Doctoral theses at NTNU, 2019:303

Sigurd Hofsmo Jakobsen

# Frequency control and stability requirements on hydro power plants

## System identification for performance and stability assessment

Doctoral thesis

Sigurd Hofsmo Jakobsen

ISBN 978-82-326-4202-1 (printed ver.)
ISBN 978-82-326-4203-8 (electronic ver.)
ISSN 1503-8181

NTNU
Norwegian University of
Science and Technology

NTNU
Norwegian University of Science and Technology
Thesis for the Degree of
Philosophiae Doctor
Faculty of Information Technology and Electrical
Engineering
Department of Electric Power Engineering

Doctoral theses at NTNU, 2019:303

NTNU
Norwegian University of
Science and Technology

Sigurd Hofsmo Jakobsen

# Frequency control and stability requirements on hydro power plants

## System identification for performance and stability assessment

Thesis for the Degree of Philosophiae Doctor

Trondheim, October 2019

Norwegian University of Science and Technology
Faculty of Information Technology and Electrical Engineering
Department of Electric Power Engineering

NTNU
Norwegian University of
Science and Technology

**NTNU**
Norwegian University of Science and Technology

Thesis for the Degree of Philosophiae Doctor

Faculty of Information Technology and Electrical Engineering
Department of Electric Power Engineering



ISBN 978-82-326-4202-1 (printed ver.)
ISBN 978-82-326-4203-8 (electronic ver.)
ISSN 1503-8181

Doctoral theses at NTNU, 2019:303

Printed by NTNU Grafisk senter

# Preface

This work has partly been conducted at the Department of Electric Power Engineering at NTNU in Trondheim and partly at Laboratoire Ampère in Ecole Centrale de Lyon (Ecully, France).

The project was financed by the Norwegian Research Council in the Norwegian In-dian research cooperation project OperaGrid project number 246784. My first stay at Ampere lab was financed by the European 7th framework programme project ELECTRA.

This work demonstrates and analyses how the stability and performance of frequency containment reserves delivered by hydro power plants can be checked using system identification techniques.

# Acknowledgments

First of all I would like to thank my family, friends and colleagues. I have had a lot of fun over the course of my PhD both at work and after work. Obviously, this would not be the case if I didn't have any of you. I also made many new friends during my PhD across Norway, India, Sweden and France where I have stayed. I am very grateful that I was welcomed so nicely by so many people.

For the scientific part I would like to thank my supervisor Kjetil and co-supervisor Xavier, who both contributed greatly to the scientific quality of my work. I also want to thank Luigi who put me in touch with Xavier, helped me in the beginning of my PhD and invited me to KTH. From the Indian side, Nand was very helpful and a good host during our visit in India and provided useful input on modelling of hydro power plants. Similarly, Thuc who wrote one of the papers that greatly inspired my work, provided a lot of good advice and help during the PhD. Trond has also been very helpful and he is a gold mine of insight into power system dynamics. Of course I have talked and discussed my PhD with several other people during the course of my work and I could probably fill a whole page with names. You should know that I thank you too.

I also want to thank Åshild and Bodil for helping me with all the annoying paper-work a PhD student has to endure.

A big thanks also goes to Statkraft, as represented by Petter and Rolf, who shared datasets with me and conducted experiments for me in a Statkraft-owned power plant. It was fun working with you guys and doing some sightseeing in Romsdalen while waiting for the power plant to run.

# Summary

The Nordic transmission system operators (TSOs) have proposed new draft requirements for the providers of frequency containment reserves. These requirements include extensive tests to determine the dynamics of hydro power plants. The dynamics of the hydro power plant are used to verify whether or not the power plants qualify to provide these reserves. To be more precise, the tests require the power plant owners to measure the plants' response when operating in open loop and with various sine sweep signals modulating the turbine governor setpoint. This is an intrusive approach and alternatives should therefore be investigated.

In this work, three novel methods have been investigated as alternatives to the one proposed by the TSOs. The main novelties of these methods are that plants are allowed to continue closed loop operation during testing and that the added excitation is limited. The three methods are characterised by different requirements on input data, as follows:

1. Phasor measurement units (PMU) measurements close to the power plant, without added extra excitation.
2. Control system measurements from the power plant, without added extra excitation.
3. Control system measurements from the power plant, with added extra excitation.

For all of the proposed methods it was analysed under which conditions the results are consistent (non biased). Although consistency cannot in general be guaranteed, it was argued that the bias due to lack of consistency is small. Moreover, the bias can be further reduced by adding external excitation to the identification procedure.

To validate the methods, tests at two different power plants in the Norwegian power system were performed. The first test compared the PMU method to the one pro-

posed in the coming draft requirements. From this test it can be seen that the PMU method yields similar results to the one proposed in the draft requirements. It was also shown that only one dataset is needed per operating state under investigation. That is true even if the method outlined in the draft requirements is used. This is an important observation as the draft proposes to use 10 tests per operating state under investigation. During the test at the other power plant it was demonstrated that the proposed method using control system measurements without added excitation could detect changes in the settings of the plant's turbine governor (PID) parameters. Moreover, it was shown that this method is capable of estimating steady state gains of the governor controller that correspond very closely with the actual permanent droop setting of the plant .

The methods were also demonstrated using the simulation softwares SIMULINK and PSS/E and a Monte Carlo Simulation (MCS) approach. This approach was used to investigate how large nonlinearities could be present before the results became too biased as well as some other aspects presented below.

When using a PMU for the identification, the power system frequency is used as an estimate of the angular speed of the machine. Consequently, a natural question is, how large an error will this lead to? The MCS approach showed that frequency is indeed a good approximation of speed. This is perfectly true when studying the slowest turbine and governor dynamics, but for the faster dynamics there will be a bias in the estimate.

When it comes to the performance of the three methods, the best results are obtained when the turbine governor uses angular speed of the rotor as feedback signal, and at the same time measurements from the power plant control system is utilized and extra excitation is added to the governor setpoint. It is possible to obtain a good estimate in the other cases too, but then some bias in the estimation should be expected, especially for the faster dynamics.

# Contents

# Chapter 1

# Introduction

## 1.1 Motivation

Recent concerns in relation to the frequency quality in the Nordic power system [1]–[3] have led to an increased interest in the dynamic performance of the frequency containment reserves (FCR). As a result of this it is expected that power plant owners in the future will be required to conduct extensive testing of their power plants to verify their plants' compliance with new draft requirements for prequalification for delivering FCR [4]. Since the proposed tests are quite intrusive and time consuming, it was decided to investigate whether it is possible to check the new requirements using a less intrusive method.

The proposed tests consist of disturbing the plant while it is operating in open loop with a set of sine tests and then record its response. However, is this really necessary? The power system is constantly excited by random events. Moreover, with the increased digitalisation of hydro power plants' control systems and installation of phasor measurement units (PMUs), several data sources are available. In other words, it is as if we are constantly performing an experiment, from which we are collecting data. Intuitively, it should therefore be possible to use this constant excitation and monitoring to deduce models that can be used for checking the requirements.

## 1.2 Scope

The scope of this thesis is to develop methods for checking the stability and performance of hydro power plants. More specifically, it is the stability and performance in the time range of the inertial response and frequency control. This means that faster or slower physical phenomena are not covered in this thesis. It is as-

sumed that the stability and performance can be checked using certain transfer functions, which will be introduced later. The focus will be on how these transfer functions can be deduced while keeping the influence on normal operation of the plant to a minimum. In order to achieve this, system identification is used. Other methods such as artificial intelligence could also potentially have been used. However, system identification has the advantage that it provides models on which standard control system theory can be applied.

Within the outlined scope the following research questions where formulated.

1. Can power plant dynamics be identified using a PMU?
2. Can power plant dynamics be identified using control system measurements without disturbing the operation of the plant?
3. What is the effect of nonlinearities on the identification?

## 1.3 Main contributions

In this section the papers, which directly contribute to answering the research questions are listed. How these publications contribute to answering the research questions is outlined in Chapter 4.

**Paper I** S. H. Jakobsen and K. Uhlen, "Vector fitting for estimation of turbine governing system parameters", in *2017 IEEE Manchester PowerTech*, Jun. 2017, pp. 1–6. DOI: 10.1109/PTC.2017.7980855

**Paper II** S. H. Jakobsen and K. Uhlen, "Development of a test system for identification of turbine dynamics using the dc power flow", *IFAC-PapersOnLine*, 9th Vienna International Conference on Mathematical Modelling, vol. 51, no. 2, pp. 97–102, 1st Jan. 2018, ISSN: 2405-8963. DOI: 10.1016/j.ifacol.2018.03.017. [Online]. Available: http://www.sciencedirect.com/science/article/pii/S240589631830017X (visited on 15/05/2019)

**Paper III** S. H. Jakobsen, K. Uhlen and X. Bombois, "Identification of hydro turbine governors using PMU data", in *2018 IEEE International Conference on Probabilistic Methods Applied to Power Systems (PMAPS)*, Jun. 2018, pp. 1–6. DOI: 10.1109/PMAPS.2018.8440273

**Paper IV** S. H. Jakobsen, K. Uhlen and P. Lie, "System identification techniques for validating hydro power plant's FCR performance", presented at the Cigre symposium, Aalborg: Cigre, Jun. 2019

**Paper V** S. H. Jakobsen and K. Uhlen, "Testing of a hydro power plant's stability and performance using PMU data", *IET Generation, Transmission & Distribution (submitted)*, 2019

**Paper VI** S. H. Jakobsen, X. Bombois and K. Uhlen, "Checking hydro power plants' FCR performance using system identification in closed loop", *IEEE Transactions on Power Systems (submitted)*, 2019

## 1.4 Other work not included in the thesis

During my work on the PhD I also coauthored a paper on one of the test systems I used during my work. This paper is in the appendices together with a report on the same test system as well as an alternative derivation to the frequency divider formula I use in my work. These documents are not to be considered as part of my PhD, but are included in the appendices as they may be useful for understanding or recreating my work.

**Appendix A** L. Vanfretti, S. H. Olsen, V. S. N. Arava *et al.*, "An open data repository and a data processing software toolset of an equivalent nordic grid model matched to historical electricity market data", *Data in Brief*, vol. 11, pp. 349–357, Apr. 2017, ISSN: 2352-3409. DOI: 10.1016/j.dib.2017.02.021. (visited on 13/06/2017)

**Appendix B** S. H. Jakobsen, E. H. Solvang and L. Kalemba, "The nordic 44 test network", *figshare*, 13th Dec. 2018. DOI: 10.6084/m9.figshare.7464386.v1

**Appendix C** S. H. Jakobsen and K. Uhlen, "An alternative derivation of the frequency divider formula using the dc power flow", *figshare*, 19th Dec. 2018. DOI: 10.6084/m9.figshare.7484489.v1

During my PhD work I also coauthored two papers, which have little relevance for my PhD.

- I. B. Sperstad, G. H. Kjølle, T. K. Vrana *et al.*, "Vulnerability analysis of HVDC contingencies in the nordic power system", presented at the Cigre Session, Aug. 2018
- E. H. Solvang, I. B. Sperstad, S. H. Jakobsen *et al.*, "Dynamic simulation of simultaneous HVDC contingencies relevant for vulnerability assessment of the nordic power system", presented at the Powertech, Milano, 2019

## 1.5 Organisation of thesis

In Chapter 2 the relevant theory needed to understand the requirements on the FCR is presented. In addition how the draft requirements propose to do the verification and some basic system identification theory is presented . Chapter 3 presents the approach proposed in this thesis for checking the requirements. How the work performed during my PhD answers the research questions is discussed and presented in Chapter 4. Finally, the conclusions and suggestions for further work are presented in Chapter 5.

# Chapter 2

# Background

## 2.1 Frequency control

In the Nordic power system, frequency control is primarily provided by hydro power plants. A good starting point for ensuring frequency quality in the Nordic power system is therefore to place good requirements on the stability margin and performance of hydro power plants.

To understand how to place requirements on hydro power plants in terms of frequency control it is first necessary to understand how the frequency control is implemented. To do this I will first present the dynamics of one generator connected to a stiff grid without any control, then the response of several generators without any control. Finally how this system can be controlled will be presented.

### 2.1.1 The response of one machine $G_J(s)$

The power system frequency is often used as a measure for the power balance in an electric power system. That is to say, it is a measure for the balance between the produced and consumed power. To understand this it is useful to look at the swing equation for a power plant, which is a well-known equation described in most standard textbooks for power systems, such as for instance [16] and [17].

$$\begin{aligned} \dot{\delta}_m(t) &= \omega_m(t) \\ J\dot{\omega}_m(t) + D_d\omega_m(t) &= T_m(t) - T_e(t) \end{aligned} \tag{2.1}$$

where:

$\delta_m(t)$**:** is the angular position of the machine's rotor,

$\omega_m(t)$**:** is the angular speed of the machine's rotor,

$J$**:** is the total moment of inertia of the machine,

$D_d$**:** is the damping torque,

$T_m(t)$**:** is the mechanical torque of the turbine and,

$T_e(t)$**:** is the torque of the electrical field in the machine.

Since power is torque times the angular speed (2.41) can be written as:

$$J\dot{\omega}_m(t) + D_d\omega_m(t) = \frac{P_m(t)}{\omega_m(t)} - \frac{P_e(t)}{\omega_m(m)} \tag{2.2}$$

To simplify the expression we can multiply with the synchronous machine speed $\omega_{sm}$ and use the assumption $\omega_m(t) \approx \omega_{sm}$. This is a common assumption since the machine speeds normally do not deviate to any great extent from synchronous speed even during disturbances.

$$\omega_{sm}J\dot{\omega}_m(t) + \omega_{sm}D_d\omega_m(t) = P_m(t) - P_e(t) \tag{2.3}$$

It is common to express the swing equation in terms of the inertia constant defined as follows:

$$H = \frac{J\omega_{sm}^2}{2S} \tag{2.4}$$

where $S$ is the rating of the machine. It is also common to define:

$$D_m = \omega_{sm}D_d \tag{2.5}$$

By inserting the new constants into (2.3) we get:

$$\frac{2HS}{\omega_{sm}}\dot{\omega}_m(t) + \omega_m(t)D_m = P_m(t) - P_e(t) \tag{2.6}$$

Since the primary topic of interest is the electrical angular speed $\omega(t)$ the following relation between the electrical rotor angle, mechanical rotor angle and number of poles $p$ is used:

$$\delta_m(t) = \frac{\delta(t)}{p/2} \tag{2.7}$$

Inserting (2.7) into (2.6) gives:

$$\frac{2HS}{\omega_s}\dot{\omega}(t) + \frac{2}{p}\omega(t)D_m = P_m(t) - P_e(t) \tag{2.8}$$

Notice that $\omega_s$ is the electrical synchronous speed. In the introduced notation the subscript $m$ is dropped when going from mechanical to electrical values. Now we can divide (2.8) by the machine rating to get the powers in per unit.

$$\frac{2H}{\omega_s}\dot{\omega}(t) + \frac{2}{Sp}\omega(t)D_m = P_m^{pu}(t) - P_e^{pu}(t) \tag{2.9}$$

From now on if not stated otherwise the powers will be in per unit. The speed damping $K_d$ is also defined as:

$$K_d = \frac{2}{p}\frac{D_m}{S} \tag{2.10}$$

By using this the final version of the swing equation is obtained

$$\frac{2H}{\omega_s}\dot{\omega}(t) + K_d\omega(t) = P_m(t) - P_e(t) \tag{2.11}$$

Another common representation of the swing equation, which will be used in the remainder of this thesis is the linearised version of (2.11):

$$\Delta\omega(s) = \frac{f_0}{2Hs + K_d}(\Delta P_m(s) - \Delta P_e(s)) = G_J(s)(\Delta P_m(s) - \Delta P_e(s)) \tag{2.12}$$

In (2.11) $\Delta$ denotes a small change. From (2.12) it can be seen that a change in either the electrical power $\Delta P_e(t)$ or mechanical power $\Delta P_m(t)$ will result in a change in the angular speed of the rotor. Or, in other words, if the balance between the mechanical or electrical power of the machine changes the rotational speed of the rotor will also change.

It should now be demonstrated that the rotational speed of the machines in a synchronous system should be more or less the same. To do this, the model of a generator connected to a stiff grid depicted in Fig. 2.1 will be used. The generator is represented by its internal voltage $E$, rotor angle $\delta$ and synchronous reactance $x_d$. The stiff grid is represented by the voltage $V$ at the terminals of the generator. That the grid is stiff means that it is assumed to be so large and contains so many generators that both its angle and frequency remain constant. Put differently, it means that the generator in Fig. 2.1 is so small compared to the rest of the system that it cannot affect its frequency or its angle. In this case we can write the power of the generator as: so large and contains so many generators that both its angle and frequency remain constant. Or in other words that the generator in Fig. 2.1 is so small compared to the rest of the system that it cannot affect its frequency nor its angle. In this case we can write the power of the generator as:

$$P_e = \frac{EV}{x_d}\sin(\delta) \tag{2.13}$$

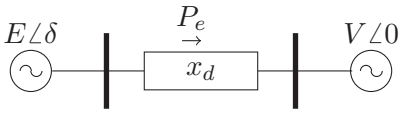


**Figure 2.1:** Generator connected to stiff grid

From (2.13) and (2.11) it can seen that it is possible to increase the electrical power of the generator by increasing the mechanical power, which will result in the the angle $\delta$ increasing, which again will increase the electrical power $P_e$. However, there is an upper limit to how much the mechanical power can be increased, which is reached at $\delta = \pi/2$. If we try to increase the power above this limit, the electrical torque will not be able to match the mechanical torque and the machine will lose synchronism. This means that if the machine were to not rotate synchronous with the grid it would eventually lose synchronism and spin out of control.

### 2.1.2 The response of several generators

Thus far the power balance of one machine has been discussed. I will now move on to discuss the power balance of a full power system. To do this a dc power flow will be used for modelling the power flowing on the lines in the power system.

The power flowing on the lines in a power system is related to the power injections at the buses through the power flow equations. Below the power flow equation for active power is written neglecting the terms related to ohmic losses and shunt elements. Basically, the equation tells us that the power injected into a bus equals all the powers flowing out on adjacent lines.

$$P_k = U_k \sum_{m \in \Omega_k} U_m x_{km}^{-1} \sin \delta_{km} \tag{2.14}$$

where:

$P_k$**:** is the power injection at node $k$,

$\delta_{km}$**:** is the voltage angle difference between node $k$ and $m$,

$x_{km}$**:** is the reactance between node $k$ and $m$,

$\Omega_k$**:** is the buses adjacent to bus $k$.

$U_k$**:** is the voltage at bus $k$.

$U_m$**:** is the voltage at bus $m$.

In real power systems the voltages are normally close to $1(p.u.)$ and the angles are small. Using these observations the DC power flow approximation is written as follows:

$$P_k \approx \sum_{m \in \Omega_k} x_{km}^{-1} \delta_{km} \tag{2.15}$$

Written in matrix form this becomes:

$$\boldsymbol{P} = \boldsymbol{Y}\boldsymbol{\delta} \tag{2.16}$$

where:

$\boldsymbol{P}$**:** is the vector of power injections,

$\boldsymbol{Y}$**:** is the nodal admittance matrix augmented with the transient reactances of the generators,

$\boldsymbol{\delta}$**:** is the vector of voltage bus angles.

Since the angles at the load buses are unknown the admittance matrix is split into submatrices to derive an expression for the power injection at the generator buses.

$$\begin{bmatrix} \boldsymbol{P}_e \\ \boldsymbol{P}_l \end{bmatrix} = \begin{bmatrix} \boldsymbol{Y}_{11} & \boldsymbol{Y}_{12} \\ \boldsymbol{Y}_{21} & \boldsymbol{Y}_{22} \end{bmatrix} \begin{bmatrix} \boldsymbol{\delta}_e \\ \boldsymbol{\delta}_l \end{bmatrix} \tag{2.17}$$

where:

$\boldsymbol{P}_e$**:** is the power injection at the generator nodes

$\boldsymbol{P}_l$**:** is the power injection at the loads

$\boldsymbol{\delta}_e$**:** is the electrical rotor angles

$\boldsymbol{\delta}_l$**:** is the voltage angle at the load nodes

The angle of the load buses can now be calculated as:

$$\boldsymbol{\delta}_l = \boldsymbol{Y}_{22}^{-1}(\boldsymbol{P}_l - \boldsymbol{Y}_{21}\boldsymbol{\delta}_e) \tag{2.18}$$

Finally the power injections at the generator buses are:

$$\boldsymbol{P}_e = \boldsymbol{Y}_{11}\boldsymbol{\delta}_e + \boldsymbol{Y}_{12}\boldsymbol{\delta}_l \tag{2.19}$$

If we are not interested in the angle of the load buses and are instead only interested in the injected power at the generator node it can be convenient to substitute (2.18) into (2.19) and rearrange to obtain:

$$\boldsymbol{P}_e = \begin{bmatrix} \boldsymbol{Y}_{11} - \boldsymbol{Y}_{12}\boldsymbol{Y}_{22}^{-1}\boldsymbol{Y}_{21} & \boldsymbol{Y}_{12}\boldsymbol{Y}_{22}^{-1} \end{bmatrix} \begin{bmatrix} \boldsymbol{\delta}_e \\ \boldsymbol{P}_l \end{bmatrix} \tag{2.20}$$

What now remains is to use (2.20) to connect several loads and generators together to model a small power system. I will assume a power system consisting of $n_g$ generators and $n_l$ loads. The loads will be assumed to be external input to the system and independent of voltages and power system frequency. Moreover, I will linearise the system and only look at small changes denoted by $\Delta$. From (2.20) it can be seen that a model for the generator rotor angles $\boldsymbol{\delta}_e$ is needed. For one generator $i$ this model is given as:

$$\Delta\delta_i(s) = \frac{1}{s}\Delta\omega_i(s) \tag{2.21}$$

where $\Delta\omega_i(s)$ is given by (2.12). By using (2.20) and (2.12) the simple graphical representation of a uncontrolled power system depicted in Figure 2.2 can be constructed. From the figure it can be seen that a change in any of the $n_l$ loads will result in a change in all electrical powers in the system, which in turn will result in a change in the rotor angular speed and position of all $n_g$ generators. Moreover, since the steady state angular speed of the machines has to be the same in a stable system it means that this value can be used as a measurement of the total balance between mechanical and electrical power.

### 2.1.3 Controlling the mechanical power $G_p(s)$

As explained in the previous sub section it is necessary to balance the electrical and mechanical power. This is performed by changing the mechanical power of all the power plants. Since the steady state angular speeds of all the machines are the same this variable can be used for a distributed control. However, all of the plants cannot try to fully compensate the power imbalance. If all the plants compensated the imbalance fully at the same time it would simply result in an imbalance in the opposite direction. Instead, the control is designed such that it should contain frequency deviations. The control is, therefore, often referred to as frequency containment control (FCP), and is the control delivered by the FCR. In this thesis the transfer function of this control is denoted $G_p(s)$.

A graphical representation of this $G_p(s)$ is depicted in Figure 2.3. If there is a difference between the speed of the machine $\Delta\omega(s)$ and the reference to the controller $r(s)$ the controller $G_c(s)$ will try to compensate for this difference by sending a

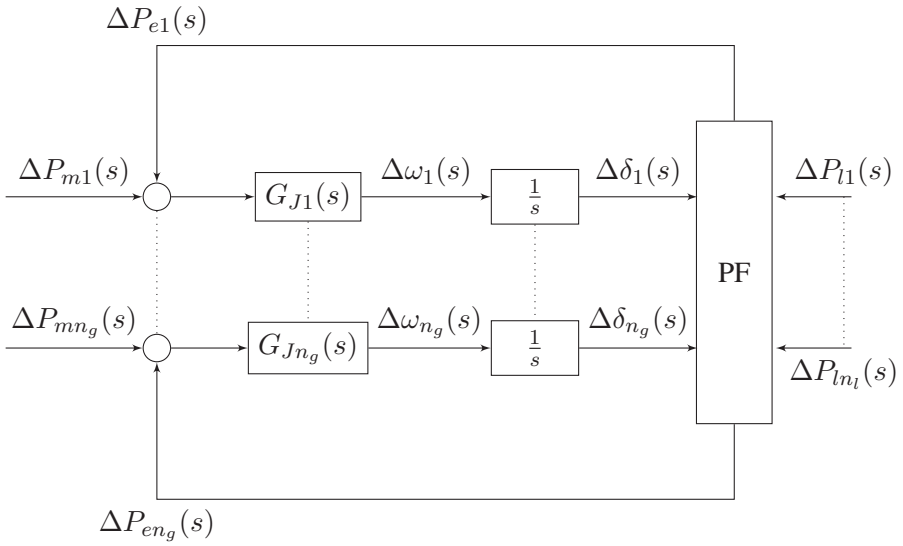


**Figure 2.2:** Uncontrolled power system with a DC power flow in the PF block

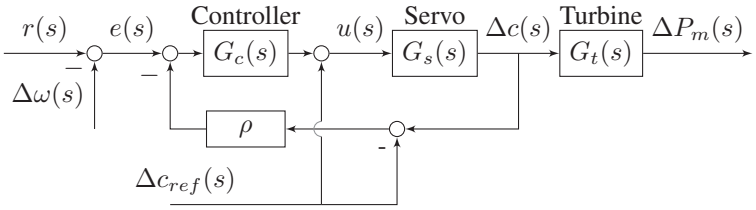


**Figure 2.3:** Block diagram of $G_p(s)$

control signal to the servo $G_s(s)$. The servo is then responsible for opening or closing the guide vane $\Delta c(s)$ to the turbine $G_t(s)$, eventually leading to a change in power. One important aspect of this process is the droop feedback $\rho$. Due to this feedback the controller will not try to fully compensate the control error $e(s)$. It is the combination of this controller $G_c(s)$, the droop feedback $\rho$, the servo $G_s(s)$ and the turbine $G_t(s)$ that make up the FCP.

Since the FCP is not designed to remove the steady state deviation of the frequency, a second process is needed to remove it. This is done by the frequency restoration process (FRP), which changes the reference for the guide vane opening $\Delta c_{ref}(s)$[1]. This is a centralised controller, which changes the power of the machines in the system such that the frequency and tie line powers are brought back to their sched-

[1]It is possible to have power droop feedback and a reference for the power instead

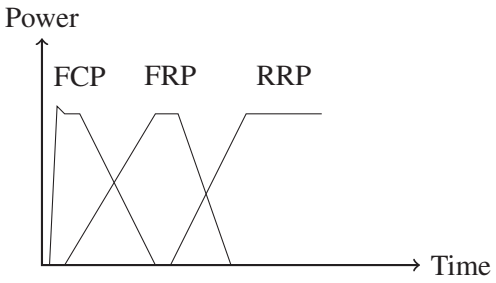


**Figure 2.4:** Temporal structure of frequency control using the ENTSO-E terminology from [18]

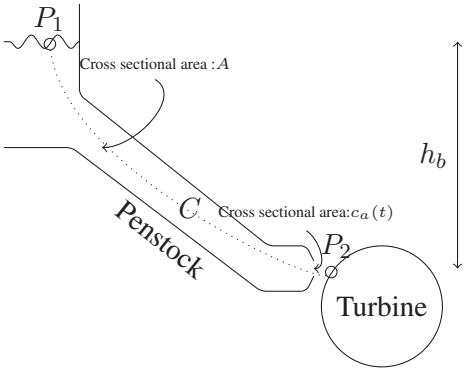


**Figure 2.5:** Hydro reservoir, waterway and turbine

uled values. In addition, it relieves the frequency containment reserves (FCR).

Finally, we have the restoration reserve process (RRP), which activates the restoration reserves (RR) relieving the frequency containment reserves (FCR). A schematic picture of how these processes relate to each other is given in Figure 2.4.

To understand how FCR is delivered a frequently used simple nonlinear model of hydro power plants will be derived. A typical hydro power plant setup is depicted in Figure 2.5. The power plant consists of a reservoir, a penstock, a servo controlling the guide vane opening and a turbine. To analyse the mechanical dynamics of the power plant we start by assuming that the flow in the penstock is steady, the flow is incompressible, the flow is frictionless, and the flow is along a single streamline [19]. With these assumptions we can use the Bernoulli equation for our system:

$$\int_1^2 \frac{\partial v(t)}{\partial t} ds + \int_1^2 \frac{dp}{\rho} + \frac{1}{2}(v_2^2(t) - v_1^2(t)) + g(z_2 - z_1) = 0 \tag{2.22}$$

where $v(t)$ is the speed of the water in the penstock, $v_1(t)$ is the speed of the water in the reservoir, $v_2(t)$ is the speed of the water out of the guide vane opening, $p$ is pressure, $g$ is the gravitational constant, $z_2$ and $z_1$ are the meters above the ocean for the points $P_2$ and $P_1$ respectively. We will make some further simplifying assumptions, namely that the flow of the water is along a line $C$, which has length $L$, the pressure at the points $P_1$ and $P_2$ are the same, and the speed of the water at the reservoir $v_1(t) = 0$. In addition we have that $z_1 - z_2$ is the head $h_b$ of the reservoir and the output speed of the water is given by

$$v_2(t) = v(t)A/c_a(t) \tag{2.23}$$

where $c_a(t)$ is the cross section area of the guide vane opening, and $A$ is the cross section area of the penstock. With the above simplifications we obtain the following expression:

$$\frac{\partial v(t)}{\partial t} = \frac{gh_b}{L} - \frac{1}{2L}\left(\frac{Av(t)}{c_a(t)}\right)^2 \tag{2.24}$$

We will now rewrite the equation in terms of mass flow instead of speed. We will also use the base values defined in [20] to get the equation in per unit. The mass flow through the penstock in per unit is given by:

$$q(t) = \frac{Av(t)}{q_b} \tag{2.25}$$

where $q_b$ is the mass flow with the guide vane opening fully opened. We also introduce the time constant

$$T_w = \frac{L}{A}\frac{q_b}{h_b g} \tag{2.26}$$

In addition, we have the following expression for the guide vane opening in per unit

$$c(t) = \sqrt{2gh_b}\frac{c_a(t)}{q_b} \tag{2.27}$$

With the above definitions we obtain the following expression for the turbine dynamics

$$\dot{q}(t) = \frac{1 - h(t)}{T_w} \tag{2.28}$$

with $h(t) = q^2(t)/c^2(t)$. It should be noted that (2.28) is the same equation as that used in [20] except that we have assumed a frictionless flow. If we neglect the damping in the turbine the mechanical power produced by the turbine can now easily be calculated as

$$P_m(t) = A_t h(t)(q(t) - q_{nl}) \tag{2.29}$$

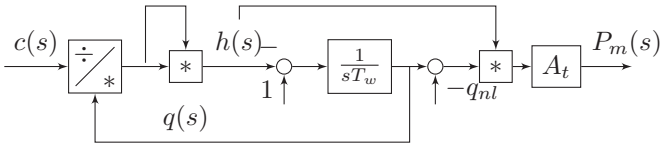


**Figure 2.6:** Simple nonlinear turbine model

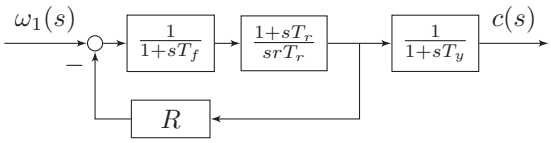


**Figure 2.7:** Classical governor model

where $q_{nl}$ is the per unit no load flow accounting for fixed losses in the turbine and $A_t$ is a proportionality factor used for going between the turbine MW rating to the generator MVA rating [20]. The dynamics of the turbine are presented graphically in Figure 2.6. This representation together with the governor depicted in Figure 2.7 is the one commonly referred to as HYGOV in several simulation softwares.

Since we will use linear system identification for identifying the dynamics we will introduce a linearisation of the dynamics depicted in Figure 2.6. This will help in comparing the results from the identification with the actual dynamics. From [20] we have the following linear expression for the turbine dynamics.

$$\frac{\Delta P_m(s)}{\Delta c(s)} = \frac{A_t(1 - sT_1)}{1 + sT_2} \tag{2.30}$$

with

$$T_1 = (q_o - q_{nl})T_w \tag{2.31}$$

and

$$T_2 = c_0 T_w/2 \tag{2.32}$$

The subscript $0$ denotes a variable at the operating point where we are linearising.

There are still some nonlinearities that may be present in a hydro power plant. For instance in [21] it is reported that a backlash was found, between the servo and guide vane opening, for some plants. Another nonlinearity that may play an important role is the frequency response deadband. This is a deadband at the input to the governor to reduce unnecessary wear and tear on the physical components of the plant due to constant small changes in the power system frequency. However, there is an upper allowed size for this deadband specified for the different classes of generators given in [22], which means it is always possible to know approximately the magnitude of this deadband.

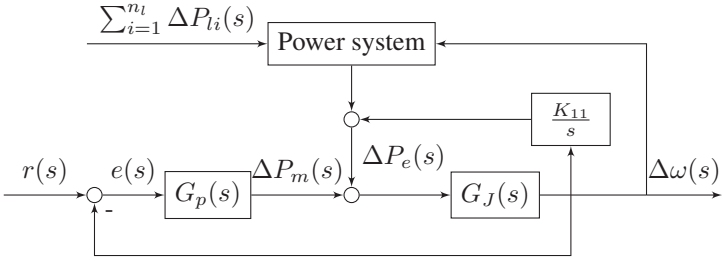


**Figure 2.8:** Hydro power plant in a power system

### 2.1.4 Closed loop transfer function of a power plant

To further understand how requirements on the stability of the frequency control can be made the closed loop system involving $G_J(s)$ and $G_p(s)$ of one of the plants in a power system is presented in Figure 2.8. The constant $K_{11}$ in the figure can be derived from (2.20) or by linearising (2.13) and the block power system represents the rest of the power flow equations, and power plants.

The system depicted in Fig. 2.8 is a multi-input single output (MISO) system. The stability of such systems will not be covered here, but a good reference source for the interested reader is [23]. For this thesis it suffices to say that if one of the loops in a MISO system is unstable, then the whole system will be unstable. Based on this reasoning it makes sense that for all power plants it should be required that the loop containing $G_p(s)$ and $G_J(s)$ to be stable. The remainder of this thesis will explain how the stability margin and performance for this loop can be defined and how this can be checked using measurements.

## 2.2 The new requirements on FCR

There already exist requirements on hydro power plants as described in the network codes for grid connection of generators [22]. However, these are stated in terms of time domain performance. Intuitively time domain requirements are quite appealing as it is possible to define the plant's response to different situations. A simple example of this approach is demonstrated in Figure 2.9 where the input to a power plant's governor has been replaced with a step signal. It is possible, for instance, put requirements on maximal activated FCR $\Delta P_{\max}$ and time to full activation $\Delta t_P$. In the frequency domain this would mean putting a requirement on the steady state gain and bandwidth of $G_p(s)$. These are just simple examples and a list of such requirements in use is provided in [18]. Another proposal from the research community is given in [24], where it is also proposed to look at the time domain performance of the plant in normal operation.

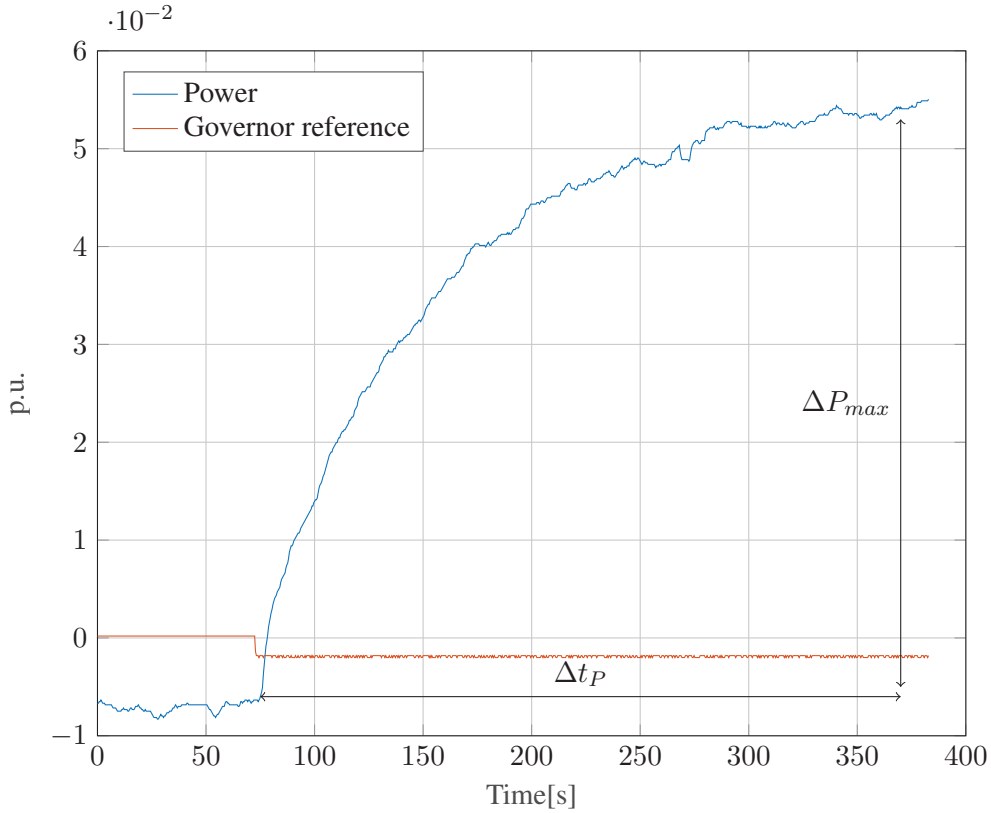


**Figure 2.9:** Step response test at a power plant in Norway

In the new draft requirements where the theoretical background is given [25], [26] they define stability and performance requirements in the frequency domain for FCR-N and FCR-D[2] respectively. The idea for the stability and performance requirements presented in this work is from [25] and the reference used for stability theory for linear time invariant (LTI) systems are from [23].

To understand how to develop requirements for a hydro power plant in the frequency domain one can start with the classical control loop depicted in Figure 2.10. It consist of a controller $K(s)$ trying to keep the output $y(s)$ of the process $G(s)$ close to the reference signal $r(s)$. The process is assumed to be subjected to noise $v(s)$ and the controller therefore does not only have to be tuned such that the system is stable and track the reference signal effectively, but it should also reject the disturbance as well as possible. From looking at Figure 2.8, it can be seen that the loop containing $G_p(s)$ and $G_J(s)$ has the same structure as the classical structure

[2]N denotes normal operation and D disturbance

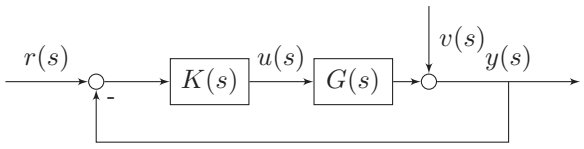


**Figure 2.10:** Classical control loop

depicted in Figure 2.10. I will therefore use classical control theory to explain the new requirements for the loop depicted in Figure 2.8.

From classical control system theory it is known that the stability of the closed loop system containing $G_p(s)$ and $G_J(s)$ depicted in Figure 2.8 can be deduced from the loop transfer function $L(s)$ given by:

$$L(s) = G_p(s)G_J(s) \tag{2.33}$$

What is also of interest is how far away the system is from instability. This distance will be referred to as the stability margin and will be denoted $M_s$. An easy way of deriving the expression for the stability margin is to look at the Nyquist diagram depicted in Figure 2.11. In this diagram the loop transfer function is plotted as a function of frequency in the complex plane. The stability of the system can be deduced from the figure by checking whether or not the curve encircles the point -1. From the diagram it can be seen that the distance to instability (distance to the point -1) is given by $-1 - L(j\Omega)$. We therefore define the stability margin as:

$$1/M_s = \min |-1 - L(j\Omega)| \tag{2.34}$$

Consequently, it is possible to check the stability margin of a hydro power plant's FCR by investigating $L(s)$. However, it is more common to use the sensitivity function $S(s)$ which is given by:

$$S(s) = \frac{1}{1 + G_p(s)G_J(s)} \tag{2.35}$$

From (2.35) one can see that the stability margin can be calculated as:

$$M_s = \max |S(j\Omega)| \tag{2.36}$$

Based on (2.36) the stability requirement for the FCR is thus stated as in [25] as:

$$\max |S(j\Omega)| < M_s \tag{2.37}$$

What remains is to formulate the performance requirements for a hydro power plant. An approach often used by engineers is to look at the time domain performance [23]. Such requirements already exists for generators and are given in [22].

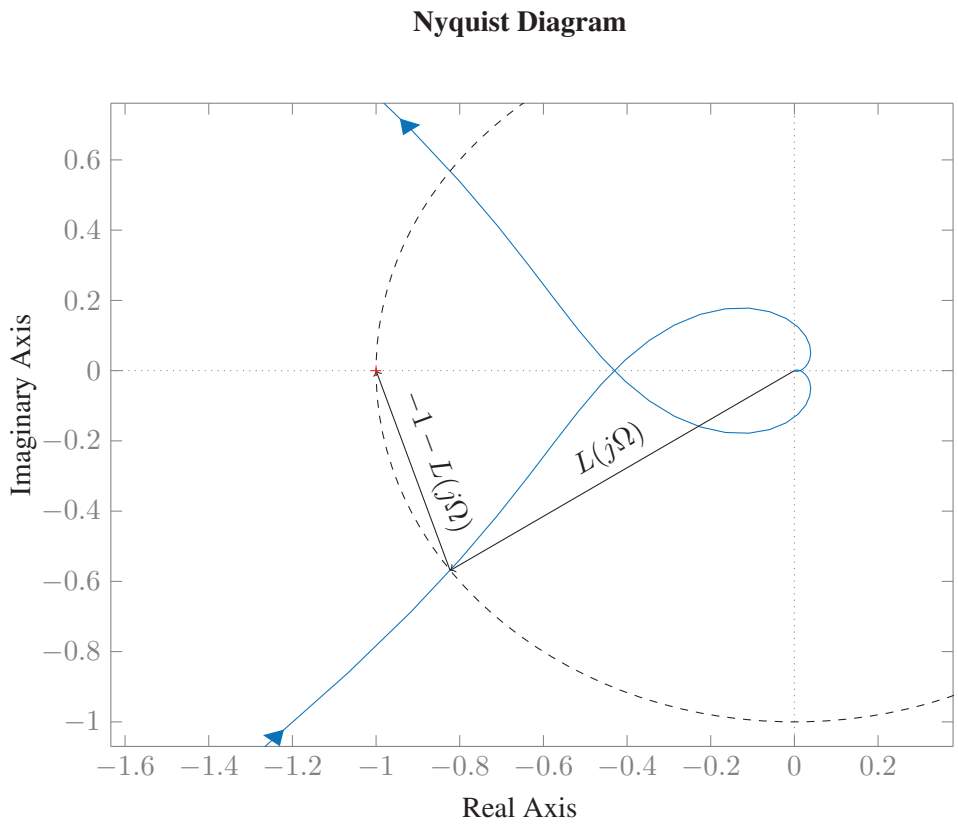


**Figure 2.11:** Nyquist diagram for a hydro power plant

The approach used in [25] is from a technique referred to as loop shaping for disturbance rejection [23]. To explain the idea, we start with the limit on the power system frequency $\Delta f_s$, which should be within the range $\Delta f_s < \pm 0.1Hz$ [18]. Since the hydro power plants under study use synchronous generators it is possible to use the limit on the power system frequency to put a limit on the deviation of the electrical angular speed of the hydro power plant's rotor as:

$$\Delta\omega(s) = G_J(s)S(s)d(s) = G_1(s)\Delta P_e(s) \tag{2.38}$$

It can now be seen that if the power of $\Delta P_e(s)$ is known, it is possible to put requirements on the plant's disturbance rejection given by $G_1(s)$ to try to keep the frequency deviation below $0.1Hz$.

$$|G_1(j\Omega)| < \frac{\sigma_{\omega_{req}}}{\sqrt{\phi_{P_e}(j\Omega)}} \tag{2.39}$$

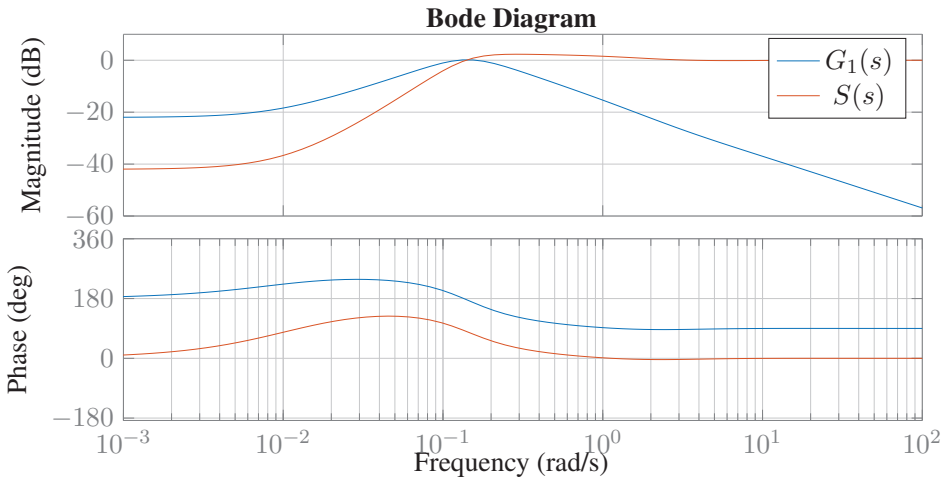


**Figure 2.12:** $G_1(s)$ and $S(s)$ for a power plant

where $\sigma_{\omega_{req}}$ is the variance of the change in electrical rotor speed when it is assumed white and subjected to $\omega(s) < 0.2\pi$.

## 2.3 Checking the new requirements

To check the new requirements in the frequency domain requires models of both $S(s)$ and $G_1(s)$, which for a hydro power plant often will look like that depicted in Figure 2.12. If the definitions from [27] are used, there are two main approaches for obtaining these models:

**Modelling** In this approach a mathematical model of a system is constructed from laws of nature, physical principles and empirical knowledge.

**System identification** In this approach a model of the system is deduced from measurements alone.

### 2.3.1 Modelling approaches for constructing power plant models

The modelling approach is well known and popular textbooks about power system modelling include [16], [17]. However, these approaches still require data to estimate the parameters of the model. Traditionally, there have been two main approaches for estimating these parameters:

- Field tests at the power plant.
- Disturbance recordings

An example of the first method is presented in [28] where parameters for a dynamic simulation model are derived using field tests and physical reasoning. The aim of the approaches is for the simulation model to produce waveforms as close as possible to those recorded during the tests. During the field tests both steady state measurements and load rejection tests were performed.

Intuitively it makes sense to use disturbance recordings for an estimation of model parameters. The reason for this is that disturbances excite most of the system's dynamics and often reveal modeling errors in previously used models. For instance during a blackout in 1996 the simulation models in use showed that the system would be stable [29]. The paper [29] therefore proceeded to use measured data from this disturbance to better tune the simulation models. Other papers such as [30]–[32] use unscented Kalman filters to estimate parameters. Another approach used in [11] is to use heuristic optimisation to find the model parameters minimising the difference between a simulated and measured signal.

### 2.3.2 System identification for constructing power plant models

Similar to the modelling approach the measurements used for system identification traditionally come from field tests or disturbance recordings. An old example of a field test where system identification is performed is [33]. The approach consisted of injecting sine signals within a specified range and to measure the plant's response in the frequency domain. By doing this they constructed Bode and Nichols plots of the plant. In other words they created graphical models of the plant. A similar approach was also performed recently in [21] where sine injection was used to derive a plant's response in the frequency domain.

With the introduction of increasing numbers of wide area monitoring devices in the power system the use of PMU measurements from disturbance recordings has also been tested to identify models as presented in [34], which used disturbance recordings for performing the identification assuming an ARX model structure. In [2] identifying governor dynamics using PMU measurements from normal operation was also tested.

### 2.3.3 ENTSO-E Nordic's proposal for checking the new requirements

In [25] they propose replacing input to the governor with sine signals with different frequencies to test the plant's response to these frequencies. The setup is presented in Figure 2.13, where $r(s)$ represents the sine signals.

The power plant owners have to measure the plant's response in electric power while the input signal to the governor has been replaced by ten sine sweeps. The time periods of the sine signals to be injected are given in Table 2.1. If we look at

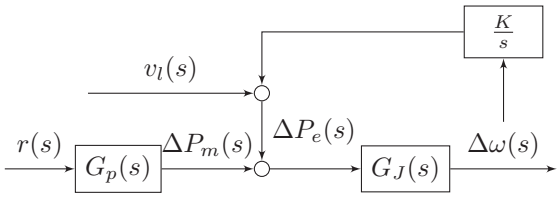


**Figure 2.13:** The setup used to find the transfer functions in [4], [25]

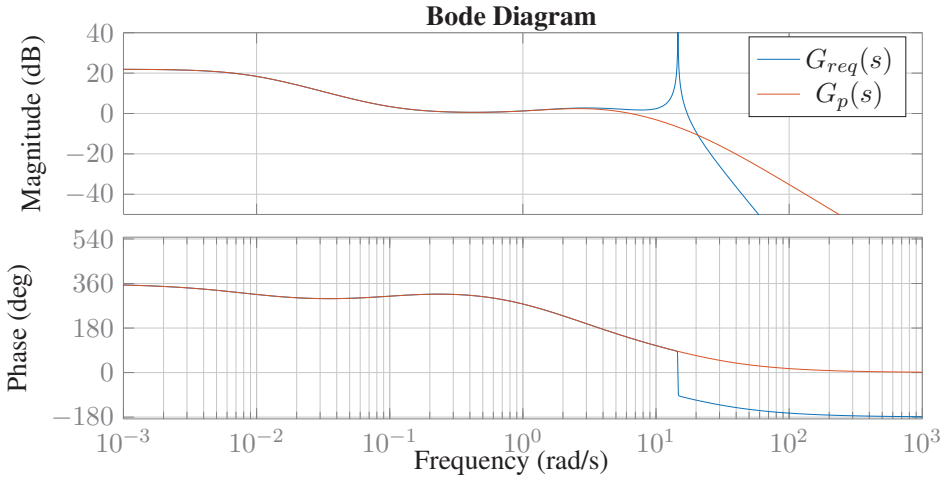


**Figure 2.14:** Comparison of $G_p(s)$ and $G_{req}(s)$

Figure 2.13 we can see that the transfer function from $r(s)$ to $\Delta P_e(s)$ is:

$$G_{req}(s) = \frac{G_p(s)G_J(s)K_{11}}{s + G_J(s)K_{11}} \tag{2.40}$$

To check if $G_{req}(s)$ is a good estimate of $G_p(s)$ we can insert the following expression for $G_J(s)$ into (2.40)

$$G_J(s) = \frac{1}{2Hs + K_d} \tag{2.41}$$

With this we get

$$G_{req}(s) = \frac{G_p(s)K_{11}}{K_{11} + s(K_d + 2Hs)} \tag{2.42}$$

**Table 2.1:** Time periods of the injected sine signals

| | | | | | | | | | |
|---|---|---|---|---|---|---|---|---|---|
| 10 | 15 | 25 | 40 | 50 | 60 | 70 | 90 | 150 | 300 |

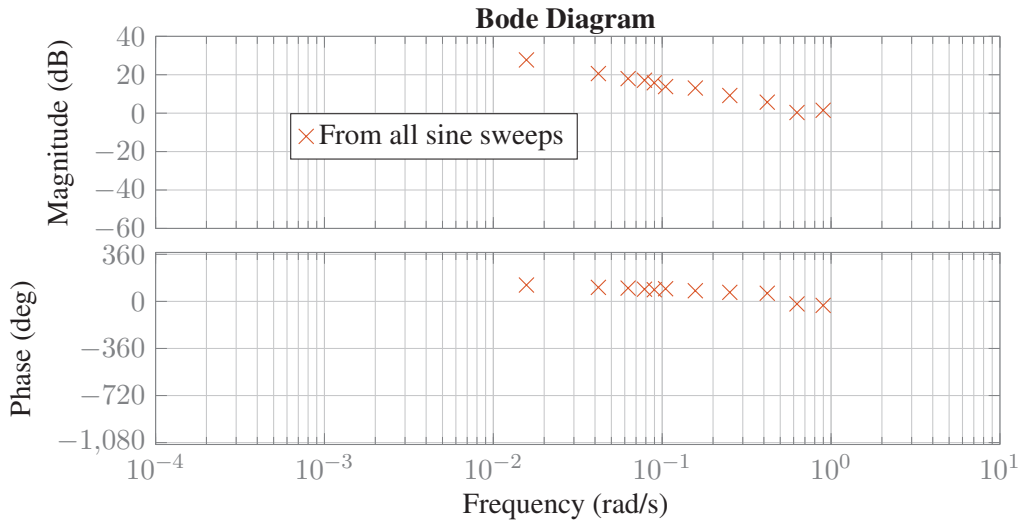


**Figure 2.15:** $G_{req}(s)$ calculated at ten frequencies

In other words $G_{req}(s)$ is the transfer function $G_p(s)$ and a low pass filter. This is demonstrated in Figure 2.14 where $G_p(s)$ and $G_{req}(s)$ are plotted together and we can see them following each other closely up to a certain frequency.

To obtain the transfer function the draft requirements propose obtaining the fourier transforms $r(j\Omega_p)$ and $\Delta P_{e1}(j\Omega_p)$ where $\Omega_p$ is the frequency of the injected sine signal. By doing this it is possible to calculate $G_{req}(j\Omega_p) = \Delta P_e(j\Omega_p)/\Delta\omega(j\Omega_p)$ for several frequencies to obtain an estimate for $G_{req}(s)$. In Figure 2.15 the result of applying this approach to a power plant in the Norwegian power system is presented. This figure clearly shows the ten frequencies at which the transfer function was calculated.

What remains is to obtain estimates for $S(s)$ and $G_1(s)$. To achieve this an estimate of the total swing dynamics has been estimated given in [25].

$$G_{J_{sys}}(s) = \frac{600MW}{0.1Hz}\frac{f_0}{S_{sys}}\frac{1}{2H_{sys}s + K_{d_{sys}}f_0} \tag{2.43}$$

To use the system swing dynamics for each plant the following per unit system was defined. The base value for each plant is given as it's static gain[3] that is

$$G_p^{(p.u.)}(s) = G_p(s)/G_p(0) \tag{2.44}$$

[3]The static gain of the plant is closely related to its droop

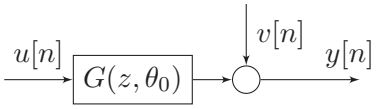


**Figure 2.16:** System assumed by the identification

The base value for $G_{J_{sys}}(s)$ is given as the sum of the static gains of all the power plants in the system, that is

$$G_{J_{sys}}^{(p.u.)}(s) = \frac{G_J(s)}{\sum_i^{N_g} G_{p_i}(0)} \tag{2.45}$$

The transfer functions $S^{(p.u.)}(s)$ and $G_1^{(p.u.)}(s)$ are then estimated as

$$S^{(p.u.)}(s) = \frac{1}{1 + G_{J_{sys}}^{(p.u.)}(s) G_p^{(p.u.)}(s)} \tag{2.46}$$

and

$$G_1^{(p.u.)}(s) = S^{(p.u.)}(s) G_p^{(p.u.)} \tag{2.47}$$

## 2.4 Checking the requirements using prediction error identification

In this work prediction error identification is used for the identification. It is worth noting that this type of identification could also be used with the setup proposed in the new requirements [4], instead of using ten tests for obtaining the transfer function they could actually use only one.

In prediction error identification it is assumed that the system to be identified has the structure depicted in Figure 2.16. The system to be identified is referred to as the true system $\mathcal{S}$ and can mathematically be described as:

$$\mathcal{S} : y[n] = G(z, \theta_0)u[n] + v[n] \tag{2.48}$$

where $z^{-1}$ is the time delay operator, $v[n] = H(z, \theta_0)e[n]$, where $e[n]$ is white noise and $\theta_0$ is the parameter vector parametrising the true system $\mathcal{S}$. The signals $u[n]$ and $y[n]$ are referred to as the input and output of the system respectively. In this work it is assumed that the true system can be described by a box-Jenkins model structure:

$$G(z, \theta_0) = \frac{\sum_{i=1}^{n_b} b_i z^{-i}}{\sum_{i=0}^{n_f} f_i z^{-i}}, H(z, \theta_0) = \frac{\sum_{i=1}^{n_c} c_i z^{-i}}{\sum_{i=0}^{n_d} d_i z^{-i}} \tag{2.49}$$

The true parameter vector is thus

$$\theta_0 = \begin{bmatrix} b_1 \dots b_{n_b} & 1 & f_1 \dots f_{n_f} & c_1 \dots c_{n_c} & 1 & d_1 \dots d_{n_d} \end{bmatrix} \tag{2.50}$$

The aim of the system identification procedure is then to, given a dataset $Z^N = \{u[n], y[n] | 1 \dots N\}$ containing $N$ samples, find an estimate $\hat{\theta}_N$ of the true parameter vector $\theta_0$. For finding our estimate $\hat{\theta}_N$ we will use prediction error identification [27]. The aim of prediction error identification is to find the parameter vector $\hat{\theta}_N$ minimizing the prediction error criterion. The prediction error is defined as:

$$\epsilon[n, \theta] = H^{-1}(z, \theta)(y[n] - G(z, \theta)u[n]) \tag{2.51}$$

It can now be seen that if the true system is inserted into (2.51) the prediction error will be $e[n]$, which makes sense as even the true system cannot predict the white noise representing process noise and other unmodelled dynamics. We can now find our estimate as the argument minimising (2.51), or in other words:

$$\hat{\theta}_N = \arg\min_{\theta} \frac{1}{N} \sum_{n=1}^{N} \epsilon^2(n, \theta) \tag{2.52}$$

# Chapter 3

# Methodology

As stated in the previous chapter prediction error identification is used to identify the transfer functions needed for checking the new draft requirements. Depending on what measurements we have available and whether or not we can add extra excitation to the plant, three different approaches for checking the stability and performance of the FCR have been developed.

## 3.1 Approaches for checking the requirements

The three approaches for checking the requirements are:

1. PMU measurements close to the power plant, without added extra excitation.
2. Control system measurements from the power plant, without added extra excitation.
3. Control system measurements from the power plant, with added extra excitation.

The first approach is presented in Paper III, the second approach is presented in Paper IV and the third approach is presented in Paper VI.

All of the approaches consist of the same steps. What differs between the approaches is the dataset collected. In Table 3.1 the different measurements needed for the different approaches are explained. For the third approach it is also possible to first identify FCR dynamics $G_p(s)$ and the swing dynamics $G_J(s)$ before calculating $S(s)$ and $G_1(s)$. However, to do this it is necessary to identify the servo $G_s(s)$; how to do this is outlined in Paper VI. It is also worth noting that the

**Table 3.1:** Measured data for the different approaches

| Approach | output $y[n]$ | input 1 $u_1[n]$ | input 2 $u_2[n]$ |
|---|---|---|---|
| 1 | power system frequency | generator power | |
| 2 | generator rotor angular velocity | generator power | |
| 3 | control system error | generator power | control system reference |

measurement of the generator rotor angular velocity can be replaced with measurements of the power system frequency; however, this will lead to a biased estimate for faster dynamics.

**Data collection** In this step data are collected either from a PMU or from the control system of a hydro power plant.

**Preprocessing of data** First it is necessary to calculate the correct variables. For instance if the data are from a PMU it is necessary to calculate power from the voltages and currents. In some cases it is also necessary to take into account that the measured values may have been scaled or use the wrong units. The collected data should be passed through a low pass filter, decimated and the average removed.

**System identification** It should be ensured that the correct model order is chosen. This can be seen as an iterative process, where we first attempt a high order model. Following this we should perform a residual test on the model. The residual test for closed loop identification consists of checking whether or not the prediction error is white. If it is not white this may indicate that the results are biased. In Figure 3.1 an example of two residual tests from the system identification toolbox in MATLAB is presented. The figure shows the autocorrelation of the prediction error, if the prediction error is white there will be no autocorrelatioun. From the figure it is possible to conclude that the prediction error of the tested models most likely are white.

It is also beneficial to look for pole zero cancellation. In Figure 3.1 we can see a spike in the frequency response of some of the transfer functions. This spike represents a pole zero cancellation and can be removed by reducing the order of the of the numerator. If the model passes the tests then we can try with a lower order and then continue reducing the order until the model no longer passes the test. An example of this process is presented in Figure 3.1. Here four attempts of identifying $G_{req}(s)$ of a power plant in the Norwegian system are shown. Here, we can see that all the transfer functions except one pass the residual test. We therefore discard the one not passing the residual

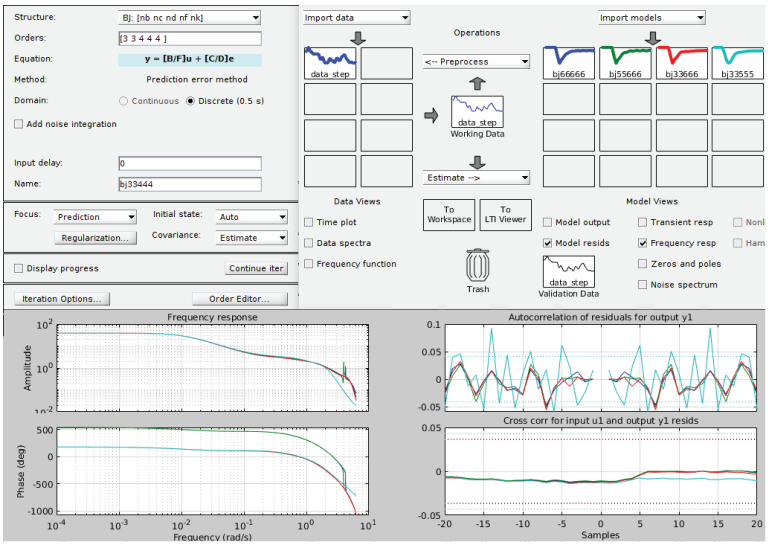


**Figure 3.1:** System identification toolbox [35] workflow

test. For the other transfer functions we see that all except one have pole zero cancellation. The pole zero cancellation can be seen as the spikes on the bode diagram. We therefore keep the transfer function drawn in red, which passes all the tests.

# Chapter 4

# Discussion and results

In this chapter it will be explained how the different papers contribute to answering the research questions (RQs) raised in the introduction. The questions are as follows:

1. Can power plant dynamics be identified using a PMU?
2. Can power plant dynamics be identified using control system measurements without disturbing the operation of the plant?
3. What is the effect of nonlinearities on the identification?

To answer these questions 36 different datasets from 4 power plants in the Norwegian power system were obtained.

**Dataset** $1-19$**:** PMU measurements from power plants 1 and 2.

**Dataset** 20**:** PMU measurements from power plant 3.

**Dataset** $21-31$**:** Control system measurements according to [25] from power plant 3.

**Dataset** $32-36$**:** Control system measurements from power plant 4, while the plant was operating in closed loop.

In addition two different test networks were used, with the first being presented in Paper II. This paper does not directly answer any of the research questions, however, it is used in all preceding papers. In Paper V a test system developed for

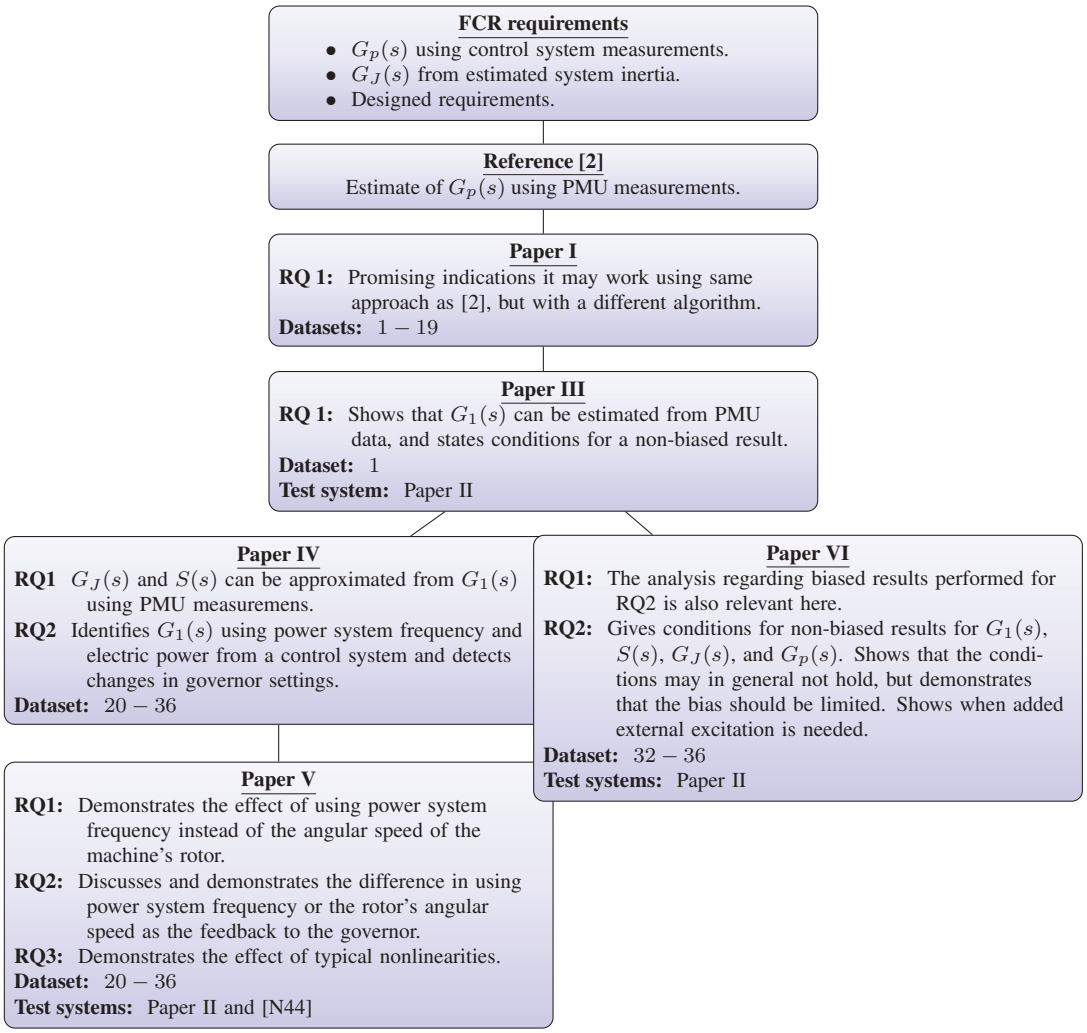


**Figure 4.1:** Overview of how the different papers answer the main research questions and how they relate to each other

a commercial power system simulator is also used. This test network is referred to as N44 and described in [11], [12].

An overview of how the different papers relate to each other, along with which dataset and test system they use is presented in Figure 4.1. Moreover, the figure provides an overview of the main contributions the different papers have towards answering the research questions. A more detailed discussion on how the papers answer the research questions is presented in the following discussion.

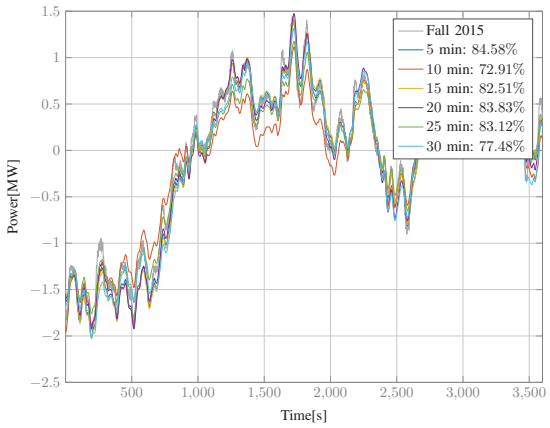


**Figure 4.2:** Cross validating of dataset

## 4.1 Initial tests using vector fitting Paper I

In the first paper the idea was to follow up on the work performed in [2]. This work was inspired by the work in the new draft requirements [4], where the transfer function from the input of the governor to the electrical power is identified, while the plant is in open loop. Similarly, the basic idea in [2] and Paper I was to attempt the same identification while the plant was operating in closed loop using PMU measurements. This would make it possible for TSOs to directly check the new requirements using PMU measurements. However, as pointed out in Paper V it is not possible to identify $G_p(s)$ by doing this. Still, there is some merit to the approach as the identified transfer function will follow $G_p(s)$ for the slowest dynamics.

Although the approach described in this paper cannot identify the full dynamics of $G_p(s)$, it did contribute to answering the first research question. In the paper several datasets with different time lengths were tested and for all of them one it was possible to obtain a transfer function resembling the slow dynamics of a governor. Furthermore, the obtained models performed very well when cross validated against other datasets. An example of this is depicted in Figure 4.2 where a dataset obtained using data from spring is cross validated against a dataset obtained during fall. This gave us clear indications that it was worth further investigating what could be obtained using PMU data.

For the paper an open source version of time domain vector fitting was developed, which can be downloaded here [36]. The paper itself [5] was presented at the conference Powertech 2017.

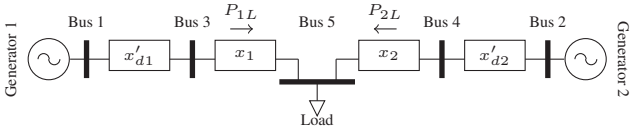


**Figure 4.3:** Single line diagram of the simple test system

To summarise the main contributions of this paper are:

- To test the idea from [2] on more datasets (dataset 1-19).
- The development of an open source toolbox for time domain vector fitting

## 4.2 Development of a simple test system Paper II

To further investigate whether or not PMUs could be used to check parts of the new requirements I entered into cooperation with my co-supervisor Xavier Bombois. To explain the system identification problem involving power system components to an expert from another domain, a simple test system was developed. The single line diagram of the test system is depicted in Figure 4.3. It consisted of two generators, a load and the lines connecting them. The power plants were modelled using the swing equation, their synchronous reactances, a linear turbine model and a governor. The power plant at bus 1 is the power plant where we wanted to perform the identification and the other power plant is an aggregated power plant representing a strong grid. To model random switching events and load changes in the power system an aggregated load was used. The power flow on the lines was modelled using a dc power flow. The rationale behind this is that the voltage dynamics are not important for explaining the underlying dynamics of the FCR. By combining these three power system components we could capture the main dynamics relevant for identification of FCR dynamics.

The work was presented in a paper [6] at MATHMOD 2018. In the presented paper the focus was on the modelling of the power plant and load and how to connect these elements together to obtain a test system relevant for analysing the identifiability of hydro power plant dynamics. This test system was used for conducting simple simulations in the papers III, VI and V. However, the linear turbine model was replaced with the nonlinear model, presented in Chapter 2, in the two last papers. The test system was also used for developing some of the transfer functions used for the analytical analysis of the identification problem presented in Paper III.

Although the paper did not directly contribute to answering any of the research questions, the developed test network was heavily used in the preceding papers.

Moreover, the simple derivations presented in the paper can be useful for power system engineers who want to understand the modelling choices and assumptions in the preceding papers. To summarise the main contribution of this paper is:

- The development of a simple test system capturing the main dynamics relevant for FCR, which could be used in the following papers.

## 4.3 Theoretical validation of the PMU approach Paper III

In Paper III it was decided to look further into what could possibly be identified using PMU measurements. To achieve this the test system developed in Paper II was used to show that when the plant is operating in closed loop the transfer function from the electrical power to the electrical rotor speed of the machine is in fact the disturbance rejection function $G_1(s)$. This means that it is not possible to identify $G_p(s)$ using PMU measurements as was attempted in Paper I. This fact is further investigated in Paper V. However, since the paper shows that the TSOs can identify $G_1(s)$ using PMU measurements, it means that parts of the requirements can actually be checked online using PMUs.

In addition to present which transfer function can actually be identified using PMU measurements, the paper also looks into the conditions for ensuring a consistent estimate. To do this the following was assumed:

**Assumption A1** *The frequency measured by the PMU is a good estimate of the electrical angular speed of the machine's rotor if the PMU is sufficiently close to the generator.*

**Assumption A2** *The random load changes in the power system can be modelled as filtered white noise and are uncorrelated to any process noise at the power plant*

**Assumption A3** *The measurement noise of the PMU is negligible.*

If the above assumptions hold it was shown that a consistent estimate of $G_1(s)$ can be obtained if the following condition holds

**Condition C1** *There is a delay in either the swing equation or the transfer function from the electrical angle of the generator to the electrical power at the bus bar of the power plant.*

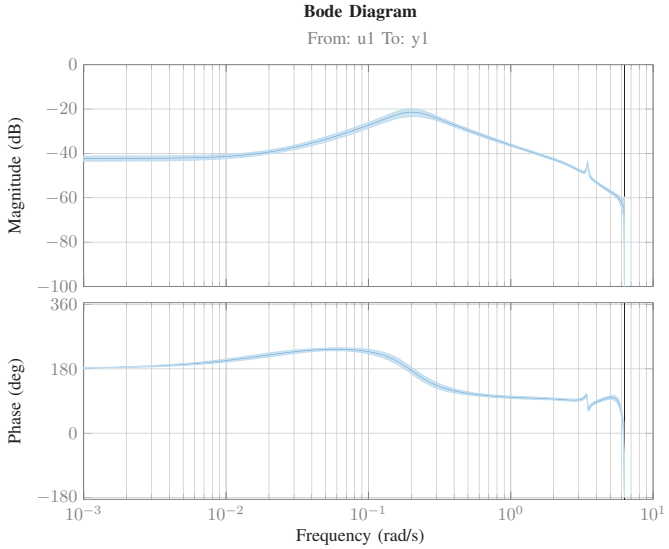


**Figure 4.4:** Identification of $G_1(s)$ on dataset 20

In this paper it was assumed that Condition C1 holds. However, as pointed out in Paper VI this, may not be the case. The results were demonstrated using the test system developed in Paper II and dataset 20. In Figure 4.4 the transfer function obtained using dataset 20 is presented.

To summarise the main contributions of this paper are:

- To show that the transfer function that can be identified using PMU measurements is $G_1(s)$ and not $G_p(s)$
- To show that the TSOs can check parts of the requirements using PMU measurements
- To present under which conditions this transfer function can be identified

## 4.4 Comparison of a PMU-based approach and the draft requirements approach using tests from two of Statkraft's power plants Paper IV

In Paper III it was demonstrated that it is possible to obtain the disturbance rejection function $G_1(s)$ using PMU measurements, given some assumptions and conditions. In Paper IV it is demonstrated that it is possible to use these measurements to obtain an estimate of the sensitivity function $S(s)$. Or, in other words, it

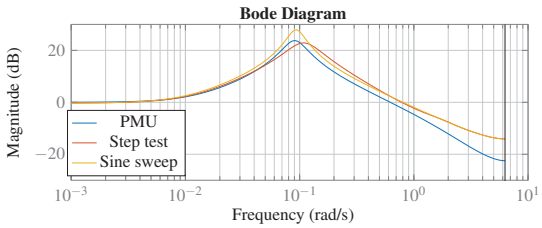


**Figure 4.5:** Comparison of estimate of $G_1(s)$ obtained using my approach and the one proposed in [4]

shows how $S(s)$ can be approximated from an estimate of $G_1(s)$. The method is compared with the draft requirements using results from a power plant owned by Statkraft. Results from another power plant are used to test whether or not $G_1(s)$ obtained using measurements of electrical power and power system frequency can capture governor parameter changes, and whether or not the static gain of obtained estimate of $G_1(s)$ is reasonable.

The first power plant is suitable for a comparison between the PMU approach and the draft requirement approach. The reason for this is that Statkraft already had performed tests according to the new draft requirements, which they were willing to share with me. In addition I was provided PMU measurements from the high voltage side of the plant's step-up transformer. This enabled me to compare the results obtained using my approach and the draft requirements. There are, however, two aspects that reduces the value of the comparison: the first being that the measurements were taken at different dates, the second being that Statkraft's measurements were from one generator and the PMU measurements capture the effect of four generators. However, since the four machines were very similar and the results were presented in per unit, the results should not differ to any great extent. The comparison is most easily visualised on the estimate of $G_1(s)$. An example of this is presented in Figure 4.5. Here it can be seen that the transfer functions follow each other quite well for slow dynamics and start to differ for faster dynamics. It is, however, quite reasonable that the results differ for faster dynamics. These dynamics are determined by the inertia constant of the machine, and since my approach uses an estimate of the inertia constant of the machine and [4] uses an estimate of the total system inertia, we cannot expect the same results for these dynamics.

In the draft requirements they calculate the phase and amplitude of the transfer function they identify at 10 frequencies, which corresponds to those used to excite the plant. Paper IV demonstrates that the same transfer function can be obtained at all frequencies up to the Nyquist frequency using only one dataset. An example of

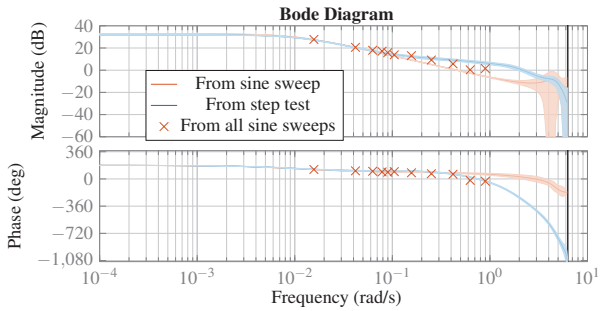


**Figure 4.6:** Comparision of estimating $G_p(s)$ using the Fourier transform and ten sine sweeps and estimating $G_p(s)$ using one dataset and prediction error identification.

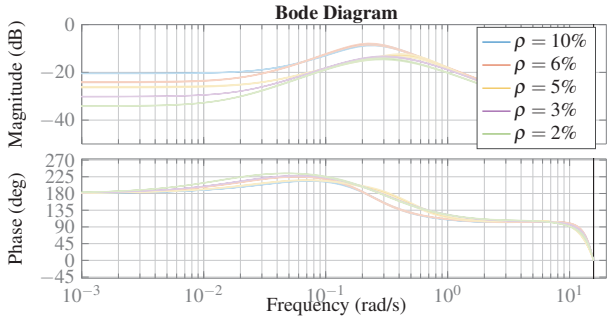


**Figure 4.7:** Identification of $G_1(s)$ with different governor settings.

this is depicted in Figure 4.6 where we can see the identification using the approach proposed in the new draft requirements and the identification using prediction error identification and either a sine or step test. This means that it is possible to greatly simplify the identification procedure even if we are using the proposal from the draft requirements.

At the second power plant only measurements from the plant's control system were used. However, unlike the draft requirements no extra excitation was added to the plant and it was operating in closed loop. During the test the electric power and power system frequency were collected from the control system of the plant. This makes this comparable to having a PMU as close as possible to the generator. During the tests the power plant was run with different droop settings and control system parameters. The identification approach successfully captured all changes and the droop estimated from the identified transfer functions corresponded well with the actual droop settings, as can be seen in Figure 4.7. Different lengths of the datasets were also tested and good results were obtained with dataset lengths as short as $15min$.

To summarise the main contributions of this paper are:

- Presentation of a method for checking the requirements using only PMU measurements.
- Comparison of the draft requirements and PMU approach on a power plant.
- Demonstrates that only one dataset is needed to check the draft requirements instead of ten.
- Checking if an approach where electrical power and power system frequency is measured can estimate the droop settings and detect governor parameter changes.

## 4.5 An extension of Paper IV, with more discussions, simulation comparisons and more simulation validations Paper V

This paper builds on the previous paper, in the sense that it compares the PMU approach and the approach in the draft requirements. However, as will be outlined below it adds several other contributions.

The paper demonstrates the fact that previous papers [2], [5] assume the opposite causality with respect to the input and output of the system compared to the approach in this thesis. It is argued through physical reasoning that the approach in this thesis is the correct one. Moreover, Monte Carlo Simulations (MCS)s are used to demonstrate that the approach in this thesis is the correct one.

Another aspect that may influence the identification is whether or not the hydro power plant is operated using power system frequency as the feedback to the governor or the electrical angular speed of the rotor. In a previous paper assumptions A1 assumes these signals to be equal. This assumption is tested using MCS and the simple test system developed in Paper II where it can be seen that there is no difference for slow dynamics and that there will be some difference for the faster dynamics. Assumption A1 is also tested using MCS and the simulation software PSS/E. It is shown that when using the power system frequency instead of the electrical angular speed of the rotor in the identification that the slope of $G_1(s)$ will be incorrect as can be seen in Figure 4.8. However, the rest of the transfer function is still estimated correctly well within the frequency range investigated in the new draft requirements. This result should not be very surprising since the angular velocity of the rotor of synchronous machines should be the same for slow dynamics. Otherwise, they would not be synchronous.

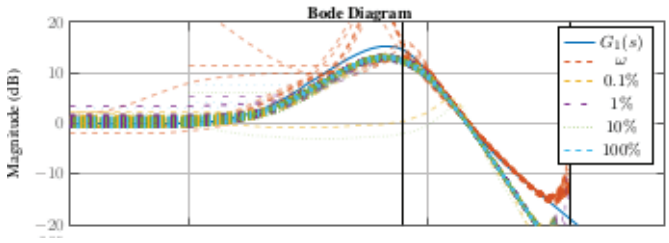


**Figure 4.8:** Identification of $G_1(s)$ using the electrical angular speed of the rotor, and the power system frequency measured at different distances from the machine

The effect of deadband on the input to the governor and backlash on the servo on the identification is also investigated. As can be expected a large deadband or backlash will result in no identification. However, as long as the deadband and backlash is reasonably small the identification should still be possible.

To summarise the main contributions of this paper not included in IV are:

- A clarification of the difference between identifying from the electrical power to the frequency instead of vice versa
- An analysis of the importance of the type of governor feedback
- A test of Assumption A1 using MCS and PSS/E
- A test of the importance of nonlinearities such as the deadband and backlash using MCS

## 4.6 Checking the requirements using measurements from the control system of a hydro power plant Paper VI

After having analysed what can be done in terms of checking the requirements using a PMU a natural next step is to move on to control system measurements and the possibility to add external excitation. This is an approach closer to what is proposed in the new draft requirements; however, in this paper the plant is operating in closed loop.

In the paper it was proven under which conditions a consistent estimate of $G_1(s)$ and $S(s)$ can be identified if extra excitation is added. It is also proven under which conditions an estimate of $G_J(s)$ and $G_p(s)$ can be estimated if extra excitation is added. To estimate $G_J(s)$ and $G_p(s)$ it was also necessary to estimate a model of the servo $G_s(s)$. It was therefore also proven under which conditions it is possible to obtain a consistent estimate of $G_s(s)$ as well.

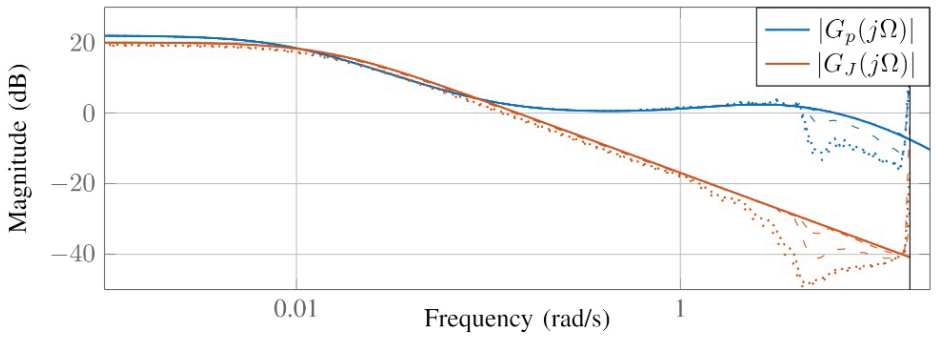


**Figure 4.9:** The mean value of $|G_p(e^{j\Omega}, \hat{\theta}_N)|$ and $|G_J(e^{j\Omega}, \hat{\theta}_N)|$ calculated from the MCS. The solid lines are the analytical calculated versions and the dashed, loosely dashed, dotted, and loosely dotted lines represent an SNR of $50dB$, $26dB$, $6dB$, and $3dB$ respectively

The same delay condition as in Paper III is still used in the proofs for the consistency. However, unlike the previous paper it is pointed out that due to the physics of the power system this delay condition will generally not hold. It is argued that the bias introduced by the lack of the delay can be expected to be small. This is also demonstrated using MCS. Another important point is that the bias introduced by the delay will be smaller when extra excitation is added. An example of the effect of the lack of the delay condition is presented in Figure 4.9. In the figure the process noise at the plant, which may create biased results if the delay condition does not hold has been varied. The relation between the useful excitation of the plant and the process noise is expressed as the signal to noise ratio (SNR). From the figure it can be seen that quite good results are obtained for quite low SNRs. Moreover, the bias first occurs for the faster dynamics.

When estimating the transfer functions MISO identification is used, except for the servo and the disturbance rejection function. One important point to keep in mind when doing MISO identification is that the system identification toolbox has trouble initialising the identification properly if a box-Jenkins model structure is used. It was therefore chosen to use an ARX model structure, which does not involve a problem with the initialisation. The drawback with using the ARX model structure is that a high order model has to be chosen to prevent bias from the choice of the model structures, this will lead to higher variance.

The results from the power plant where control system measurements were used were also included in this paper.

To summarise the main contributions of this paper are:

- An approach for identifying $G_1(s)$ and $S(s)$ directly while the plant is operating in closed loop
- An approach for identifying $G_p(s)$ and $G_J(s)$ and $G_s(s)$ while the plant is operating in closed loop
- A more correct discussion of the delay condition presented in Paper III
- It was shown that there may be introduced a bias in the estimate due to the lack of delay, however, it will likely be small
- Adding excitation reduces the bias

## 4.7 Some aspects not discussed in the papers

Notice that the new requirements do not say anything about the loop made up of $G_J(s)K_{11}/s$. Moreover, the true disturbance to the plant is $v_l(s)$ since $\Delta P_e(s)$ is made up of both $v_l(s)$ and a contribution from the plant itself. However, the stability of this loop is influenced by the excitation and voltage controller of the power plant as well as any potential power system stabiliser. These control systems operate at faster timescales than the FCR and we will therefore not analyse the stability of this loop in this work. However, this is something that could be interesting to analyse in future works.

One important thing to keep in mind is that the papers assume that there is no significant backlash in the servo of the plant. This is normally the case if the turbine is a Pelton turbine or a low pressure Francis turbine. In the case of high pressure Francis or a Kaplan turbine there may be a significant backlash. In these cases it is not possible to achieve good results, as pointed out in Paper V. However, if one uses the approach presented in Paper VI it may, for instance, be possible to manage the backlash in a similar manner as that proposed in [21].

# Chapter 5

# Conclusions and recommendations for further work

## 5.1 Conclusions

To move in the direction of writing the requirements for hydro power plants in the frequency domain is a promising idea. However, it should be a goal to do this in a way which is as gentle as possible with regards to the economic losses of the power plant owner as well as the mechanical strain on the plant. In this work it has been investigated whether or not the requirements of a hydro power plant in the frequency domain can be checked while the plant is in normal operation. The investigation not only included the development of three novel methods, but also the analysis of whether or not these methods would give consistent results.

For normal operation, that is, in closed loop operation without added external excitation, it is possible to identify the disturbance rejection function $G_1(s)$ with measurements of the plant's electrical power output and angular speed of the rotor. These are measurements that are often available from the power plant's control system. However, using these measurements it is not possible to guarantee a consistent estimate, due to the lack of the delay mentioned in Condition C1. In practice, the introduced bias can be expected to be small as long as the external excitation to the plant is large compared to the plant noise. Furthermore, using these measurements it is possible to find an approximate estimate of the plant's inertia

and the plant's sensitivity function $S(s)$. In case access to the control system of the plant is unavailable it is still possible to obtain these transfer functions using measurements from a PMU, if it is located sufficiently close to the plant. However, when using the power system frequency measurement instead of the angular speed of the rotor the identified transfer function will be biased for faster dynamics.

If external excitation is added to the power plant it is possible to identify both the sensitivity function and the disturbance rejection function directly. This only requires access to typical control system measurements. The other advantage of adding extra excitation is reduced bias due to the lack of the delay. It is also possible to identify the swing dynamics and FCR dynamics of the plant separately with access to control system measurements and added extra excitation. In both cases it is sufficient to record only one dataset. This is in contrast to what has been suggested in the new draft requirements where they recommend several datasets per identification. Another important observation is that, even with the setup proposed in the new requirements, only one dataset is needed, if prediction error identification is used.

The answers to the main research questions outlined in the introduction serve to summarise the conclusions:

- **Can the requirements be checked using PMU measurements?** Yes, they can, but the estimate will be biased, especially for faster dynamics. The reason for this is twofold. Most importantly, the power system frequency and the angular speed of the rotor may differ for faster dynamics. Secondly, there is a delay condition that most likely is not fulfilled. However, the bias due to the lack of this delay condition is expected to be small.
- **Can the requirements be checked using control system measurements, while the plant is in normal operation?** Yes, but the estimate will be biased. However, it will be less biased than when using PMU measurements. The reason for this is that we can normally expect the measurements obtained closer to the plant to be better for the identification. Moreover, if we have access to measurements of the electrical angular speed of the rotor, the only bias will be due to the lack of the delay condition.
- **Can the requirements be checked using control system measurements and added excitation?** Yes, and the bias will be negligible. This is because when we control the excitation, we are able to make the signal to noise ratio sufficiently high. This is decisive for the identification.

The conclusions are based on prediction error identification. It is still an open

research question if other methods will yield the same conclusions.

## 5.2 Future work

A possible direction for future work may involve an investigation of what type of plants the proposed methods works for. In this work it is assumed that the servo controlling the water flow in the plant does not have any backlash. This should normally be true for pelton turbines and low pressure kaplan turbines. For plants where the servo has a significant backlash it is necessary to determine what the best way to check the requirements is.

More tests on actual power plants should also be performed. Most importantly the difference between using the power system frequency to the electrical angular speed of the rotor should be investigated. Moreover, it should be verified that the measurements of the electrical angular speed are of good enough quality. Empirical results on the different noises that may be detrimental to the results should also be obtained. In particular, measurement noise and process noise may introduce a bias in the estimate. In this work some simulation comparisons were performed, but the only way to determine whether or not this noise will be a problem is to conduct tests on real plants. One possible approach for mitigating the bias introduced by the process noise could be to perform the identification from the voltage angle of the generator bus bar instead of the electrical power. However, this still remains to be investigated.

Finally, as demonstrated, in many cases external excitation should be added for the identification. In this work it was only tested with white noise. It should be investigated what signal will give the desired accuracy while keeping the disturbance of the plant to a minimum.

# Bibliography


[1] L. Saarinen, P. Norrlund, U. Lundin, E. Agneholm and A. Westberg, "Full-scale test and modelling of the frequency control dynamics of the nordic power system", in *2016 IEEE Power and Energy Society General Meeting (PESGM)*, Jul. 2016, pp. 1–5. DOI: 10.1109/PESGM.2016.7741711.

[2] Dinh Thuc Duong, Kjetil Uhlen, Stig Løvlund and Erik Alexander Jansson, "Estimation of hydro turbine-governor's transfer function from PMU measurements", presented at the IEEE PES General Meeting, Boston: IEEE, Jul. 2016.

[3] Statnett, Fingrid, E. dk and S. Kraftnät, "Challenges and opportunities for the nordic power system", 15th Aug. 2016.

[4] P. W. Group, "Technical requirements for frequency containment reserve provision in the nordic synchronous area", Draft, 26th Jun. 2017.

[5] S. H. Jakobsen and K. Uhlen, "Vector fitting for estimation of turbine governing system parameters", in *2017 IEEE Manchester PowerTech*, Jun. 2017, pp. 1–6. DOI: 10.1109/PTC.2017.7980855.

[6] S. H. Jakobsen and K. Uhlen, "Development of a test system for identification of turbine dynamics using the dc power flow", *IFAC-PapersOnLine*, 9th Vienna International Conference on Mathematical Modelling, vol. 51, no. 2, pp. 97–102, 1st Jan. 2018, ISSN: 2405-8963. DOI: 10.1016/j.ifacol.2018.03.017. [Online]. Available: http://www.sciencedirect.com/science/article/pii/S240589631830017X (visited on 15/05/2019).

[7] S. H. Jakobsen, K. Uhlen and X. Bombois, "Identification of hydro turbine governors using PMU data", in *2018 IEEE International Conference on Probabilistic Methods Applied to Power Systems (PMAPS)*, Jun. 2018, pp. 1–6. DOI: 10.1109/PMAPS.2018.8440273.

[8] S. H. Jakobsen, K. Uhlen and P. Lie, "System identification techniques for validating hydro power plant's FCR performance", presented at the Cigre symposium, Aalborg: Cigre, Jun. 2019.

[9] S. H. Jakobsen and K. Uhlen, "Testing of a hydro power plant's stability and performance using PMU data", *IET Generation, Transmission & Distribution (submitted)*, 2019.

[10] S. H. Jakobsen, X. Bombois and K. Uhlen, "Checking hydro power plants' FCR performance using system identification in closed loop", *IEEE Transactions on Power Systems (submitted)*, 2019.

[11] L. Vanfretti, S. H. Olsen, V. S. N. Arava, G. Laera, A. Bidadfar, T. Rabuzin, S. H. Jakobsen, J. Lavenius, M. Baudette and F. J. Gómez-López, "An open data repository and a data processing software toolset of an equivalent nordic grid model matched to historical electricity market data", *Data in Brief*, vol. 11, pp. 349–357, Apr. 2017, ISSN: 2352-3409. DOI: 10.1016/j.dib.2017.02.021. (visited on 13/06/2017).

[12] S. H. Jakobsen, E. H. Solvang and L. Kalemba, "The nordic 44 test network", *figshare*, 13th Dec. 2018. DOI: 10.6084/m9.figshare.7464386.v1.

[13] S. H. Jakobsen and K. Uhlen, "An alternative derivation of the frequency divider formula using the dc power flow", *figshare*, 19th Dec. 2018. DOI: 10.6084/m9.figshare.7484489.v1.

[14] I. B. Sperstad, G. H. Kjølle, T. K. Vrana, S. H. Jakobsen, J. Turunen and L. Haarla, "Vulnerability analysis of HVDC contingencies in the nordic power system", presented at the Cigre Session, Aug. 2018.

[15] E. H. Solvang, I. B. Sperstad, S. H. Jakobsen and K. Uhlen, "Dynamic simulation of simultaneous HVDC contingencies relevant for vulnerability assessment of the nordic power system", presented at the Powertech, Milano, 2019.

[16] J. Machowski, J. W. Bialek and J. R. Bumby, *Power System Dynamics : Stability and Control*. Chichester, U.K.: Wiley, 2008, vol. 2nd ed, ISBN: 978-0-470-72558-0. (visited on 28/06/2017).

[17] P. Kundur, N. J. Balu and M. G. Lauby, *Power system stability and control*. McGraw-hill New York, 1994, vol. 7. (visited on 16/12/2015).

[18] ENTSO-E, "Commission regulation (EU) 2017/1485 of 2 august 2017 establishing a guideline on electricity transmission system operation (text with EEA relevance. )", 2nd Aug. 2017.

[19] F. M. White, *Fluid mechanics*, 6th ed. 2008.

[20] Working Group on Prime Mover and Energy Supply Models for System Dynamic Performance Studies, "Hydraulic turbine and turbine control models for system dynamic studies", *IEEE Transactions on Power Systems*, vol. 7, no. 1, pp. 167–179, Feb. 1992, ISSN: 0885-8950. DOI: 10.1109/59.141700.

[21] L. Saarinen, P. Norrlund and U. Lundin, "Field measurements and system identification of three frequency controlling hydropower plants", *IEEE Transactions on Energy Conversion*, vol. 30, no. 3, pp. 1061–1068, Sep. 2015, ISSN: 0885-8969. DOI: 10.1109/TEC.2015.2425915.

[22] E. Commission. (14th Apr. 2016). Network code on requirements for grid connection applicable to all generators, [Online]. Available: http://eur-lex.europa.eu/legal-content/EN/TXT/HTML/?uri=CELEX:32016R0631&from=EN (visited on 01/09/2016).

[23] S. Skogestad and I. Postlethwaite, *Multivariable feedback control: analysis and design*. Wiley New York, 2007, vol. 2.

[24] D. I. Jones, S. P. Mansoor, F. C. Aris, G. R. Jones, D. A. Bradley and D. J. King, "A standard method for specifying the response of hydroelectric plant in frequency-control mode", *Electric Power Systems Research*, vol. 68, no. 1, pp. 19–32, 1st Jan. 2004, ISSN: 0378-7796. DOI: 10.1016/S0378-7796(03)00152-4. [Online]. Available: http://www.sciencedirect.com/science/article/pii/S0378779603001524.

[25] R. Eriksson, N. Modig and A. Westberg, "FCR-n DESIGN OF REQUIREMENTS", ENTSO-E report, 4th Jul. 2017. [Online]. Available: https://www.statnett.no/for-aktorer-i-kraftbransjen/utvikling-av-kraftsystemet/prosjekter-og-tiltak/nordisk-frekvensstabilitet

[26] M. Kuivaniemi, N. Modig and R. Eriksson, "FCR-d design of requirements", Jul. 2017. [Online]. Available: https://www.statnett.no/for-aktorer-i-kraftbransjen/utvikling-av-kraftsystemet/prosjekter-og-tiltak/nordisk-frekvensstabilitet/.

[27] L. Ljung, *System identification*. Springer, 1998. (visited on 29/03/2016).

[28] L. N. Hannett, J. W. Feltes and B. Fardanesh, "Field tests to validate hydro turbine-governor model structure and parameters", *IEEE Transactions on Power Systems*, vol. 9, no. 4, pp. 1744–1751, Nov. 1994, ISSN: 0885-8950. DOI: 10.1109/59.331426.

[29] D. Kosterev, "Hydro turbine-governor model validation in pacific northwest", *IEEE Transactions on Power Systems*, vol. 19, no. 2, pp. 1144–1149, May 2004, ISSN: 0885-8950. DOI: 10.1109/TPWRS.2003.821464.

[30] H. Aghamolki, Z. Miao, L. Fan, W. Jiang and D. Manjure, "Identification of synchronous generator model with frequency control using unscented kalman filter", *Electric Power Systems Research*, vol. 126, pp. 45–55, 2015, ISSN: 0378-7796. DOI: 10.1016/j.epsr.2015.04.016.

[31] N. D. Hatziargyriou, E. S. Karapidakis, G. S. Stavrakakis, I. F. Dimopoulos and K. Kalaitzakis, "Identification of synchronous machine parameters using constrained optimization", in *Power Tech Proceedings, 2001 IEEE Porto*, vol. 4, 2001, 5 pp. vol.4–-. DOI: 10.1109/PTC.2001.964812.

[32] J. C. N. Pantoja, A. Olarte and H. Díaz, "Simultaneous estimation of exciter, governor and synchronous generator parameters using phasor measurements", in *2014 Electric Power Quality and Supply Reliability Conference (PQ)*, Jun. 2014, pp. 43–49. DOI: 10.1109/PQ.2014.6866781.

[33] G. W. Bryce, P. W. Agnew, T. R. Foord, D. J. Winning and A. G. Marshal, "On-site investigation of electrohydraulic governors for water turbines", *Proceedings of the Institution of Electrical Engineers*, vol. 124, no. 2, pp. 147–153, Feb. 1977, ISSN: 0020-3270. DOI: 10.1049/piee.1977.0026.

[34] B. Mogharbel, L. Fan and Z. Miao, "Least squares estimation-based synchronous generator parameter estimation using PMU data", in *2015 IEEE Power Energy Society General Meeting*, Jul. 2015, pp. 1–5. DOI: 10.1109/PESGM.2015.7286559.

[35] Mathworks. (2018). System identification toolbox, [Online]. Available: https://se.mathworks.com/products/sysid.html (visited on 03/12/2018).

[36] (). Hofsmo/vectorFitting, GitHub, [Online]. Available: https://github.com/Hofsmo/vectorFitting (visited on 21/04/2016).

# Papers

# Paper I

# Vector fitting for estimation of turbine governing system parameters

# Vector fitting for estimation of turbine governing system parameters

Sigurd Hofsmo Jakobsen, Kjetil Uhlen
Department of Electric Power Engineering
Norwegian University of Science and Technology
Trondheim, Norway
sigurd.h.jakobsen@ntnu.no

***Abstract*—With the introduction of more and more renewables into the power system both the inertia and the primary frequency reserves are expected to decrease. It is therefore a growing concern that the frequency quality will deteriorate. One way of mitigating these problems may be a more detailed monitoring of the generators providing the primary reserves.**

**A promising approach for monitoring the generators is to identify turbine governing system parameters using system identification. This will allow for estimating the droop and the bandwidth of the governor, parameters that are important for the primary control. Furthermore, if this can be reliably done on ambient data, updated estimates of these parameters can be obtained relatively fast.**

**In this paper we will look into how vector fitting can be used for this purpose. The algorithm possesses some interesting properties for automatically constructing models from ambient data. How this can be done will be presented together with results obtained using real data from the Norwegian power system. A simple criterion for reducing the obtained model order is also proposed.**

***Keywords*—Turbine governors, PMUs, ambient data, system identification, time domain, vector fitting**

## I. Hydro governor parameter estimation using vector fitting

The introduction of more and more renewables into the power system has lead to a concern for the system's frequency, since these units often do not provide inertia or the ability to provide frequency containment reserves (FCR). To mitigate these problems for continental Europe one proposal is to use hydro power plants in the Nordic, as providers of FCR thorough interconnectors. For the Nordic countries this is both an opportunity and a challenge as their systems will have to both handle their own intermittent production and large shifts in power flows on interconnectors to continental Europe. These challenges are well understood by the Nordic transmission system operators (TSOs) and are thoroughly covered in their challenges and opportunities report [1].

In this paper we will investigate the possibility to use phasor measurement units (PMUs) to monitor the FCR. One advantage of this approach is that TSOs can use their own equipment to monitor generators, which are important power system equipment not owned by the generators. Furthermore, we propose to use ambient PMU data to not disturb the operation of the power plant. This will serve as a supplement to the required data exchange between generators and TSOs and can also be used on generators not covered by the grid code on requirement for grid connection of generators (RfG)[2].

System identification techniques have previously been applied to real system data in papers such as [3]–[5]. The authors of [5] use constrained optimization on disturbance data from the Crete power system and the authors of [4] apply an unscented Kalman filter to the measurements from a trip event in the Midcontinent Independent System. Common for these papers is the use of data from disturbances. For the purpose of model validation this is sufficient, however, for a more continuous monitoring one would need to use data from normal system operation. An example on how this can be achieved is presented in [3] where an auto regressive exogenous (ARX) model structure is applied to recordings from normal system operation in the Norwegian grid.

One disadvantage of the ARX model structure is that one needs to select an appropriate model order to get a good fit. For the purpose of performing a continuous monitoring it would be an advantage if less tuning was needed. One method that may have these properties is time domain vector fitting [6]. Therefore, we will in this paper present how this method can be applied to estimate model of turbine governors. Furthermore, we will show that the method does indeed possess interesting properties for online applications, due to its performance with respect to speed, accuracy and the amount of tuning needed.

Time domain vector fitting is presented in section II and the code used is available at [7]. Hydro governors are discussed in section III and the results are presented and discussed in section IV. The final section covers the conclusion regarding the methods performance and how it should be tuned.

## II. Time domain vector fitting

Vector fitting was introduced for the frequency domain in [8] and later extended to the time domain in [6]. It is an iterative algorithm where each step start with a set of starting poles that are updated at the end of the step until convergence is reached.

### A. The algorithm

In the vector fitting algorithm it is assumed that the transfer function of the system can be expressed using the rational transfer function:

$$H(s) = d + \sum_{i=1}^{n_p} \frac{r_i}{s - p_i} \tag{1}$$

In (1) the unknowns to be estimated are $d$, $r_i$ and $p_i$. Since some of the unknowns are situated in the denominator the problem is not linear. To make the problem linear it is multiplied by an unknown scaling function $\sigma(s)$ with known poles $\tilde{p}_i$ defined such that:

$$\sigma(s)H(s) = d + \sum_{i=1}^{n_p} \frac{r_i}{s - \tilde{p_i}} \tag{2}$$

It can be proven that the zeros of $\sigma(s)$ will be equal to the poles of (1) [9]. $\sigma(s)$ is unknown, hence the following approximation for $\sigma(s)$ given in [8] is introduced as:

$$\sigma(s) \approx 1 + \sum_{i=1}^{n_p} \frac{k_i}{s - \tilde{p_i}} = \frac{\prod_{i=1}^{n_z}(1 - \tilde{z_i})}{\prod_{i=1}^{n_p}(1 - \tilde{p_i})} \tag{3}$$

Notice that if the zeros $\tilde{z}_i$ of (3) equal the starting poles $\tilde{p}_i$ (3), the weighted problem (2) equals the original problem (1). This implies that if the correct poles of the system is identified, $k_i$ equals zero.

Vector fitting in the time domain can now be obtained by multiplying (2) by the input signal $u(t)$ and performing laplace inverse.

$$y(t) \approx \tilde{d}x(t) + \sum_{i=1}^{n_p} \tilde{r}_i x_i - \sum_{i=1}^{n_p} \tilde{k}_i y_i \tag{4}$$

Notice that the unknowns in (4) are denoted with a ˜ to mark that these are recalculated every iteration. The waveforms $x_i(t)$ and $y_i(t)$ are obtained from the following convolution integrals:

$$x_i = \int_0^t e^{\tilde{p}_i(t-\tau)} x_i(\tau) d\tau \tag{5}$$

$$y_i = \int_0^t e^{\tilde{p}_i(t-\tau)} y_i(\tau) d\tau \tag{6}$$

These integrals can be solved using an IIR filter [6].

$$x_i[k] = \alpha_i x_i[k-1] + \beta x[k] + \beta x[k-1] \tag{7}$$

In (7) we use the coefficients defined in [10], which implements the trapezoidal method for numerical integration.

$$\alpha = \frac{1 + \tilde{p}_i \frac{\Delta t}{2}}{1 - \tilde{p}_i \frac{\Delta t}{2}}, \beta = \frac{\Delta t}{2 - \tilde{p}_i \Delta t} \tag{8}$$

where $\Delta t$ is the sampling time.

The unknowns of (4) are now obtained using least square fitting. Then the updated poles to be used in the next iteration of the vector fitting is obtained as the zeros of (3).

### B. Starting poles for vector fitting

Unlike the (autoregressive moving average exogenous) ARMAX type model structures, vector fitting does not require one to find an appropriate model order for the system. One only needs to define a set of starting poles, which should be given according to the rule of thumbs described in [8] that is the starting poles should be:

- Linearly or logarithmically spaced
- Real or complex conjugate

Real poles should only be used to fit smooth functions, whereas complex conjugate poles should be chosen in the general case. Furthermore, for complex conjugate starting poles the real part should be $1/100$ of the complex part.

When it comes to the order of the model [8] states that the starting poles that converge towards poles that are not in the system one tries to fit will have low values of the corresponding residues. This fact is used to make an automatic order reduction procedure. The procedure is inspired by the following convergence criterion from [9]:

$$\|\frac{\tilde{k}_1}{\tilde{p}_1}, \cdots, \frac{\tilde{k}_{n_p}}{\tilde{p}_{n_p}}\| < \epsilon \tag{9}$$

which states that the vector norm of the normalized residues of $\sigma(s)$ should be below a certain tolerance limit $\epsilon$. A similar criterion can also be stated for the residues of the function we are fitting, that is:

$$|\frac{r_i}{p_i}, | < \epsilon, i \in n_p \tag{10}$$

where the normalized residue below the tolerance limit $\epsilon$ are discarded. Other model reduction schemes have been proposed in [11] where single value decomposition (SVD) and balanced realization model is compared.

### C. Indicator for goodness of fit

Various indicators exist for measuring the goodness of fit when performing system identification. Typically theses indicators try to give an indication on which model performs best with respect to both ability to predict and complexity. In this paper, however, we will use the simple indicator normalised root mean square error (NRMSE) as defined in (11) from [12].

$$\text{NRMSE} = 100(1 - \frac{||y - \hat{y}||}{||y - \bar{y}||}) \tag{11}$$

where $y$ is the measured response and $\hat{y}$ is the estimated response. The reason is that it is intuitively easy to understand. Furthermore, as will be shown later, vector fitting normally provides low order models meaning that the penalty term for higher order models, included in most other indicators, becomes less relevant. For an introduction to indicators on goodness of fit please refer to a standard text book in system identification such as [13].

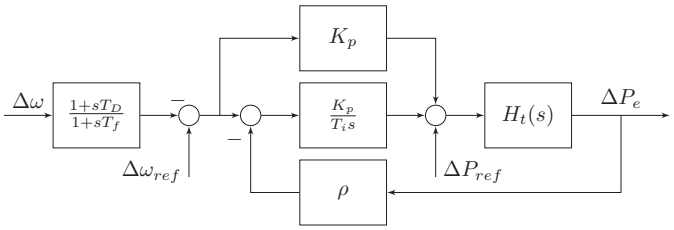


Fig. 1: PID hydro turbine governor

TABLE I: Hydro turbine governor parameters

| Variable | Explanation | Approximate value |
|---|---|---|
| $T_D$ | Derivative time | $1-2s$ |
| $T_f$ | Low pass filter time constant | $0.2s$ |
| $K_p$ | Controller gain | $1-3$ |
| $T_i$ | Integral time | $2-10s$ |
| $\rho$ | Droop | $0.04-0.12$ |

## III. Hydro turbine governors

Since the Norwegian system is dominated by hydro units our study will only consider hydro units. Therefore, a few basic properties of hydro governors useful for understanding identification of these will be briefly covered.

### A. Transfer function of hydro turbine governors

In Fig. 1 a simple block system representation of a governor and a turbine is depicted. The turbine and generator are represented by the transfer function $H_t(s)$, and their dynamics are assumed to be negligible in the frequency range under study. Unlike [14] the derivative action of the governor is moved before the frequency reference to prevent changes in the frequency reference to influence the derivative. The parameters in the model are presented in Table I.

As explained in section II the vector fitting algorithm requires a set of starting poles. To get an indication on what range to choose from, the transfer function of the governor can be analyzed.

$$H = -K_p \frac{1+sT_D}{1+sT_f} \cdot \frac{1+sT_i}{\rho K_p + sT_i} \tag{12}$$

From (12) one can see that the system's poles will be placed at:

$$p_1 = -\frac{1}{T_f},\ p_2 = -\frac{\rho K_p}{T_i} \tag{13}$$

This means that it is possible to get purely real poles or one complex conjugate pair. Using the parameter values from Table I one can see that the maximum range of the poles will be $5Hz$ and $0.18Hz$.

### B. Potential problems when performing the fitting

In our approach we will try to identify the transfer function of the governor by measuring the frequency and the power at a generator busbar. As can be seen from Fig. 1 the results may be influenced by changes in the frequency and power reference set points. The power reference is typically changed as a ramp around the hour change. Unless the ramp is known an identification during such an event will risk identifying the ramp, instead of the governor dynamics. One also has to be careful to select a filter that filters out electromechanical dynamics. Furthermore both the governor and turbine contain nonlinearities such as dead bands and limiters [14]. However, in this paper it is assumed that the governor behaves linearly around the operating point where its behaviour is observed. Furthermore, when working with ambient data it is important to choose a measurement time window where the relevant dynamics of the governor is excited.

## IV. Vector fitting on real system PMU data

To test the applicability of vector fitting on real data, PMU measurements from five generators at two different location in Norway were collected. When testing vector fitting for online identification there are some properties we want to look for:

1) Easy configuration.
2) Results valid outside of the measurement window.
3) A small measurement time window.
4) Low execution time

### A. Identification approach

The approach used for performing the identification consists of five main steps:

1) Data collection: This step consists of collecting PMU data measurements from locations in the Norwegian grid.
2) Partitioning of data set: When performing identification It is important to ensure that a good fit is obtained. To do this it is normal to partition the data set into one identification part and one validation part, an approach referred to as cross validation [13]. In principle cross validation could be done by merely splitting the data set into two parts. However, due to nonlinearities, lack of dynamics or ramping, parts of a data sets may be unfit for either identification or validation. To circumvent this problem each data set is partitioned into partitions of equal lengths. For a data set of one hour and partitions of five minutes this gives 132 cross validation possibilities.
3) Preprocessing of data: All data is detrended, decimated and filtered through a low pass filter. The decimation

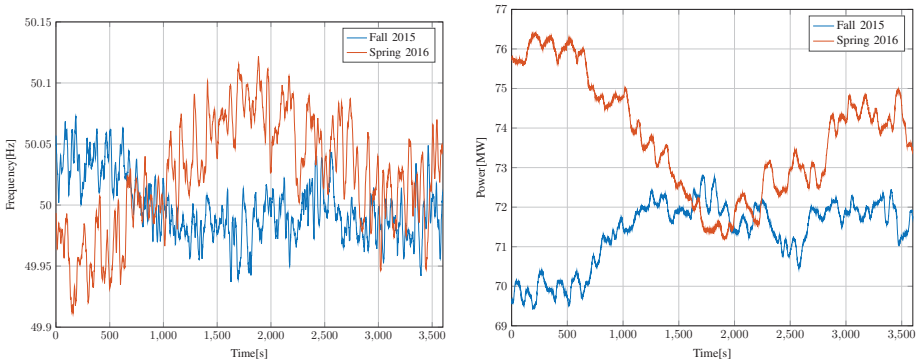


(a) Frequency of datasets

(b) Power output of datasets

Fig. 2: Datasets for fall 2015 and spring 2016

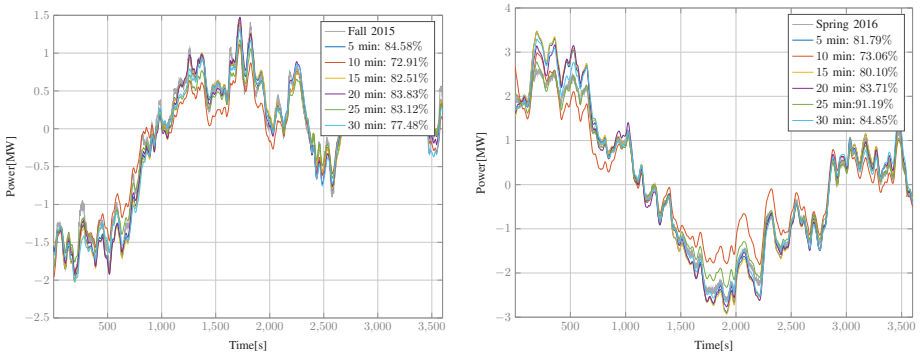


(a) Validating the constructed models against the fall dataset

(b) Validating the constructed models against the spring dataset

Fig. 3: Validation of models constructed from spring and fall dataset

factor and filter cut-off frequency is chosen such that dynamics up to $0.5Hz$ can be captured. At this frequency one may have electromechanical dynamics, however, it is unlikely that dynamic that close to the Nyquist frequency will be identified.

4) Vector fitting is performed on all partitions
5) Cross validation and model selection All cross validation possibilities are attempted and the model with the highest NRMSE is selected.

### B. *Starting order for vector fitting*

As explained in section II the vector fitting algorithm takes a set of starting poles as input. It is therefore of interest to investigate which starting orders are best for performing vector fitting on hydro governor data. To test this 19 data sets with a measurement time window of 60 minutes were selected.

To decide what ranges of starting poles to test it is useful to further investigate how many poles one can expect to find and what values they will take. From the sampling rate of the processed signal a natural upper bound of $0.5$ is easy to deduce using the Nyquist criterion. Furthermore, if one considers the results obtained from (13) and the values from Table I one can see that the maximum value of a pole should be no more than $0.18Hz$. However, when testing different starting poles we will try up to $0.5Hz$ which is the maximum we can identify.

To find the best starting poles for hydro governor fitting different combinations of both real starting poles, complex conjugate starting poles and combinations were tested for the ranges reported in Table II. The purely real and purely complex starting poles were linearly spaced and consisted of ten starting poles. The mixed starting poles were a superposition of the purely real and purely complex. Furthermore, different time windows were also tested.

From Table II it is evident that best fits are obtained when the starting poles contains complex conjugate pairs. When it comes to the distribution of the poles there are no significant difference. It is therefore reasonable to choose the maximum starting pole as half of the sampling frequency. The important

TABLE II: Fit for the different starting poles and time windows

| Minutes | Poles | [0, 0.5] | [0, 0.1] | [0, 0.05] |
|---|---|---|---|---|
| 5 | Real | 66.66% | 66.66% | 66.66% |
| | Complex | 73.07% | 74.60% | 73.53% |
| | Mixed | 74.89% | 74.69% | 74.42% |
| 10 | Real | 68.45% | 68.45% | 68.45% |
| | Complex | 72.49% | 73.84% | 72.75% |
| | Mixed | 73.49% | 72.60% | 73.73% |
| 15 | Real | 66.01% | 66.01% | 66.01% |
| | Complex | 69.72% | 70.40% | 70.33% |
| | Mixed | 70.86% | 70.43% | 70.12% |
| 20 | Real | 70.73% | 70.73% | 70.73% |
| | Complex | 72.53% | 72.27% | 71.16% |
| | Mixed | 71.28% | 71.91% | 72.38% |
| 25 | Real | 60.27% | 60.27% | 60.27% |
| | Complex | 63.45% | 62.31% | 63.45% |
| | Mixed | 63.14% | 63.45% | 63.45% |
| 30 | Real | 68.01% | 68.01% | 68.01% |
| | Complex | 71.75% | 71.45% | 72.54% |
| | Mixed | 72.52% | 71.44% | 72.21% |

decision then reduces to which cut-off frequency to use in the antialiasing filter.

### C. Measurement time window

Preferably one would want to obtain a good fit with a time window as short as possible. Furthermore, one would want the results to be valid for a wide as possible time range. In subsection IV-B we investigated the best starting poles for different time windows and as can be seen from Table II good *NRMSE* values were obtained for all time windows. This should not be very surprising as we look at dynamics in the minute time range, which means that a time window of a couple of minutes should be enough. It is also of interest to investigate the validity range of a constructed model in terms of time. To do this we will cross validate models constructed from datasets that are measured half a year apart. The datasets are from one measurement site and are from fall 2015 and spring 2016 and are depicted in Fig. 2.

In Fig. 3 the result of using the frequency signal from the spring dataset as input to the fall model and vice versa is depicted. From this one can see that models constructed half a year apart from the validation data perform satisfactory. It should also be noted that all time windows perform well, however, it varies which one is the best. The reason for this is that the fit is more dependent on the dynamics contained in the signal than the length of the signal.

Another aspect relevant for choosing the time window is the execution time. Since, the execution time increases with the number of samples a too large time window may result in a too long execution time. However, with a time window of half an hour one identification takes approximately half a second, which should for all practical purposes be fast enough. It is also worth noticing that the maximum model order obtained using vector fitting and the proposed model reduction scheme is third order models.

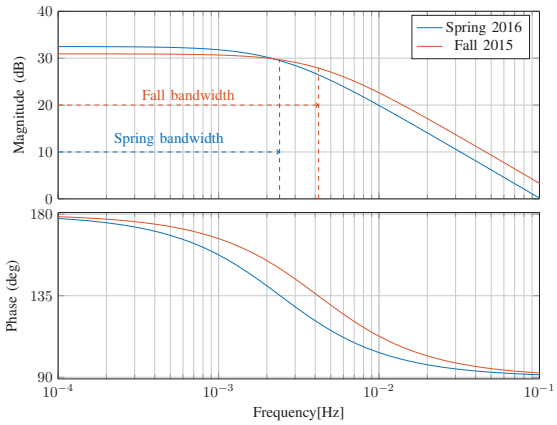


Fig. 4: Bode plot showing governor gain and bandwidth

TABLE III: Estimated droop for generator at two different times

| Dataset | Droop[%] | Bandwidth[mHz] |
|---|---|---|
| Fall 2015 | 10 | 4.16 |
| Spring 2016 | 8 | 2.41 |

### D. Applications

The most obvious application for identifying governor models are system validation. As one can see from Fig. 3 the identified models represent the real system behaviour well and can be used for this purpose. Another useful application is the ability to estimate the droop and bandwidth of the turbine governor. This can be used to check whether or not generator droop settings are close to their reported values or to validate that generators actually change their droop when instructed.

In Fig. 4 the Bode plots of the transfer functions constructed from five minute time windows using the data sets presented in Fig. 2 are presented. From the bode plot one can see both the available bandwidth as well as the droop. Bode plots are useful for graphical presenting the dynamics of the transfer functions. However, one is also quite likely to be interested in the values of the droop and the bandwidth. These values are reported in Table III. An interesting observation is that the estimated values of the droop and the bandwidth differ in between the fall and spring dataset. This observation rises an important question, that is out of the scope of this paper. Namely, is the deviation due to an actual change in the droop settings or due to uncertainties in the estimation technique.

## V. CONCLUSIONS

Vector fitting shows very promising results for identifying governor parameters obtaining good fits for all the considered datasets. The most notable feature being the ability to obtain good fits with little tuning. In short the tuning decisions that has to be made are:

1) The cut off-frequency of the antialiasing filter

2) The time window

To choose the time window the decisive factor should be the dynamics contained in the signal a discussion not covered in this paper.

The algorithm also obtains the results quickly and the proposed model reduction scheme results in low order models.

## ACKNOWLEDGEMENTS

The work presented in this paper was carried out in the project OperaGrid funded by the Norwegian research council. The authors would also like to thank Dinh Thuc Duong for valuable discussions and feedback on the work.

## REFERENCES

[1] Statnett, Fingrid, Energinet.DK, and Svenska Kraftnt. (2016). Challenges and opportunities report, [Online]. Available: http://www.statnett.no/Global/Dokumenter/Challenges%20and%20opportunities_Report.pdf (visited on 08/30/2016).

[2] European Commission. (Apr. 14, 2016). Network code on requirements for grid connection applicable to all generators, [Online]. Available: http://eur-lex.europa.eu/legal-content/EN/TXT/HTML/?uri=CELEX:32016R0631&from=EN (visited on 09/01/2016).

[3] Dinh Thuc Duong, Kjetil Uhlen, Stig Lvlund, and Erik Alexander Jansson, "Estimation of hydro turbine-governors transfer function from PMU measurements," presented at the IEEE PES General Meeting, Boston: IEEE, Jul. 2016.

[4] H. G. Aghamolki, Z. Miao, L. Fan, W. Jiang, and D. Manjure, "Identification of synchronous generator model with frequency control using unscented kalman filter," *Electric Power Systems Research*, vol. 126, pp. 45–55, Sep. 2015, ISSN: 0378-7796. DOI: 10.1016/j.epsr.2015.04.016. [Online]. Available: http://www.sciencedirect.com/science/article/pii/S0378779615001224 (visited on 01/18/2016).

[5] N. D. Hatziargyriou, E. S. Karapidakis, G. S. Stavrakakis, I. F. Dimopoulos, and K. Kalaitzakis, "Identification of synchronous machine parameters using constrained optimization," in *Power Tech Proceedings, 2001 IEEE Porto*, vol. 4, 2001, 5 pp. vol.4–. DOI: 10.1109/PTC.2001.964812.

[6] S. Grivet-Talocia, "Package macromodeling via time-domain vector fitting," *IEEE Microwave and Wireless Components Letters*, vol. 13, no. 11, pp. 472–474, Nov. 2003, ISSN: 1531-1309. DOI: 10.1109/LMWC.2003.819378.

[7] S. H. Jakobsen. (2016). Hofsmo/vectorFitting, GitHub, [Online]. Available: https://github.com/Hofsmo/vectorFitting (visited on 04/21/2016).

[8] B. Gustavsen and A. Semlyen, "Rational approximation of frequency domain responses by vector fitting," *IEEE Transactions on Power Delivery*, vol. 14, no. 3, pp. 1052–1061, Jul. 1999, ISSN: 0885-8977. DOI: 10.1109/61.772353.

[9] Stefano Grivet-Talocia and Bjrn Gustavsen, *Passive macromodeling theory and applications*, ser. Wiley Series in Microwave and Optical Enineering. John Wiley & Sons, 2016, ISBN: 978-1-118-09491-4.

[10] A. Ubolli and B. Gustavsen, "Applicability of time domain and z-domain vector fitting to rational modeling from time domain responses with consideration to circuit solver integration method," in *2010 IEEE 14th Workshop on Signal Propagation on Interconnects (SPI)*, May 2010, pp. 69–72. DOI: 10.1109/SPI.2010.5483573.

[11] A. Ramirez, "Vector fitting-based calculation of frequency-dependent network equivalents by frequency partitioning and model-order reduction," *IEEE Transactions on Power Delivery*, vol. 24, no. 1, pp. 410–415, Jan. 2009, ISSN: 0885-8977. DOI: 10.1109/TPWRD.2008.921139.

[12] MATLAB. (2016). Loss function and model quality metrics - MATLAB & simulink - MathWorks nordic, [Online]. Available: http://se.mathworks.com/help/ident/ug/model-quality-metrics.html (visited on 04/28/2016).

[13] L. Ljung, *System identification*. Springer, 1998. [Online]. Available: http://link.springer.com/chapter/10.1007/978-1-4612-1768-8_11 (visited on 03/29/2016).

[14] Working Group on Prime Mover and Energy Supply Models for System Dynamic Performance Studies, "Hydraulic turbine and turbine control models for system dynamic studies," *IEEE Transactions on Power Systems*, vol. 7, no. 1, pp. 167–179, Feb. 1992, bibtex: ieee_wg_1992, ISSN: 0885-8950. DOI: 10.1109/59.141700.

## Paper II

# Development of a test system for identification of turbine dynamics using the dc power flow

# Development of a test system for identification of turbine dynamics using the dc power flow

**Sigurd Hofsmo Jakobsen** * **Kjetil Uhlen** *

* *Department of Electric Power Engineering, Norwegian University of Science and Technology, Trondheim, Norway, sigurd.h.jakobsen@ntnu.no*

**Abstract:** Recent concerns about the frequency quality in the Nordic power system has lead to increased research on hydro turbine governors. Among this research is the use of system identification methods. However, there has been no theoretical validation of the approaches used. To be able to do a theoretical validation a simple test system is needed. In this paper it is described how one can develop such a simple test system using the dc power flow equations. In addition the system is tuned according to parameters given by recent studies to have a realistic frequency response.

## 1. INTRODUCTION

In the power system there is a strong coupling between active power and frequency. The frequency dynamics are mostly determined by the turbine governors of the large synchronous machines in the power system. Studying the dynamics of these therefore makes sense with respect to analysing frequency quality problems.

Different approaches have been proposed for identifying hydro turbine dynamics. For instance one could identify the dynamics by exciting the system externally and using measurements at the plant as in Saarinen et al. (2015). Another approach is to use Phasor measurement units (PMUs) and assume that the power system itself sufficiently excites the turbine dynamics as in Sigurd Hofsmo Jakobsen and Kjetil Uhlen (2017); Dinh Thuc Duong et al. (2016); Mogharbel et al. (2015). Common for the approaches using PMUs is that they don't consider how the input and output signals of the identification are related through the power system. Essentially what we are doing is identification in a network a topic covered in more detail in Van den Hof et al. (2013).

A simple model often used in the literature for studying generators connected to a larger power system is the single machine infinite bus (SMIB) system. This system can be found in for instance the text book Kundur et al. (1994). A SMIB system consists of a generator, an infinite bus and line connecting them. The infinite bus is characterised by having, constant voltage, voltage angle and frequency and is meant to represent a large power system. One famous example is the Heffron-Phillips system Heffron and Phillips (1952), that was proposed for studying voltage regulators. For our purpose voltages and reactive power are not important and we will therefore use a dc power flow equation with constant voltages. Although, a dc power flow have some shortcomings when it comes to accuracy, it is believed to be acceptable for studying low frequency dynamics. However, care should be taken as voltage control has significant influence on electromechanical dynamics. It also has many advantages when it comes to computational speed and convergence Stott et al. (2009).

The proposed test system can be seen as an extension of a classical SMIB system. Opposed to a classical SMIB system there will be no infinite bus, rather an aggregated generator. Furthermore, a load bus will be included. The load bus is important to include the effects of the stochastic and frequency dependent loads. It is important to notice that the modelling techniques in this paper are all standard power system modeling techniques. The novelty lies in applying these techniques to create a small test system that can be used for easily analysing identification problems including power and frequency. In addition the approach used for developing the test system can be applied for analysing frequency control strategies and power system frequency response.

The paper will be organized such that modelling of frequency dynamics are presented in Section 2. How the different elements are connected together to form a system is described in Section 3. To show the performance of the methodology some simulation results are presented in Section 4 before the conclusions in Section 5.

## 2. FREQUENCY DYNAMICS

One of the main task of the power system is to maintain a constant frequency Kundur et al. (1994). This is achieved by constantly balancing the power consumed and the power produced in the system, a process often referred to as frequency control. Typically one talks about three levels of frequency control. The frequency containment control is the fastest acting control. It is a local controller situated at all synchronous machines above a certain size. The next level of control is the frequency restoration control, which is responsible for bringing the frequency back to its nominal value and to bring tie line powers back to their scheduled values. This is a slower centralized control. The last level is the replacement reserves. These are standby reserves that should be activated to ensure that the

system has enough restoration and containment reserves. In addition the inertia in the synchronous machines and rotating loads influence the frequency of the power system, this effect is often referred to as the inertial response.

In this section the elements relevant in the frequency range of the inertial response and the frequency containment response will be presented.

### *2.1 The swing equation*

The inertial response of the power system is related to the energy stored in the rotating mass of the synchronous machines, which rotates at a speed synchronous to the grid frequency, and can be mathematical described as:

$$\begin{aligned} \dot{\theta}_m &= \omega_m \\ J\dot{\omega}_m + D_d\omega_m &= T_m - T_e \end{aligned} \tag{1}$$

where:

$\theta_m$**:** is the angular position of the machines' rotor,
$\omega_m$**:** is the angular velocity of the machines' rotor,
$J$**:** is the total moment of inertia of the machine,
$D_d$**:** is the damping torque,
$T_m$**:** is the mechanical torque of the turbine and,
$T_e$**:** is the torque of the electrical field in the machine.

The equation is well known and described in most standard text books for power systems such as for instance Machowski et al. (2008) and Kundur et al. (1994). Since power is torque times the angular velocity (1) can be written as:

$$J\dot{\omega}_m + D_d\omega_m = \frac{P_m}{\omega_m} - \frac{P_e}{\omega_m} \tag{2}$$

To simplify the expression we multiply with the synchronous machine speed $\omega_{sm}$ and the assumption $\omega_m \approx \omega_{sm}$ is used. This is a common assumption since the machine speeds normally not deviate a lot from synchronous speed even during disturbances.

$$\omega_{sm}J\dot{\omega}_m + \omega_{sm}D_d\omega_m = P_m - P_e \tag{3}$$

It is common to express the swing equation in terms of the inertia constant defined as follows:

$$H = \frac{J\omega_{sm}^2}{2S} \tag{4}$$

where $S$ is the rating of the machine. We also define

$$D_m = \omega_{sm}D_d \tag{5}$$

By inserting the new constants into (3) we get.

$$\frac{2HS}{\omega_{sm}}\dot{\omega}_m + \omega_m D_m = P_m - P_e \tag{6}$$

Since we are mostly interested in the electrical angular speed $\omega$ the following relation between the electrical, mechanical angular speed and number of poles $p$ is used:

$$\omega_m = \frac{\omega}{p/2} \tag{7}$$

Inserting (7) into (6) gives:

$$\frac{2HS}{\omega_s}\dot{\omega} + \frac{2}{p}\omega D_m = P_m - P_e \tag{8}$$

Notice that $\omega_s$ is the electrical synchronous speed. In our notation the subscript $m$ is dropped when going from mechanical to electrical values. Now we divide (8) by the machine rating to get the powers in per unit.

$$\frac{2H}{\omega_s}\dot{\omega} + \frac{2}{Sp}\omega D_m = P_m^{pu} - P_e^{pu} \tag{9}$$

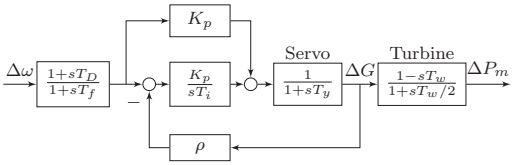


Fig. 1. Hydro turbine governor and turbine

From now on if not stated otherwise the powers will be in per unit. We also define:

$$K_d = \frac{2}{p}\frac{D_m}{S} \tag{10}$$

By using this the final version of the swing equation is obtained

$$\frac{2H}{\omega_s}\dot{\omega} + K_d\omega = P_m - P_e \tag{11}$$

### *2.2 Frequency containment control*

After the inertial response the primary frequency control or frequency containment control takes over. It is a local controller at each synchronous machine of a certain size, which governs how much a turbine should change its power output given a frequency deviation. An example on how this controller could be implemented and it's relation to the turbine dynamics are depicted in Fig. 1. The signals in the figure are as follows:

$\Delta P_m$**:** is the change in turbine mechanical power,
$\Delta G$**:** is the change in the gate position, and
$\Delta\omega$**:** is the speed deviation

The parameters in Fig. 1 and the values used are given in TABLE 1. Fig. 1 depicts a governor and its connection

Table 1. Hydro turbine governor parameters

| Variable | Explanation | Value |
|---|---|---|
| $T_D$ | Derivative time | 0 |
| $T_f$ | Low pass filter time constant | 0 |
| $K_p$ | Controller gain | 1.5 |
| $T_i$ | Integral time | $5s$ |
| $\rho$ | Droop | 0.1 |
| $T_y$ | Servo time constant | $0.2s$ |
| $T_w$ | Water starting time | $1.01s$ |

to the turbine. In between the PID regulator is a servo controlling the gate, which normally is modeled as a first order lag Working Group on Prime Mover and Energy Supply Models for System Dynamic Performance Studies (1992). The constant $\rho$ in the feedback determines how much the power output of the generator should change given a frequency deviation and is referred to as the droop. The feedback could also be from the measured power. In this case when it's from the measured gate opening a look up table relating gate opening to produced mechanical power is used to determine the gate opening.

Other more detailed models commonly used are described in Working Group on Prime Mover and Energy Supply Models for System Dynamic Performance Studies (1992) and a review of what can be found in the literature is given in Kishor et al. (2007).

### 2.3 Frequency dependent loads

In addition to the inertial response of the system's generators and the primary frequency response there are also frequency dependent loads. The equation used for describing the load behavior is as follows:

$$\Delta P_{load} = \Delta P_f + \Delta P_s \tag{12}$$

where:

$\Delta P_f$**:** is frequency dependent part of the load
$\Delta P_s$: is the stochastic part of the load assumed to be the integral of white noise.

For the frequency dependent part the following model will be used:

$$\Delta P_f = \frac{1}{D}\Delta f + \frac{W_0}{f_0}\Delta \dot{f} \tag{13}$$

where:

$\Delta P_f$ : is the change in electrical power due to frequency dependent loads,
$D$ : is a constant,
$W_0$ : is the energy stored in the rotating masses at the linearization point and,
$f_0$ : is the frequency at the linearization point.

On the load bus the swing equation cannot be used for calculating the frequency. The two main approaches for calculating the frequency at such buses are to use a weighted sum of the generator speeds or the derivative of the voltage angle at the bus Hsu et al. (1998). In this study the load bus frequency will be calculated as a weighted sum of the generator speeds.

$$f_L = \frac{\sum_{i=1}^{n_g} H_i \omega_i}{2\pi \sum_{i=1}^{n_g} H_i} \tag{14}$$

where:

$f_L$**:** is the load frequency,
$\omega_i$**:** is the speed at generator bus $i$,
$n_g$**:** is the number of generators in the system,
$H_i$**:** is the inertia constant of bus $i$.

Other approaches for modelling frequency at load buses exist such as the recent frequency divider equation Milano and Ortega (2017). This approach could be useful if one need to model spatial variation of the frequency. As it gives an algebraic expression for the frequency at load buses dependent on the system reactances.

### 2.4 Model of an aggregated generator

A model for an aggregated generator consisting of $N_g$ generators will also be derived. We will refer to the set of generators as $\Omega_g$. The derivation shown here is based on Göran Andersson (2012). We start with (11) and multiply it with $S_i$ which is the rating of generator $i$. Furthermore, we use that $\omega = \dot{\theta}$.

$$\frac{2H_i S_i}{\omega_s}\dot{\omega}_i + K_{di} S_i \omega_i = P_{mi} - P_{ei} \tag{15}$$

Now we sum over (15) for all the generators on the bus:

$$2\sum_{i\in\Omega_g}\left(\frac{H_i S_i}{\omega_s}\dot{\omega}_i + K_{di} S_i \omega_i\right) = \sum_{i\in\Omega_g}(P_{mi} - P_{ei}) \tag{16}$$

To simplify (16) we define the following quantities:

$$\omega = \frac{\sum_{i\in\Omega_g} H_i \omega_i}{\sum_{i\in\Omega_g} H_i} \tag{17}$$

$$S = \sum_{i\in\Omega_g} S_i \tag{18}$$

$$H = \frac{\sum_{i\in\Omega_g} H_i S_i}{\sum_{i\in\Omega_g} S_i} \tag{19}$$

$$K_d = \frac{\sum_{i\in\Omega_g} K_{di} S_i}{\sum_{i\in\Omega_g} S_i} \tag{20}$$

$$P_m = \sum_{i\in\Omega_g} P_{mi} \tag{21}$$

$$P_e = \sum_{i\in\Omega_g} P_{ei} \tag{22}$$

We can now write the swing equation for the bus as

$$\frac{2HS}{\omega_s}\dot{\omega} + K_d S\omega = P_m - P_e \tag{23}$$

In addition to aggregating the swing equation the turbine, governor and reactances also have to be aggregated. The turbine and governor can be represented by a transfer function $G_t(s)$. At the bus there will be $N_g$ of these transfer functions all contributing to the mechanical power.

$$P_m = \sum_{i\in\Omega_g} G_{t2} \tag{24}$$

For the reactances of the machines at the aggregated bus it is reasonable to assume them to be connected in parallel.

$$\frac{1}{x'_d} = \sum_{i\in\Omega_g} \frac{1}{x'_{di}} \tag{25}$$

## 3. THE DC POWER FLOW

In this section the version of the dc power flow used for this paper is presented. A description on how one can interface the dc power flow with the necessary power system components is also provided.

### 3.1 Grid interface of the synchronous machine

Before moving on to describing the dc power flow we will first introduce how the models presented in the previous section can be interfaced with the dc power flow. In the literature one can find that it is normal to represent synchronous generators as a source behind an impedance Kundur et al. (1994). The impedance is also dominated by the reactance, hence, we will model it as a reactance. Furthermore, the reactance will be dependent on the transients such that the value will be larger for faster transients. Typically, one will divide the analysis into a sub-transient, transient and a steady state period. In our analysis we will use the transient reactance. Schematically this representation of a synchronous generator is depicted in Fig. 2.

### 3.2 DC power flow

The power flowing on the lines in a power system is related to the power injections at the buses through the power flow equations. Below the power flow equation for active power

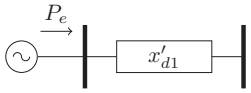


Fig. 2. Generator behind a transient reactance

is written neglecting the terms related to ohmic losses and shunt elements. Basically the equation tells us that the power injected into a bus equals all the powers flowing into it from adjacent lines.

$$P_k = U_k \sum_{m \in \Omega_k} U_m x_{km}^{-1} \sin \theta_{km} \tag{26}$$

where:

$P_k$**:** is the power injection at node $k$,
$\theta_{km}$**:** is the voltage angle difference between node $k$ and $m$,
$x_{km}$**:** is the reactance between node $k$ and $m$,
$\Omega_k$**:** is the buses adjacent to bus $k$.
$U_k$**:** is the voltage at bus $k$.
$U_m$**:** is the voltage at bus $m$.

In real power systems the voltages are normally close to $1(p.u.)$ and the angles are small. Using these observations the DC power flow approximation is written as follows:

$$P_k \approx \sum_{m \in \Omega_k} x_{km}^{-1} \theta_{km} \tag{27}$$

Written on matrix form this becomes:

$$\mathbf{P} = \mathbf{Y}\theta \tag{28}$$

where:

**P:** is the vector of power injections,
**Y:** is the nodal admittance matrix,
$\theta$**:** is the vector of voltage bus angles.

Since the angles at the load buses are unknown we split the admittance matrix into submatrices to derive an expression for the power injection at the generator buses.

$$\begin{bmatrix} \mathbf{P}_e \\ \mathbf{P}_l \end{bmatrix} = \begin{bmatrix} \mathbf{Y}_{11} & \mathbf{Y}_{12} \\ \mathbf{Y}_{21} & \mathbf{Y}_{22} \end{bmatrix} \begin{bmatrix} \theta_e \\ \theta_l \end{bmatrix} \tag{29}$$

where:

$\mathbf{P}_e$**:** is the power injection at the generator nodes
$\mathbf{P}_l$**:** is the power injection at the loads
$\theta_e$**:** is the voltage angle at the generator nodes
$\theta_l$**:** is the voltage angle at the load nodes

The angle of the load buses can now be calculated as:

$$\theta_l = \mathbf{Y}_{22}^{-1}(\mathbf{P}_l - \mathbf{Y}_{21}\theta_e) \tag{30}$$

Finally the power injections at the generator buses are:

$$\mathbf{P}_e = \mathbf{Y}_{11}\theta_e + \mathbf{Y}_{12}\theta_l \tag{31}$$

If one is not interested in the angle of the load buses and are only interested in the injected power at the generator node it can be convenient to substitute (30) into (31) and rearrange to obtain.

$$\mathbf{P}_e = \begin{bmatrix} \mathbf{Y}_{11} - \mathbf{Y}_{12}\mathbf{Y}_{22}^{-1}\mathbf{Y}_{21} & \mathbf{Y}_{12}\mathbf{Y}_{22}^{-1} \end{bmatrix} \begin{bmatrix} \theta_e \\ \mathbf{P}_l \end{bmatrix} \tag{32}$$

From (32) one can see that the input needed to the DC power flow are the change in generator angles and the change in the demand. The change in the generator angles are easily calculated as the integral of the generator

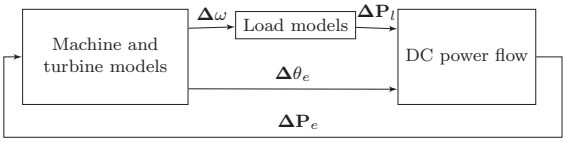


Fig. 3. Conceptual connection between device models and DC power flow

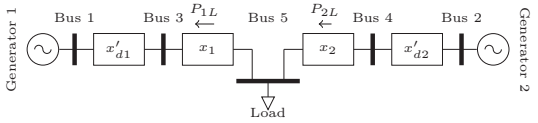


Fig. 4. System set up

speeds. Furthermore, the calculated injected power at the generators are input to the swing equation. This means that the machine models, loads and dc power flow equation together form a feedback loop, as depicted in Fig. 3.

## 4. SIMULATION RESULTS

In this section simulation results from the test system is presented and compared to PMU data. The PMU data was collected using a PMU installed close to a generator in the Nordic power system.

To study the identifiability of turbines using PMU measurement the system depicted in 4 is proposed. It consists of a generator at bus 1, a load at bus 5 and an aggregated generator at bus 2. At bus 2 it is assumed to be 10 generators that have exactly the same parameters. If one increases the number of generators at bus the system will gradually go towards a single machine infinite bus system. The idea behind the layout of the system is that bus 1 represents the bus where one has PMU measurements and will attempt the identification, bus 2 represents the rest of the generators, and bus 5 represents the loads in the system. The block diagram is depicted in 4. In addition to what have been described earlier the diagram also contains block for changing between the different per unit systems and also for going from frequency to radians. The parameters used are given in 2. In the table base voltages for the machines and transmission system are also reported. These are used for converting the sub transient reactances to the same base as the transmission grid. A block diagram representation of the system is depicted in Fig. 5. The constants denoted $K$ in the figure corresponds to the elements of the matrix in (32).

To get a realistic frequency response the values reported in the paper Saarinen et al. (2016) were used for tuning the governor.

To check whether or not the system response is reasonable a random load with a standard deviation of 0.025 was simulated. This signal was sent through an integrator to represent the load as the integral of white noise. This is a commonly used method for representing stochastic loads in the power system Perić and Vanfretti (2014). The results from this simulation was used to plot the power spectral density of the simulated frequency against a measured

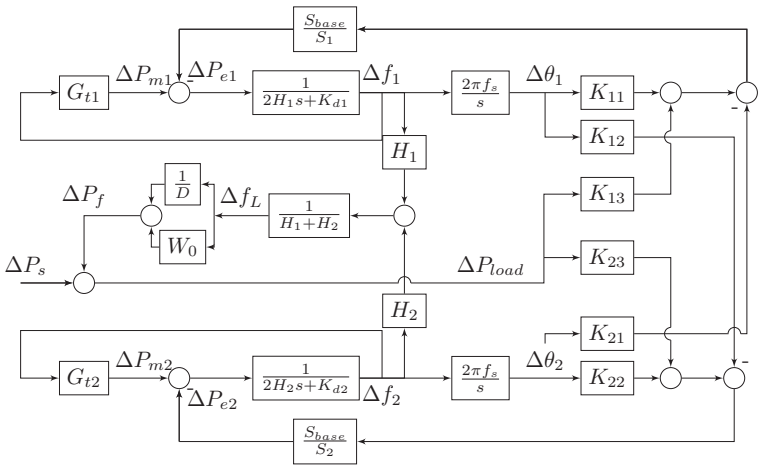


Fig. 5. Block diagram of Fig. 4

signal. The result of this is shown in Fig. 6. As one can see it is a reasonably good match.

In Fig. 7 the system frequency's response to a one per unit load step is plotted. One can see that the change in frequency is less than expected given the applied step, if one assumed the change to be directly proportional to the droop of the governors. However, since the damping $K_{d2}$ is quite large this also contributes to the final change in the frequency deviation. Since the model used is quite simple some of the damping provided by for instance the damper windings have to be included in the model and it is common to choose the damping factors larger to overcome this problem. To obtain a steady state change directly proportional to the droop one could choose to model the damping as only acting while the frequency is changing as in Andersen (2016).

A plot of the powers flowing on the lines is also given in Fig. 8. As one could expect most of the load change is being compensated by the larger generator at bus 2.

Table 2. The parameters used for Fig. 5

| Variable | Explanation | Value | |
|---|---|---|---|
| $S_1$ | Machine 1 base power | $300MW$ | - |
| $S_2$ | Machine 2 base power | $3GW$ | - |
| $S_{base}$ | System base power | $3.3GW$ | - |
| $U_{base}$ | Base voltage for the transmission system | $400kV$ | - |
| $U_M$ | base voltage for the machines | $20kV$ | - |
| $D$ | Proportional load frequency dependency | 50 | $S_{base}$ |
| $W_0$ | Energy stored in rotating loads | 0.01 | $S_{base}$ |
| $H_1$ | Generator 1 inertia constant | $9.68s$ | |
| $H_2$ | Generator 2 inertia constant | $968s$ | |
| $K_{d1}$ | Damping constant | 0.5 | - |
| $k_{d2}$ | Damping constant | 5 | - |
| $x_1$ | Reactance between bus 3 and 5 | 5 | $S_{base}$ |
| $x_2$ | Reactance between bus 4 and 5 | 5 | $S_{base}$ |
| $x_{d1}$ | Sub transient reactance generator 1 | 0.2 | $S_1$ |
| $x_{d2}$ | Sub transient reactance generator 2 | 0.2 | $S_1$ |

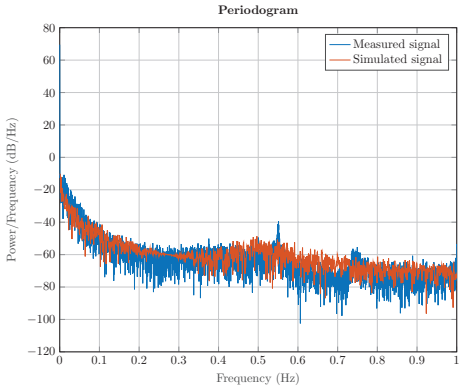


Fig. 6. Power spectrum density of measured system frequency and simulated frequency

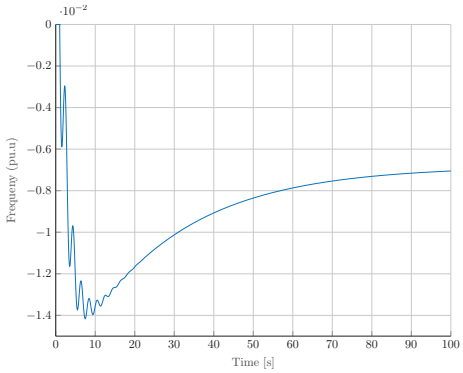


Fig. 7. Frequency response to a 1(p.u.) load step

## 5. CONCLUSIONS

In the paper it has been shown how one can create a simple test system for studying frequency control. The system shows similar frequency dynamics to the real power system

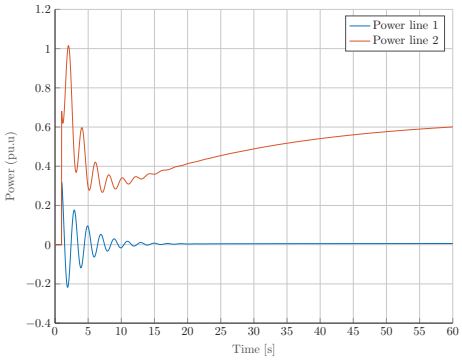


Fig. 8. Generator power response to a 1(p.u.) load step

when tuned with parameters from a recent study and should be suited for studying identification of turbine and turbine governor dynamics. Furthermore, the methodology can easily be adapted for other frequency studies. However, if one want a more correct representation of the system's droop characteristic another model of the damping will have to be implemented.

## ACKNOWLEDGEMENTS

The work presented in this paper was carried out in the project OperaGrid funded by the Norwegian research council. In addition the ELECTRA IRP FP7 project funded the research exchange between NTNU and Ampere Lab.

## REFERENCES

Andersen, K.G. (2016). *Area Based Secondary Frequency Control in the Nordic Power System*. Ph.D. thesis, Norwegian University of Science and Technology.

Dinh Thuc Duong, Kjetil Uhlen, Stig Løvlund, and Erik Alexander Jansson (2016). Estimation of Hydro Turbine-Governor's Transfer Function from PMU Measurements. IEEE, Boston.

Göran Andersson (2012). *Dynamics and Control of Electric Power Systems*.

Heffron, W.G. and Phillips, R.A. (1952). Effect of a Modern Amplidyne Voltage Regulator on Underexcited Operation of Large Turbine Generators [includes discussion]. *Transactions of the American Institute of Electrical Engineers. Part III: Power Apparatus and Systems*, 71(1). doi:10.1109/AIEEPAS.1952.4498530.

Hsu, C.S., Chen, M.S., and Lee, W.J. (1998). Approach for bus frequency estimating in power system simulations. *Transmission and Distribution IEE Proceedings - Generation*, 145(4), 431–435. doi:10.1049/ip-gtd:19982028.

Kishor, N., Saini, R.P., and Singh, S.P. (2007). A review on hydropower plant models and control. *Renewable and Sustainable Energy Reviews*, 11(5), 776–796. doi:10.1016/j.rser.2005.06.003.

Kundur, P., Balu, N.J., and Lauby, M.G. (1994). *Power system stability and control*, volume 7. McGraw-hill New York.

Machowski, J., Bialek, J.W., and Bumby, J.R. (2008). *Power System Dynamics : Stability and Control*, volume 2nd ed. Wiley, Chichester, U.K.

Milano, F. and Ortega, A. (2017). Frequency Divider. *IEEE Transactions on Power Systems*, 32(2), 1493–1501. doi:10.1109/TPWRS.2016.2569563.

Mogharbel, B., Fan, L., and Miao, Z. (2015). Least squares estimation-based synchronous generator parameter estimation using PMU data. In *2015 IEEE Power Energy Society General Meeting*, 1–5. doi:10.1109/PESGM.2015.7286559.

Perić, V.S. and Vanfretti, L. (2014). Power-System Ambient-Mode Estimation Considering Spectral Load Properties. *IEEE Transactions on Power Systems*, 29(3), 1133–1143. doi:10.1109/TPWRS.2013.2292331.

Saarinen, L., Norrlund, P., and Lundin, U. (2015). Field Measurements and System Identification of Three Frequency Controlling Hydropower Plants. *IEEE Transactions on Energy Conversion*, 30(3), 1061–1068. doi:10.1109/TEC.2015.2425915.

Saarinen, L., Norrlund, P., Lundin, U., Agneholm, E., and Westberg, A. (2016). Full-scale test and modelling of the frequency control dynamics of the Nordic power system. In *2016 IEEE Power and Energy Society General Meeting (PESGM)*, 1–5. doi:10.1109/PESGM.2016.7741711.

Sigurd Hofsmo Jakobsen and Kjetil Uhlen (2017). Vector fitting for estimation of turbine governing system parameters. In *Powertech*.

Stott, B., Jardim, J., and Alsac, O. (2009). DC Power Flow Revisited. *IEEE Transactions on Power Systems*, 24(3), 1290–1300. doi:10.1109/TPWRS.2009.2021235.

Van den Hof, P.M.J., Dankers, A., Heuberger, P.S.C., and Bombois, X. (2013). Identification of dynamic models in complex networks with prediction error methods—Basic methods for consistent module estimates. *Automatica*, 49(10), 2994–3006. doi:10.1016/j.automatica.2013.07.011. URL `http://www.sciencedirect.com/science/article/pii/S000`

Working Group on Prime Mover and Energy Supply Models for System Dynamic Performance Studies (1992). Hydraulic turbine and turbine control models for system dynamic studies. *IEEE Transactions on Power Systems*, 7(1), 167–179. doi:10.1109/59.141700. Bibtex: ieee_wg_1992.

## Paper III

# Identification of hydro turbine governors using PMU data

# Identification of hydro turbine governors using PMU data

Sigurd Hofsmo Jakobsen, Kjetil Uhlen
Department of Electric Power Engineering
Norwegian University of Science and Technology,
Trondheim, Norway,
sigurd.h.jakobsen@ntnu.no

Xavier Bombois
Laboratoire Ampère UMR CNRS 5005
Ecole Centrale de Lyon,
Ecully, France

***Abstract*—Recent concerns for the frequency quality in the Nordic power system has lead to an increased interest in hydro turbine governors. Among this research have been papers on identification of turbine and turbine governor dynamics from PMU measurements. However, no attempt at a theoretical validation has been made. This paper fills in this gap by a theoretical validation using a DC power flow model for modelling the power flows in the grids. By doing this it is shown that it is indeed possible to identify the closed loop transfer function of the turbine, turbine governor and electromechanical dynamics. An experimental validation using results from a real life power system are also presented.**

## I. Introduction

Recent concerns for the frequency quality in the Nordic power system [1] have lead to an increased interest in the dynamic performance of hydro turbine governors. Among the research being carried out is identification of turbine governors using local measurements from phasor measurement units (PMUs). The added value for the TSOs is the possibility to validate the performance of the governors using their own measurements instead of relying on information from the production plant owners.

In this article the aim is to test the hypothesis that turbine governor dynamics can be identified using PMU measurements at generator bus bars. In the literature one can already find papers where identification methods have been applied to PMU measurements for the identification of turbine dynamics [2]–[6]. In [2] an unscented Kalman filter is used to identify both turbine and electromechanical dynamics using data from a generator trip event. Another paper using data from disturbance[1] recordings is [4] who uses constrained optimization to perform the identification. Other papers such as [3], [5], [6] use data from normal operation to do the identification. This is of particular interest since the system is not always subjected to large disturbances. We will therefore focus on measurements from normal operation in this paper. The papers [3], [6] uses the ARX and ARMAX model structure to perform the identification whereas [5] uses time domain vector fitting. In the present paper the same dataset as in [3], [5] will be used for the experimental validation.

[1]In this context disturbance refers to a larger power system event, i.e. load or generation tripping and not normal load variations

What lacks in the previous papers is an explicit study on how the input and output to the identification is related to each other through the power system. In other words there is no analysis of whether or not the proposed methods will yield consistent results. In this paper we give conditions under which a consistent estimate of the transfer function between the electrical power and the speed of a generator can be deduced using only PMU data from normal operation.

The structure of the paper will be as follows. The system under study is presented in Section II, the theoretical validation in Section III, simulation results are give in Section IV, results from a real life power system is given in Section V, and finally the conclusions in Section VI.

## II. Test system for identification

To be able to analyze the identifiability of turbine and turbine governors the components influencing the input and output signals to the identification has to be modeled. To do this we will consider a turbine located at bus 1 in a power system. The location will be denoted by adding the number 1 to the subscript for the considered signals and functions. In Fig. 1 the model used for representing a hydro turbine governor and the turbine used in this paper is presented. For the model of the turbine we have chosen a linearised model represented by a first order transfer function with a time constant $T_w$. Physically this time constant represents the time the water uses to flow from the reservoir to the turbine at the operating point of the linearization. The governor is a PID regulator with a droop feedback $\rho$, which uses the generator speed $\Delta\omega_1(s)$ to modify the power output $\Delta P_{m1}(s)$ of the turbine. The transfer function between $\Delta\omega_1(s)$ and $\Delta P_{m1}(s)$ will be denoted $G_{t1}(s)$:

$$\Delta P_{m1}(s) = G_{t1}(s)\Delta\omega_1(s) \tag{1}$$

It is worth noting that the steady state gain of $G_{t1}(s)$ is always equal to the inverse of the droop $1/\rho$. The power output is changed by adjusting the guide vane opening $\Delta g_1(s)$. Other modelling choices are available and a reference for many common choices are [7].

To identify $G_{t1}(s)$, one would need to use a data set with $\Delta\omega_1(s)$ as input and $\Delta P_{m1}(s)$ as output. Unfortunately, $\Delta P_{m1}(s)$ is not available to the TSOs. Instead, they can install

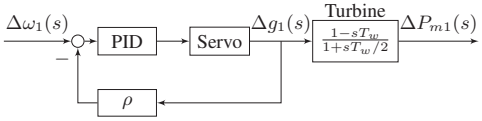


Fig. 1: Hydro turbine governor and turbine $G_{t1}(s)$

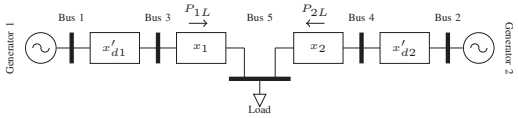


Fig. 2: Single line diagram of the system

PMUs at the bus bar where the generator is connected to their system. This will allow them to measure the electrical power and frequency at the bus bar. The relation between the electrical power, mechanical power, and generator speed is given by the swing equation:

$$\Delta\omega_1(s) = \frac{\Delta P_{m1}(s) - \Delta P_{e1}(s)}{2\mathcal{H}_1 s + K_{d1}} \tag{2}$$

where:

$\mathcal{H}_1$**:** is the inertia constant of the machine, which is the inertia of the machine scaled according to its rating.

$K_{d1}$**:** is the damping constant.

From now on we will denote $G_{J1}(s) = 1/(2\mathcal{H}_1 s + K_{d1})$. We will also combine (1) and (2) to obtain:

$$\Delta\omega_1(s) = -\frac{G_{J1}(s)}{1 + G_{J1}(s)G_{t1}(s)}\Delta P_{e1}(s) + v_1(s) \tag{3}$$

where $v_1(s)$ is an additional contribution representing the process disturbance acting on generator 1. It will be modeled as white noise $e_1(s)$[2] filtered by the transfer function $H_1(s)$. One should take note of that $H_1(s)$ can also be a closed loop transfer function.

Consequently, using measurements of $\Delta\omega_1(s)$ and $\Delta P_{e1}(s)$ we will never be able to identify $G_{t1}(s)$. If we can identify a transfer function based on these data it will be the closed-loop transfer function $G_1(s) = -G_{J1}(s)/(1+G_{t1}(s)G_{J1}(s))$. It should be noted that the steady state gain of $G_1(s)$ is approximately equal to the droop $\rho$, which means that we will still be able to deduce information on the turbine governor's droop settings.

What remains to be proven is whether or not $G_1(s)$ can be consistently identified from normal operation data. For this purpose it is important to analyze how $\Delta P_{e1}(s)$ is generated in the power system. We will therefore introduce the simple power system depicted in Fig 2. The system consists of two power plant buses, one load bus and the lines connecting them. As already mentioned, our objective is to identify $G_1(s)$ for the power plant at bus 1. The power plant at bus 2 is an aggregated plant designed to represent the rest of the production capacity in the network and the load at bus 5 is meant to represent all loads in the system. In the power system there is a strong coupling between active power and frequency. Due to this we will assume that reactive power and voltages can be assumed constant for our analysis, allowing us to model the flow on the lines using a dc power flow. This design choice allows us to include the most relevant dynamics in our analysis, while keeping the system small.

[2]This is abuse of notation since white noise has no Laplace transform.

In Fig. 2 there are four reactances, $x_1$ and $x_2$ are line reactances, and $x'_{d1}$ and $x'_{d2}$ are the subtransient reactances of the generators at bus 1 and bus 2 respectively. It is important to notice that the subtransient reactances are internal to the generators. Therefore, our PMU measurements used for identifying $G_1(s)$ will be taken at bus 3 not bus 1. We have already assumed a dc power flow, hence the electrical power measured at bus 3 will be the same as for bus 1. Furthermore, we will also assume the frequency measured at bus 3 $\Delta f_3(s)$ is a good estimate of the electric speed at bus 1, in other words $\omega_1(s) \approx 2\pi f_3(s)$.

For the load it is assumed that the load has a frequency dependency given by the transfer function $G_l(s)$, this is commonly due to rotating loads. The frequency at the load is estimated using the centre of inertia equation.

$$f_5(s) = 2\pi\frac{\sum_{i=1}^{2}\omega_i(s)\mathcal{H}_i}{\sum_{i=1}^{2}\mathcal{H}_i} \tag{4}$$

In addition to frequency dependent part the load consists of a stochastic part $v_5(s) = H_5(s)e_5(s)$, which represents the load changes due to random load switching. It is modeled as white noise $e_5(s)$ filtered by the filter $H_5(s)$.

The dc power flow assumption allows us to establish the following relationship between the electrical angle at the two production plant buses and the active power at the load bus [8].

$$\mathbf{P}_e = \begin{bmatrix}\mathbf{Y}_{11} - \mathbf{Y}_{12}\mathbf{Y}_{22}^{-1}\mathbf{Y}_{21} & \mathbf{Y}_{12}\mathbf{Y}_{22}^{-1}\end{bmatrix}\begin{bmatrix}\theta_e \\ \mathbf{P}_l\end{bmatrix} \tag{5}$$

where the $\mathbf{Y}_{ij}$ are submatrices of the nodal admittance matrix, $\theta_e$ is vector of generator angles, $\mathbf{P}_e$ is the vector of generator bus active powers, and $\mathbf{P}_l$ is the vector of load active powers. We can now derive a linear relationship between the plants and load. This linear relationship is presented in Fig. 3 where the $K$ factors are constants derived from (4) and (5).

In Fig. 3 the process noise acting on the power plants are depicted and we see that the second power plant like power plant 1 is perturbed by filtered white noise $v_2(s) = H_2(s)e_2(s)$. An important assumption is that the noise terms $v_1(s)$, $v_2(s)$, and $v_5(s)$ are all statistically uncorrelated. This assumption should easily hold for $v_5(s)$ as consumers are unlikely to change their consumption due to process noise at production plants. It is also very unlikely that the process noises at power plants situated at geographical distant locations are dependent on each other.

Based on Fig. 3 one can deduce, that in normal operation, $\Delta P_{e1}(s)$ is made of a contribution of the two process noises $v_1(s) = H_1(s)e_1(s)$ and $v_2(s) = H_2(s)e_2(s)$ as well as the

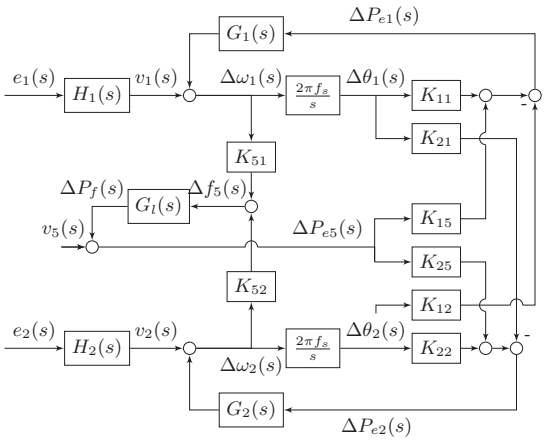


Fig. 3: Block diagram of the system depicted in Fig. 2

random load changes $v_5(s) = H_5(s)e_5(s)$. We can now write $P_{e1}(s)$ as a function of the white noises.

$$\Delta P_{e1}(s) = T_5(s)e_5(s) + T_1(s)e_1(s) + T_2(s)e_2(s) \tag{6}$$

where $T_5(s)$, $T_1(s)$ and $T_2(s)$ are stable transfer functions. The contribution of $e_2(s)$ and $e_5(s)$ are important, indeed, these contributions show that $\Delta P_{e1}(s)$ will be made up of external signals even under normal operations. These external signals will excite the dynamics of $G_1(s)$ and help in the identification. Opposed to this $e_1(s)$ could be detrimental as it introduces a correlation between $\Delta P_{e1}(s)$ and the process disturbance $v_1(s)$. However, we will show that this correlation will not lead to identification problems if a certain technical condition is satisfied.

## III. Theoretical validation

For the validation we suppose that, after the application of an antialiasing filter, we have collected N samples of $\Delta P_{e1}(t)$ and $\Delta\omega_1(t)$ with a certain sampling frequency. We will denote these samples $u[n]$ and $y[n]$ respectively, where $[n]$ denotes discrete time. These sampled signals make up the dataset $Z^N = \{u[n], y[n] | n = 1 \dots N\}$, and they are assumed related by:

$$\mathcal{S} : y[n] = G_1(z, \theta_0)u[n] + H_1(z, \theta_0)e_1[n] \tag{7}$$

where $G_1(z, \theta_0)$ and $H_1(z, \theta_0)$ are discrete versions of the transfer functions $G_1(s)$ and $H_1(s)$, $H_1(z, \theta_0)$ is assumed monic, $e_1[n]$ is discrete time white noise, $\theta_0$ is the vector that parametrize the true system $\mathcal{S}$, and $z^{-1}$ is the delay operator.

For the input signal $u[n]$ we have that:

$$u[n] = T_5(z)e_5[n] + T_1(z)e_1[n] + T_2(z)e_2[n] \tag{8}$$

where $T_5(z)$, $T_1(z)$, and $T_2(z)$ are discrete versions of the transfer functions in (6). We also define $\sigma^2_{e_1}$, $\sigma^2_{e_2}$, and $\sigma^2_{e_5}$ as the power spectra of $e_1[n]$, $e_2[n]$, and $e_5[n]$.[3]

Before moving on to the proof what we mean by identification should be defined. It is simply that given the dataset $Z^N$ and a full order model structure $\mathcal{M} = \{G_1(z, \theta), H_1(z, \theta)\}$ we can deduce an estimate of the unknown parameter vector $\hat{\theta}_N$ using prediction identification [9]:

$$\hat{\theta}_N = \arg\min_{\theta} \frac{1}{N} \sum_{n=1}^{N} \epsilon^2(n, \theta) \tag{9}$$

with:

$$\epsilon(n, \theta) = H_1^{-1}(z, \theta)(y[n] - G_1(z, \theta)u[n]) \tag{10}$$

In order to validate our identification setting it is important to verify whether or not (9)-(10) will lead to a consistent estimate of $\theta_0$ when the input signal is given by (8), or in other words, whether or not (8) is a sufficiently informative signal for the identification of $\mathcal{S}$. For $\hat{\theta}_N$ to be a consistent estimate, one needs to verify that the true parameter vector $\theta_0$ is the unique solution to the asymptotic prediction criterion:

$$\theta^* = \arg\min_{\theta} \bar{E}\epsilon^2(n, \theta) \tag{11}$$

with

$$\bar{E}\epsilon^2(n, \theta) = \lim_{N \to \infty} \frac{1}{N} \sum_{t=1}^{N} E\epsilon^2(n, \theta) \tag{12}$$

The operator $E$ denotes the expectation operator.

**Theorem 1.** *Consider the dataset $Z^N = \{u[n], y[n] | n = 1 \dots N\}$ where $Z^N$ is generated by* (7) *and* (8)*. Suppose also that $e_1[n]$, $e_2[n]$, and $e_5[n]$ are independent white noises. Then the prediction error criterion* (9)-(10) *yields a consistent estimate of $\theta_0$ if there is a delay in either $G_1(z, \theta_0)$ or $T_1(z)$.*

*Proof.* We start by writing the prediction error in terms of the input at node *1* by inserting (7) into (10) to get.

$$\epsilon[n, \theta] = e_1[n] + \frac{\Delta H_1(z, \theta)}{H_1(z, \theta)} e_1[n] + \frac{\Delta G_1(z, \theta)}{H_1(z, \theta)} u[n] \tag{13}$$

with $\Delta H_1(z, \theta) = H_1(z, \theta_0) - H_1(z, \theta)$ and $\Delta G_1(z, \theta) = G_1(z, \theta_0) - G_1(z, \theta)$. By inserting (8) into (13) we can write $\epsilon[n, \theta]$ as:

$$\begin{aligned} \epsilon[n, \theta] = e_1[n] + \nu(z, \theta)e_1[n] \\ + \Gamma_2(z, \theta)e_2[n] + \Gamma_5(z, \theta)e_5[n] \end{aligned} \tag{14}$$

with:

$$\nu(z, \theta) = \frac{\Delta H_1(z, \theta) + \Delta G_1(z, \theta)T_1(z)}{H_1(z, \theta)} \tag{15}$$

and

$$\Gamma_{m \in 2,5}(z, \theta) = \frac{\Delta G_1(z, \theta)}{H_1(z, \theta)} T_{m \in 2,5}(z) \tag{16}$$

Due to the fact that $H_1(z)$ is monic and the fact that $\Delta G_1(z, \theta)T_1(z)$ contains a delay, we conclude that when

[3]For a white noise process the spectrum is its variance.

non zero $\nu(z,\theta)$ also contains a delay. This property and the assumption on the independence of $e_1[n]$, $e_2[n]$, and $e_5[n]$ can be used to write $\bar{E}\epsilon^2(n,\theta)$ as:

$$\begin{aligned}\bar{E}\epsilon^2[n,\theta] = \sigma_{e_1}^2 \\ + \frac{1}{2\pi}\int_{-\pi}^{\pi} \nu(e^{j\omega},\theta)\sigma_{e_1}^2\nu^*(e^{j\omega},\theta)d\omega \\ + \frac{1}{2\pi}\int_{-\pi}^{\pi} \Gamma_2(e^{j\omega},\theta)\sigma_{e_2}^2\Gamma_2^*(e^{j\omega},\theta)d\omega \\ + \frac{1}{2\pi}\int_{-\pi}^{\pi} \Gamma_5(e^{j\omega},\theta)\sigma_{e_5}^2\Gamma_5^*(e^{j\omega},\theta)d\omega\end{aligned} \tag{17}$$

To prove the consistency, we will show that $\theta_0$ is the unique minimizer of (17), that is it is the unique parameter vector $\theta^*$ yielding $\bar{E}\epsilon^2[n,\theta^*] = \sigma_{e_1}^2$. We observe that this only holds if $\nu(z,\theta^*) = \Gamma_2(z,\theta^*) = \Gamma_5(z,\theta^*) = 0$. From (15) and (16) we see that the latter statement implies that $\Delta G_1(z,\theta^*) = \Delta H_1(z,\theta^*) = 0$. This again implies $\theta^* = \theta_0$. □

## IV. Simulation results

In this section validation of the identification of turbine dynamics using a simulation model developed in Simulink will be presented. The system is depicted in Fig. 2 and was presented in Section II. It was tuned to give a response similar to the one area system in [10].

To obtain the models a Box-Jenkins model structure was assumed, which has the following structure:

$$y(t) = \frac{B(z)}{F(z)}u(t) + \frac{C(z)}{D(z)}e(t) \tag{18}$$

The reason for this choice is that it is a general model structure that allows for modelling the denominator dynamics of $G_1(z,\theta_0)$ and $H_1(z,\theta_0)$ separately. The model order used was $[4,6,6,5,0]$ where the model orders are given in alphabetical order and the last number represents the time delay. The simulated signals were given with a sampling frequency of $50Hz$ to be the same as for a PMU signal. In addition the signals were decimated using a factor of 25. The system identification toolbox developed for MATLAB was used for the filtering and identification [11].

It should be noted that the order of the delay is chosen to be zero. This means that if there is a delay in $G_1(z,\theta_0)$ it is shorter than $0.5s$. If one considers the condition stated in 1 one realizes that this implies that there has to be a delay longer than $0.5s$ in $T_1(z)$.

To validate the results we first start by plotting the analytical transfer function of the true system against an estimated one. This is depicted in Fig. 4, where one can see that there is an almost perfect match between $G_1(s)$ and $G_1(z,\hat{\theta}_N)$. One can also observe how the identified function follows the dynamics of the inverse of $G_{t1}(s)$ for low frequencies. Although, in Fig. 4 one can also see that the transfer function starts deviating from the governor as the frequency raises, one can still extract information on the steady state gain of the transfer function. This implies that one can derive information

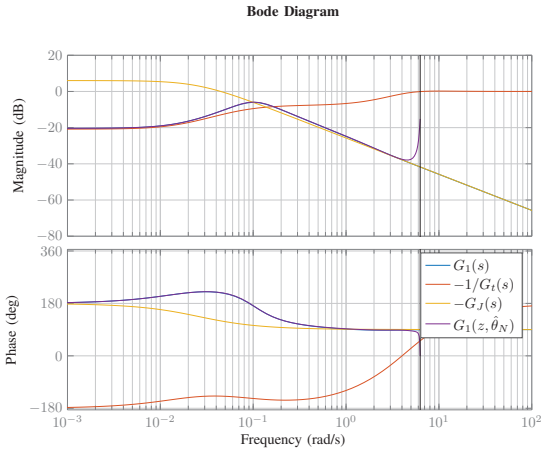


Fig. 4: Bode plots of actual transfer functions and identified transfer function using simulation data

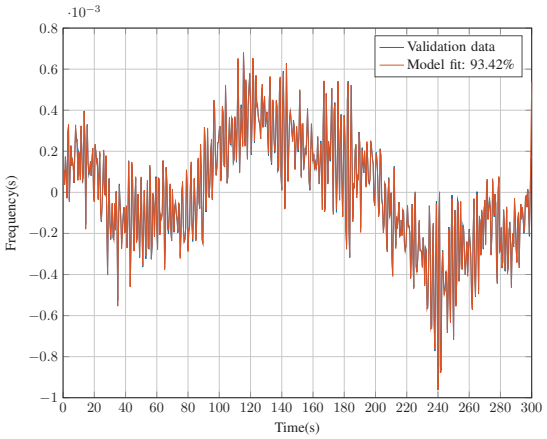


Fig. 5: Comparison of actual and identified transfer function subjected to a signal using simulation data

on the steady state gain of $G_{t1}(s)$, which is related to the droop settings, from the measurements. In general it will be difficult to say something about the bandwidth of the governor since the dynamics will be a mix of the electromechanical and governor dynamics, however, one will still be able to say something about the plants response as a whole.

A common method for benchmarking the performance of identified transfer functions is to measure a second data set $Z_v = \{u_v[n], y_v[n] | n = 1 \dots N_v\}$. We then apply $u_v[n]$ to the identified model $G_1(z,\hat{\theta}_N)$ to obtain a signal $\hat{y}[n]$ that is:

$$\hat{y}[n] = G_1(z,\hat{\theta})u_v[n] \tag{19}$$

$\hat{y}[n]$ can then be plotted against $y_v[n]$ to allow for a visualization of the identified model's performance. In addition one

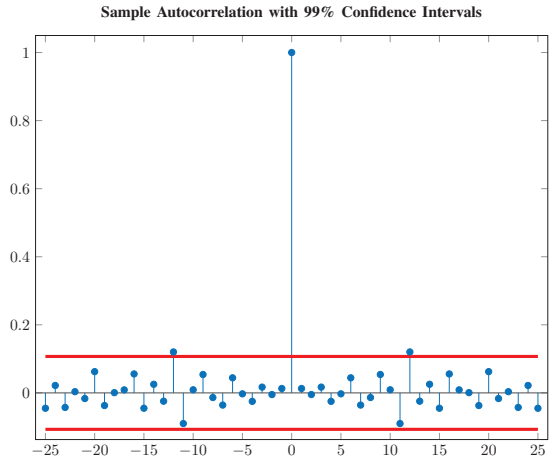


Fig. 6: Residuals for identified model using simulation data

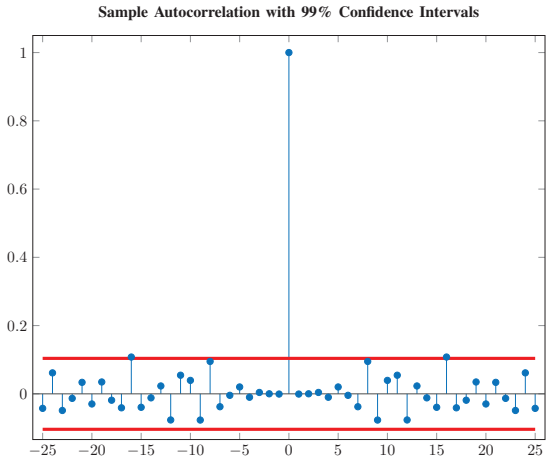


Fig. 7: Residuals of identified transfer function using data from PMU

can calculate the normalized root mean square error (NRMSE) given by the following equation.

$$\text{NRMSE} = 100(1 - \frac{||y[n] - \hat{y}[n]||}{||y[n] - \bar{y}||}) \tag{20}$$

where:

$y[n]$: is a measured output signal.
$\hat{y}[n]$: is a signal simulated using a $u[n]$ as the input signal to the identified model $G_1(z, \hat{\theta}_N)$.
$\bar{y}[n]$: is the average of $y[n]$.

The result of such a cross validation is presented in Fig. 5. One will see that the response of the estimated function follows the analytical one closely. One can also see that the NRMSE value is very high, further indicating that the model performs well.

Another useful test is the residual test for the model structure. This test is useful, because it gives information on whether or not the correct model structure was chosen. The idea behind the test is to take the autocorrelation of (13), with the autocorrelation defined by (21).

$$\hat{R}_\epsilon^N(\tau) = \frac{1}{N}\sum_{n=1}^{N-\tau} \epsilon[n+\tau, \hat{\theta}]\epsilon[n, \hat{\theta}] \tag{21}$$

From the proof for consistent results we recall that if $\mathcal{S} \in \mathcal{M}$ all the terms of (13) except for the first term will approach zero. This means that if $\mathcal{S} \in \mathcal{M}$ the autocorrelation of (13) will approach zero for all $\tau \neq 0$. For $\tau = 0$ it will approach the variance of $e_1[n]$. The idea behind the test is then to use this fact to plot values of $\hat{R}_\epsilon^N(\tau)$ for different values of $\tau$ against the 99% confidence interval. The results from the residual test is presented in Fig. 6, where one can see that the residues are within or close to the confidence interval. From this we can conclude that a good model structure was chosen.

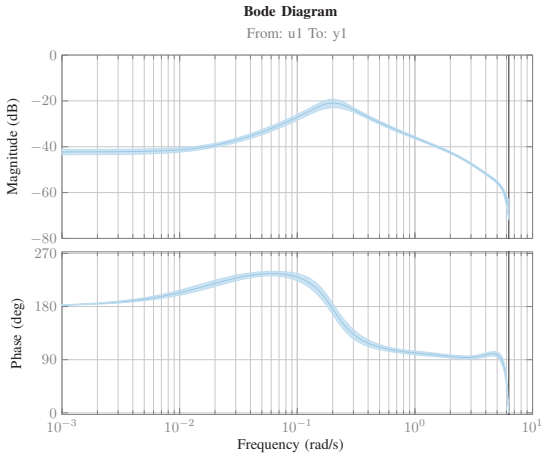


Fig. 8: Bode plot of identified transfer function using data from PMU

## V. Results using PMU measurements

Since some assumptions were made for both the analytical validation and the simulation results it is also useful to investigate whether or not one will get good results using data from a real power system. This was done by collecting data from a generation plant in the Norwegian power system using a PMU. The preparation of the data was done in the same way as for the simulation case. For the PMU data the following model order was selected $[4, 5, 6, 5, 0]$.

In Fig. 7 one can see that the residues are within an acceptable range. Since we don't know the actual model of the plant we can't compare the bode plot to an analytical

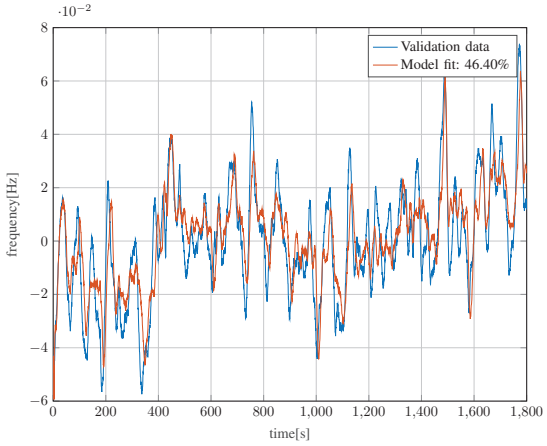


Fig. 9: Compare from PMU

function. However, one can still inspect the bode plot to see whether or not it look reasonable. It is clear from Fig. 8 that the obtained model resembles the one from the simulation validations. In addition the uncertainty corresponding to two standard deviations is shown in the plot. The confidence region of the model was calculated from the covariance of the parameter vector using the system identification toolbox in MATLAB [11]. For expressions for the covariance matrix one may refer to [9]. The plot shows that the uncertainty is rather low indicating that a decent estimate of the plant's dynamic behaviour has been obtained. However, as one can see from Fig. 9 we observe a low NRMSE that could be explained by a large noise power, but further analysis will be necessary.

## VI. Conclusions

Several papers have already investigated system identification for identifying turbine and turbine governor dynamics using PMU measurements. However, no theoretical validation have been attempted before now. It was shown that the identification is indeed possible and that consistent results can be obtained. It is also worth noting that what one identifies is both the turbine dynamics including the governor as well as the electromechanical dynamics.

It still remains to investigate the implications on some of the assumptions made in this paper. However, the proposed method should provide a quick and easy method for TSOs to check whether or not production plants are well tuned, with respect to the droop settings and frequency response.

## Acknowledgements

The work presented in this paper was carried out in the project OperaGrid funded by the Norwegian research council. In addition the ELECTRA IRP FP7 project funded the research exchange between NTNU and Ampere Lab.

## References

[1] Statnett, Fingrid, Energinet.DK, and S. Kraftnät. (2016). Challenges and opportunities report, (visited on 08/30/2016).

[2] H. G. Aghamolki, Z. Miao, L. Fan, W. Jiang, and D. Manjure, "Identification of synchronous generator model with frequency control using unscented kalman filter," *Electric Power Systems Research*, vol. 126, pp. 45–55, Sep. 2015, ISSN: 0378-7796. DOI: 10.1016/j.epsr.2015.04.016. [Online]. Available: http://www.sciencedirect.com/science/article/pii/S0378779615001224 (visited on 01/18/2016).

[3] Dinh Thuc Duong, Kjetil Uhlen, Stig Løvlund, and Erik Alexander Jansson, "Estimation of hydro turbine-governor's transfer function from PMU measurements," presented at the IEEE PES General Meeting, Boston: IEEE, Jul. 2016.

[4] N. D. Hatziargyriou, E. S. Karapidakis, G. S. Stavrakakis, I. F. Dimopoulos, and K. Kalaitzakis, "Identification of synchronous machine parameters using constrained optimization," in *Power Tech Proceedings, 2001 IEEE Porto*, vol. 4, 2001, 5 pp. vol.4–. DOI: 10.1109/PTC.2001.964812.

[5] S. H. Jakobsen and K. Uhlen, "Vector fitting for estimation of turbine governing system parameters," in *2017 IEEE Manchester PowerTech*, Jun. 2017, pp. 1–6. DOI: 10.1109/PTC.2017.7980855.

[6] B. Mogharbel, L. Fan, and Z. Miao, "Least squares estimation-based synchronous generator parameter estimation using PMU data," in *2015 IEEE Power Energy Society General Meeting*, Jul. 2015, pp. 1–5. DOI: 10.1109/PESGM.2015.7286559.

[7] Working Group on Prime Mover and Energy Supply Models for System Dynamic Performance Studies, "Hydraulic turbine and turbine control models for system dynamic studies," *IEEE Transactions on Power Systems*, vol. 7, no. 1, pp. 167–179, Feb. 1992, bibtex: ieee_wg_1992, ISSN: 0885-8950. DOI: 10.1109/59.141700.

[8] S. H. Jakobsen and K. Uhlen, "Development of a test system for identification of turbine dynamics using the dc power flow," presented at the Mathmod, Feb. 2018.

[9] L. Ljung, *System identification*. Springer, 1998. (visited on 03/29/2016).

[10] L. Saarinen, P. Norrlund, U. Lundin, E. Agneholm, and A. Westberg, "Full-scale test and modelling of the frequency control dynamics of the nordic power system," in *2016 IEEE Power and Energy Society General Meeting (PESGM)*, Jul. 2016, pp. 1–5. DOI: 10.1109/PESGM.2016.7741711.

[11] *System identification toolbox*, 2016. [Online]. Available: https://se.mathworks.com/products/sysid.html.

## Paper IV

# System identification techniques for validating power plant's compliance with new draft frequency control requirements

Symposium Aalborg, Denmark
4th-7th June 2019

126

# System identification techniques for validating hydro power plant's FCR performance

**S.H. JAKOBSEN*, K. UHLEN*, P. LIE+**
**Norwegian University of Technology and Science*, Statkraft+**
**Norway**

## SUMMARY

In response to recent years' concern of deteriorating system frequency quality in the Nordic power system, the Nordic TSOs are developing new requirements for frequency containment reserves (FCR). These requirements outline extensive tests, which the power plant owners have to perform to qualify to deliver FCR.
In the tests the power plant owners have to perform a number of open loop tests for each operating state of interest in order to document fulfillment of the requirements. The frequency input to the governor is to be replaced by a signal generator simulating frequency steps and 10 different sine tests. The transfer function from the input of the governor to the electrical power of the generator are then estimated at the frequencies of the sine tests. The drawback of this approach is that it is both time consuming and intrusive.
We suggest another approach where the transfer function from the electrical power of the generator to the electrical angular speed of the machine's rotor is estimated while the plant is in normal operation. This means that the approach is completely non-intrusive. In case measurements of the angular speed of the machine's rotor is not available we suggest to use the measured power system frequency as an estimate.
We demonstrate and compare our approach to the approach proposed in the new draft requirements using data from a PMU, and control system data obtained from two different power plants in the Norwegian power system. Results using our approach and data from a PMU is compared to results obtained using the approach and the testing procedure described in the draft requirements. In addition we test our approach on a second plant where we use data from the plant's control system. During these tests we demonstrate that the approach is able to capture changes in the parameters of the plant's governor.

## KEYWORDS

**FCR requirements, frequency control, system identification, hydro power, PMU**

**sigurd.h.jakobsen@ntnu.no**

## 1 INTRODUCTION

The Nordic transmission system operators (TSO)s are currently developing new requirements for frequency containment reserves (FCR). In the draft requirements [5] they require the power plant owners to do extensive testing on the power plants. As a response to this, the paper [3] investigated whether or not a model of a hydro plant governor could be estimated using data from a phasor measurement unit (PMU) during normal operation. The advantage of this approach is that it is non-intrusive unlike what is proposed in the draft requirements. Other non intrusive approaches have also been proposed in [1, 6, 10], however these use data from disturbance recordings.
Building on the work in [3] the paper [7] proved under which conditions a PMU based approach using measurements from normal operation would give a consistent estimate of the identfied model. Moreover, [7] showed that using PMU measurements one would find the transfer function describing the plant's disturbance rejection. This is among one of the transfer functions described in the new draft requirements. Consequently, it means that parts of the requirements can be directly checked using PMU measurements from normal operation without any disturbance to the power plant's operation.
In the present paper we will build upon the approach described in [7] and show how both the stability margin and disturbance rejection of a hydro power plant can be estimated using measurements from either a PMU or the plant's control system. We also analyse the transfer function one identifies if one follows the approach of [5]. This is important as this transfer function is not presented in [5] and it should be verified if it can indeed be used for checking the requirements. We then proceed to compare our approach with the one proposed in [5]. The comparison will be performed using datasets from a power plant in the Norwegian power system. Our approach is tested using measurements from a PMU and compared to tests done according to the procedures described in [5]. We also test our approach on a second plant where we use data collected from the control system. On this plant we also check if the approach can detect changes in the parameters of the governor.

## 2 THEORY

### 2.1 Requirements for the power plant

In [4] the requirements are derived using a power plant model consisting of all the power plants in the system aggregated together, we will instead use the generic model of one power plant depicted in Figure 1. The plant is assumed to be grid connected, however, for simplicity only the elements needed to explain the requirements are included. The model consists of $G_p(s)$, which represents the governor, turbine and servo dynamics, and $G_J(s)$, which represents the swing dynamics. The signals in the figure are the reference speed signal $\Delta\omega_{ref}(s)$, the mechanical power of the turbine $\Delta P_m(s)$, the electrical power $\Delta P_e(s)$ and the machine speed $\Delta\omega(s)$.
The stability of the closed loop depicted in Figure 1 can be analysed by investigating the loop transfer function

$$L(s) = G_p(s)G_J(s) \tag{1}$$

One common approach for analysing the stability is to plot the loop transfer function in a Nyquist diagram as the one presented in Figure 2. The stability analysis is done by investigating whether or not the point $-1$ is encircled by the loop transfer function. In the presented figure we have zoomed in to this point to demonstrate the stability margin $M_s$, which is the smallest

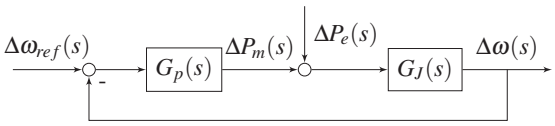


*Figure 1: Block diagram of a power plant*

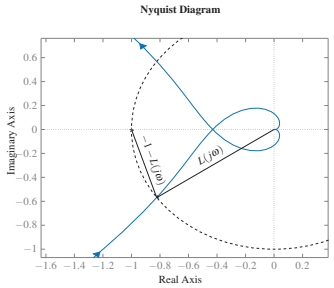


*Figure 2: Nyquist diagram of $L(s)$*

*Table 1: Time periods of the simulated sine signals*

| | | | | | | | | | |
|---|---|---|---|---|---|---|---|---|---|
| 10 | 15 | 25 | 40 | 50 | 60 | 70 | 90 | 150 | 300 |

distance between the loop transfer function and the point $-1$.

$$M_s = \min|-1-L(j\Omega)| \tag{2}$$

In the theoretical framework for the new draft requirements [4] they propose to put a lower limit on the stability margin and to analyse it using the sensitivity function

$$S(s) = \frac{1}{1+L(s)} \tag{3}$$

The limit is set on the sensitivity function as follows:

$$\max|S(j\Omega)| < \frac{1}{M_s} \tag{4}$$

For the limit on the performance we look at the transfer function from the electrical power to the speed deviation. The idea is that if random variations in electric power do not lead to large speed deviations for any of the power plants in the system, then the frequency deviation will also be small. The relation between the speed deviation and the electrical power is given by.

$$\Delta\omega(s) = G_1(s)\Delta P_e(s) \tag{5}$$

where

$$G_1(s) = -G_J(s)S(s) \tag{6}$$

The performance requirements are thus set on $G_1(s)$.

### 2.2 Checking the requirements as proposed in the draft requirements

In [4] they propose to replace the frequency input to the governor with sine signals. Ten different time periods, given in Table 1, are simulated while measuring the generating unit electric power. The setup is presented in Figure 3, where $r(s)$ represents the sine signals. In Figure 3 one can see that the transfer function from $r(s)$ to $P_e(s)$ is:

$$G_{req}(s) = \frac{G_p(s)G_J(s)K}{s+G_J(s)K} \tag{7}$$

The factor $K$ in (7) can be found by realising that the power of a synchronous machine is given by [2]

$$P_e = \frac{3V_tE_a\sin\delta}{X_s} \tag{8}$$

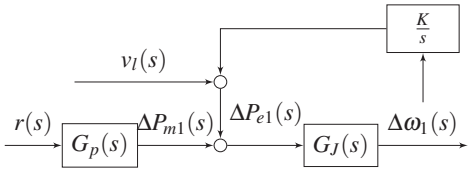


*Figure 3: The setup used to find the transfer functions in [4, 5]*

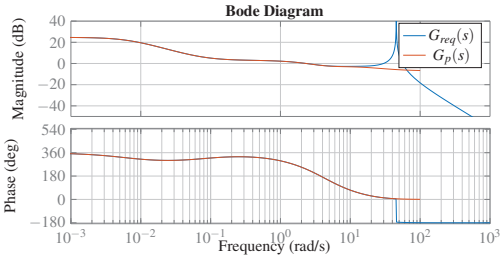


*Figure 4: Comparison of $G_p(s)$ and $G_{req}(s)$*

where $V_t$ is the terminal voltage of the machine, $E_a$ is the internal voltage, $\delta$ is the angle between the terminal and internal voltage and $X_s$ is the synchronous reactance. By assuming constant voltages and linearising we get:

$$\Delta P_e(s) = \frac{K}{s}\Delta\omega(s) + v_l(s) \tag{9}$$

where $v_l(s)$ represents the part of the change in the electric power due to changes in the rest of the power system. The contribution from $v_l(s)$ will increase the variance in the estimate of $G_{req}(s)$.

To check if $G_{req}(s)$ is a good estimate of $G_p(s)$ we will insert the following expression for $G_J(s)$ into (7)

$$G_J(s) = \frac{1}{2Hs + K_d} \tag{10}$$

With this we get

$$G_{req}(s) = \frac{G_p(s)K}{K - s(K_d + 2Hs)} \tag{11}$$

In other words $G_{req}(s)$ is the transfer function $G_p(s)$ and a low pass filter. This is demonstrated in Figure 4 where $G_p(s)$ and $G_{req}(s)$ are plotted together and we can see them following each other closely up to a certain frequency.

To obtain the transfer function the draft requirements propose to obtain the fourier transforms of the measured signals $r(j\Omega_p)$ and $\Delta P_{e1}(j\Omega_p)$ where $\Omega_p$ is the frequency of the simulated sine signal. By doing this one can calculate $G_{req}(j\Omega_p) = \Delta P_e(j\Omega_p)/\Delta\omega(j\Omega_p)$ for several frequencies to obtain an estimate for $G_{req}(s)$.

What remains is to obtain estimates for $S(s)$ and $G_1(s)$. To do this an estimate of the total swing dynamics have been estimated given by [4].

$$G_{J_{sys}}(s) = \frac{600MW}{0.1Hz}\frac{f_0}{S_{sys}}\frac{1}{2H_{sys}s + K_{d_{sys}}f_0} \tag{12}$$

To use the system swing dynamics for each plant the following per unit system was defined. The base value for each plant is given as it's static gain[1] that is

$$G_p^{(p.u.)}(s) = G_p(s)/G_p(0) \tag{13}$$

The base value for $G_{J_{sys}}(s)$ is given as the sum of the static gains of all the power plants in the system, that is

$$G_{J_{sys}}^{(p.u.)}(s) = G_J(s)\sum_i^{N_g} G_{p_i}(0) \tag{14}$$

[1] The static gain of the plant is closely related to its droop

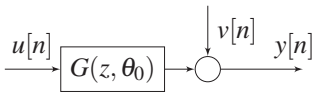


*Figure 5: System assumed by the identification*

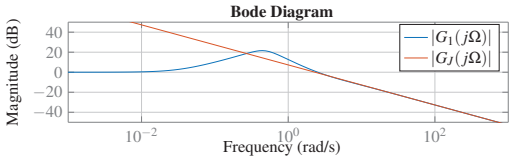


*Figure 6: Comparison of $G_J(s)$ and $G_1(s)$.*

The transfer functions $S^{(p.u.)}(s)$ and $G_1^{(p.u.)}(s)$ are then estimated as

$$S^{(p.u.)}(s) = \frac{1}{1 + G_{J_{sys}}^{(p.u.)}(s) G_p^{(p.u.)}(s)} \tag{15}$$

and

$$G_1^{(p.u.)}(s) = S^{(p.u.)}(s) G_{J_{sys}}^{(p.u.)} \tag{16}$$

### 2.3 Our proposal for checking the requirements

We propose that the requirements can be checked without actually doing any tests. That is one can just let the plant operate normally and use PMU or control system measurements to identify the models, which can be used for checking the requirements. Moreover, if one uses the system identification methods we use, one can do the open loop test proposed in the new requirements with only one dataset.

To do the identification we will use prediction error identification using discrete time. In this approach one assumes that the system one wants to identify has the structure depicted in Figure 5. We will refer to the system we want to identify as the true system $\mathscr{S}$ and we will mathematically describe it as:

$$\mathscr{S} : y[n] = G(z, \theta_0) u[n] + v[n] \tag{17}$$

where $z^{-1}$ is the time delay operator, $v[n] = H(z, \theta_0) e[n]$, where $e[n]$ is white noise and $\theta_0$ is the parameter vector parametrizing the true system $\mathscr{S}$. We will assume that our true system can be described by a box-Jenkins model:

$$G(z, \theta_0) = \frac{\sum_{i=1}^{n_b} b_i z^{-i}}{\sum_{i=0}^{n_f} f_i z^{-i}}, H(z, \theta_0) = \frac{\sum_{i=1}^{n_c} c_i z^{-i}}{\sum_{i=0}^{n_d} d_i z^{-i}} \tag{18}$$

The true parameter vector is thus

$$\theta_0 = \begin{bmatrix} b_1 \dots b_{n_b} & 1 & f_1 \dots f_{n_f} & c_1 \dots c_{n_c} & 1 & d_1 \dots d_{n_d} \end{bmatrix} \tag{19}$$

The aim of the system identification procedure is, then to, given a dataset $Z^N = \{u[n], y[n] | 1 \dots N\}$ containing $N$ samples, to find an estimate $\hat{\theta}_N$ of the true parameter vector $\theta_0$. For finding our estimate $\hat{\theta}_N$ we will use prediction error identification [8]. The aim of prediction error identification is to find the parameter vector $\hat{\theta}_N$ minimizing the prediction error. The prediction error is defined as:

$$\varepsilon[n, \theta] = H^{-1}(z, \theta)(y[n] - G(z, \theta) u[n]) \tag{20}$$

We see that if we insert the true system into (20) the prediction error will be $e[n]$, which makes sense as even the true system cannot predict the white noise representing process noise and other unmodelled dynamics. We can now find our estimate as the argument minimising (20), or in other words

$$\hat{\theta}_N = \arg\min_{\theta} \frac{1}{N} \sum_{n=1}^{N} \varepsilon^2(n, \theta) \tag{21}$$

To be more precise we should before moving onto the identification ensure that our dataset $Z^N$ will lead to a consistent estimate of what we want to identify. In our case we should investigate $G_1(s)$ using the dataset $Z_1^N = \{u_1[n], y_1[n] | 1 \dots N\}$ where $u_1[n]$ is the sampled version of $\Delta P_e(s)$ and $y_1[n]$ is the sampled version of $\Delta\omega(s)$. However, the consistency of this identification experiment has already been covered in [7].
We will also for the sake of comparison show that $G_{req}(s)$ can be identified using only one test instead of ten tests as proposed in the draft requirements. To do this we will use the dataset $Z_2^N = \{u_2[n], y_2[n]\}$ where $u_2[n]$ is the sampled version of $r(s)$, and $y_2[n]$ is the sampled version of $\Delta P_{e1}(s)$. This dataset is assumed generated when the plant is operating in open loop as depicted in Figure 3. It is therefore identification in open loop a topic thoroughly covered in [8].
As already stated our aim is to estimate a model of $G_1(s)$ and $S(s)$ using data from normal operation. What remains is to find an estimate for $S(s)$. If one investigates Figure 6 one see that the slope of $G_1(s)$ and $G_J(s)$ is almost the same for faster dynamics. This means that one can estimate the slope of $G_J(s)$ from $G_1(s)$. From Figure (10) one can see that the swing equation consists of two parameters the inertia constant $H$ and the speed damping $K_d$. Normally, one can assume that $2H >> K_d$. We will therefore assume that the slope of $G_1(s)$ is completely determined by $H$. To find an estimate of $H$ we choose to interpolate between to frequencies to reduce the effect of errors.

$$H \approx \frac{\Omega_2 - \Omega_1}{2\Omega_1\Omega_2(|G_1(j\Omega_1)| - |G_1(j\Omega_2)|)} \tag{22}$$

We can now find $S(s)$ as follows

$$S(s) \approx 2HsG_1(s) \tag{23}$$

## 3 METHODOLOGY

Our methodology for checking the requirements rely heavily on the system identification toolbox [9] available for MATLAB. We will in this section show how collected data can be used together with the system identification toolbox to deduce models which can be used for checking the requirements.
Essentially the methodology consists of the following steps:

**Data collection** In this step data is collected either from a PMU or from the control system of a hydro power plant.

**Preprocessing of data** The collected data should be passed through a low pass filter, decimated and the average removed.

**Order selection** One should make sure that the correct model order is chosen. This can be seen as an iterative process, where one first tries a high order model. Then one should do a residual test on the model. It is also good to look for pole zero cancellation, and reduce the order of the transfer function numerator to remove any. If the model passes the test one can try with a lower order and then continue reducing the order until the model doesn't pass the tests anymore. An example of this process is shown in Figure 7. Here four attempts of identifying $G_p(s)$ of a power plant in the Norwegian system is shown. One can see that all the transfer functions except one pass the residual test. We therefore discard the one not passing the residual test. For the other transfer functions we see that all except one has pole zero cancellation. The pole zero cancellation can be seen as the spikes on the bode diagram. We therefore keep the transfer function drawn in red, which passes all the tests.

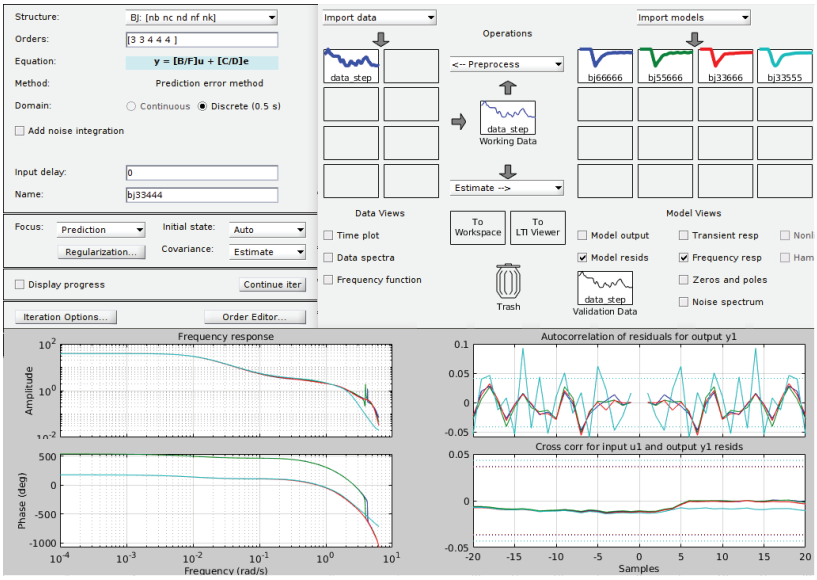


*Figure 7: System identification toolbox [9] workflow*

## 4 RESULTS

To demonstrate our approach and compare it to the draft requirements we use data sets from tests performed at two power plants in the Norwegian system. At the first power plant a test according to the new requirements were performed. Moreover, measurements from a PMU were obtained at the same plant and used for comparison. On the second plant we obtained measurements from the control system while the plant was operating normally.

### 4.1 Comparison of our approach and the one in the draft requirements

The single line diagram of the part of the plant we investigated is depicted in Figure 8. Our approach was tested on PMU data from the high voltage side of the transformer. The approach from the new requirements were tested using datasets from tests done by Statkraft according to the new draft requirements. In Figure. 9 an example of a sine sweep and a step test from the Statkraft tests are presented together with the PMU measurements.

In Figure 10 we have plotted bode diagrams of estimates of the transfer functions $G_{req}(s)$. Two of the estimates where obtained using the system identification toolbox and have been plotted with the 95% confidence interval. One estimate was obtained using measurements from one sine sweep. During the sine sweeps the plant was providing FCR-N and during the step test it was providing FCR-D. One can see from the figure that the variance is smaller using the step test recording than the sine sweep. This is to be expected as the step provides better excitation than one sine wave. We can use the sine sweep for the identification since it consists of many small steps. The third estimate is obtained by following the procedure from the draft requirements. We can see that this estimate follows the other estimates quite well. However, it only gives the transfer function at discrete frequencies. Moreover, the estimate captures a smaller range of the dynamics.

Now that we have tested two different ways of finding $G_{req}(s)$. We will compare the sensitivity function and disturbance rejection function obtained using our approach and the approach described in the draft requirements. Our approach was performed with the measurements obtained

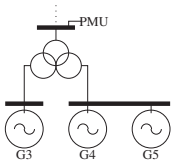


*Figure 8: Single line diagram of the power plant*

*Table 2: Droop setting and $G_1(0)$*

| Droop | 60*min* | 45*min* | 30*min* | 15*min* |
|---|---|---|---|---|
| 10% | 9.5% | 9.5% | 9.5% | 9.5% |
| 6% | 6.2% | 6.0% | 5.9% | 6.1% |
| 5% | 4.9% | 4.9% | 5.0% | 5.1% |
| 3% | 3.1% | 3.1% | 3.1% | 2.9% |
| 2% | 2.0% | 1.8% | 1.8% | 1.7% |

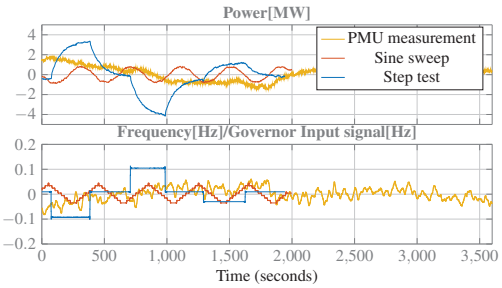


*Figure 9: Example of collected datasets*

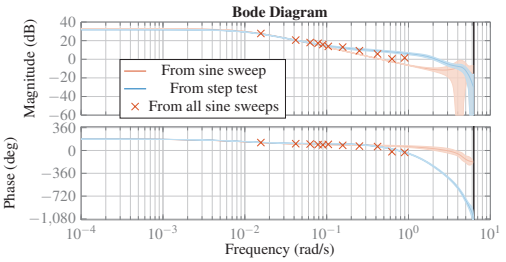


*Figure 10: Comparison of estimate of $G_{req}(s)$ obtained using box-Jenkins and fft*

from the PMU. The approach described in the draft requirements were obtained using the step test and one sine sweep. To make it easier to compare we did the draft requirement's approach using the system identification toolbox instead of the fast Fourier transform. The result of estimating the disturbance rejection function is presented in Figure 11. The results are presented in per unit, where the base value has been calculated from the steady state gain of the estimates. It is of interest to observe that the estimate obtained using the step test has a better disturbance rejection than the one obtained using the sine test, as the plant was providing FCR-D during the step test. The slope of the estimate is different for our approach than the one described in the draft requirements. This is to be expected as our approach estimates all of the dynamics using local measurements. Whereas, the fast dynamics in the other approach is derived from an estimate of the total system inertia. The estimate of the obtained sensitivity function is depicted in Figure 12. In this case we see that the steady state gain of the estimate obtained using the PMU differs quite a lot from the two other estimates. This is due to the fact that we have assumed that there is no speed damping. However, since it is the peak of the transfer function that is important for the stability margin this is not a problem.

The results using the different approaches are not directly comparable since they have been obtained at different loading levels and more than a year apart. However, at least one can see that the PMU measurement estimate and the step test estimate give similar results.

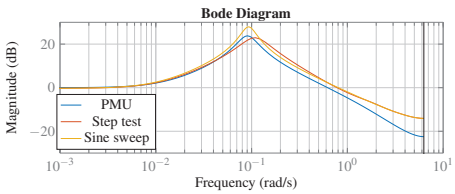


*Figure 11: Comparison of $G_1(s)$ obtained using all datasets depicted in Figure 9 and a box-Jenkins model structure*

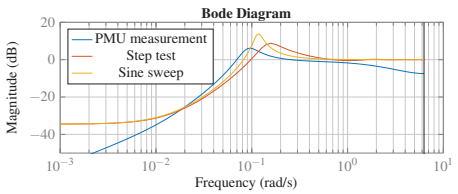


*Figure 12: Comparison of $S(s)$ obtained using all datasets depicted in Figure 9 and a box-Jenkins model structure*

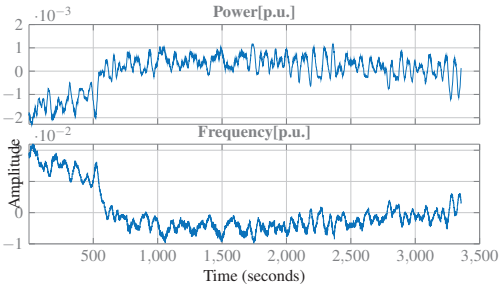


*Figure 13: Signals from control system*

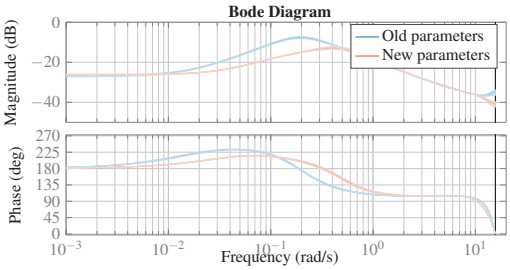


*Figure 14: Estimate of $G_1(s)$ new and old tuning*

### 4.2 Measurements from the control system of a power plant operating normally

When using PMU measurements for obtaining the estimate one have to keep in mind that there may be some losses in the active power of the plant, which are not accounted for. In addition the closer to the generator one measures the power system frequency the better we can assume it to estimate the electrical angular speed of the machine's rotor. It is therefore of interest to see how our approach performs when one uses measurements obtained as close as possible to the generator. This can be achieved if one has access to the control signals of a modern hydro turbine governor.

Another advantage of having access to the control system of a hydro power plant is that it allows us to test if the method is able to capture changes in the governor parameters. We therefore did a test at one of Statkraft's power plants where we connected a computer to the control system of the governor. The tests consisted of letting the plant run for one hour, before we changed the governor parameters. The plant was also set to operate with a constant load during the tests. While the parameters where changed we did not record anything, which means that the datasets may be a few minutes shorter than one hour. An example of a dataset is presented in Figure 13. This dataset was obtained with a droop setting of 2%.

Based on the tests performed on the other power plant, new parameters for the PID part of the governor was calculated. Although, these parameters were calculated for another plant we compared these new parameters with the old parameters for this plant. A result of this is shown in Figure 14, where one can see that the proposed approach can indeed detect the parameter change. One can also see that the new parameters give a better disturbance rejection than the old parameters.

We also tested several different droop settings. The result of this is given in Figure 15. All the estimates in this figure is performed while the plant is operated using the new PID parameters. However, for the droop setting of 10% and 6% a smaller proportional gain is used than for the other cases. One can clearly see that the approach captures both the change in the droop and the proportional gain. The approach's sensitivity to different lengths of the dataset is demonstrated in Figure 16, where one can see that the results are quite reasonable for all lengths except for the 15 minutes dataset. The steady state gain for the transfer functions in Figure 15 is presented together with the droop setting in table 2 for different lengths of the datasets. As expected the values are quite close.

## 5 CONCLUSIONS

We have in this paper demonstrated that requirements on a hydro power plant's stability margin and disturbance rejection can be checked using both PMU measurements, and data from the plant's control system under normal operation. This will save power plant owners both time

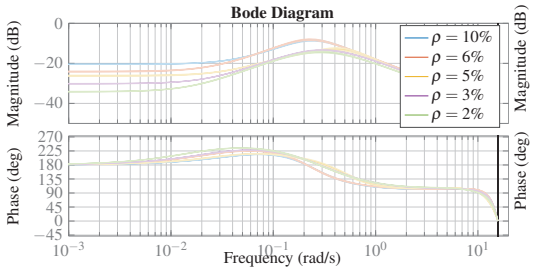


*Figure 15: $G_1(s)$ with different droop settings*

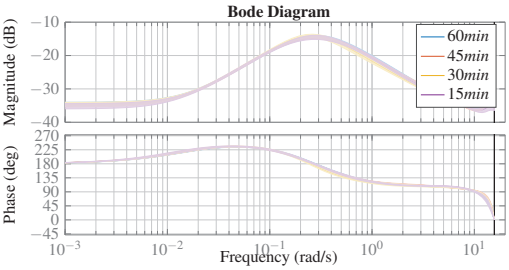


*Figure 16: $G_1(s)$ obtained using different signal length*

and money compared to approaches were it is proposed to perform multiple tests to excite the plant. The results were demonstrated using measurements from tests performed at two different power plants in the Norwegian power system and the results from both plants were promising. One of the tests showing promising results were even obtained using PMUs. This means that the TSOs can obtain an estimate of a plant's performance using their own measurements. We therefore believe that, if the TSOs will pursue the approach of setting requirements for FCR in the frequency domain, a less intrusive approach for the tests could be used.

## REFERENCES


[1] Hossein Ghassempour Aghamolki, Zhixin Miao, Lingling Fan, Weiqing Jiang, and Durgesh Manjure. Identification of synchronous generator model with frequency control using unscented Kalman filter. *Electric Power Systems Research*, 126:45–55, September 2015.

[2] Stephen J. Chapman. *Electric machinery and power system fundamentals*, volume 3. McGraw-Hill New York, 2002.

[3] Dinh Thuc Duong, Kjetil Uhlen, Stig Løvlund, and Erik Alexander Jansson. Estimation of Hydro Turbine-Governor's Transfer Function from PMU Measurements. Boston, July 2016. IEEE.

[4] Robert Eriksson, Niklas Modig, and Andreas Westberg. FCR-N DESIGN OF REQUIREMENTS. ENTSO-E report, July 2017.

[5] Prequalification Working Group. Technical Requirements for Frequency Containment Reserve Provision in the Nordic Synchronous Area. Draft, June 2017.

[6] N. D. Hatziargyriou, E. S. Karapidakis, G. S. Stavrakakis, I. F. Dimopoulos, and K. Kalaitzakis. Identification of synchronous machine parameters using constrained optimization. In *Power Tech Proceedings, 2001 IEEE Porto*, volume 4, pages 5 pp. vol.4–, 2001.

[7] S. H. Jakobsen, K. Uhlen, and X. Bombois. Identification of hydro turbine governors using PMU data. In *2018 IEEE International Conference on Probabilistic Methods Applied to Power Systems (PMAPS)*, pages 1–6, June 2018.

[8] Lennart Ljung. *System identification*. Springer, 1998.

[9] Mathworks. System Identification Toolbox, 2018.

[10] B. Mogharbel, L. Fan, and Z. Miao. Least squares estimation-based synchronous generator parameter estimation using PMU data. In *2015 IEEE Power Energy Society General Meeting*, pages 1–5, July 2015.

# Paper V

# Testing of a hydro power plant's stability and performance using PMU data

IET Research Journals

IET Journals
The Institution of Engineering and Technology

# Testing of a hydro power plant's stability and performance using PMU and control system data in closed loop

ISSN 1751-8644
doi: 0000000000
www.ietdl.org

*Sigurd Hofsmo Jakobsen Kjetil Uhlen*

*Department of Electric Power Engineering*
*Norwegian University of Science and Technology,*
*Trondheim, Norway * E-mail: sigurd.h.jakobsen@ntnu.no*

**Abstract:** In response to recent concerns for deteriorating frequency quality in the Nordic power system, the Nordic TSOs have developed draft requirements for the frequency containment reserves (FCR). These requirements outline extensive tests, which the power plant owners have to perform to qualify to deliver FCR. In this paper we demonstrate that one can check these requirements while the plant is in normal operation using measurement readily available from the plant's control system or a phasor measurement unit (PMU) and standard system identification techniques.
The validity of the proposed approach is demonstrated using Monte Carlo Simulation (MCS) to investigate the effect of the main assumption and potential nonlinearities affecting the approach. Data from real power system operation is also used to demonstrate the approach.

## 1 Introduction

The Nordic TSOs have developed draft requirements for the frequency containment reserves (FCR)[5]. These requirements outline extensive tests, which the power plant owners have to perform to qualify to deliver FCR. In the proposed tests the power plant owners have to measure the plant's response to several sine tests for each operating state of interest. This is a time consuming and expensive approach. Other approaches should therefore be investigated. In the literature it has been proposed to identify hydro power plant dynamics using data from normal system operation obtained using phasor measurement units (PMUs) [3, 6, 7, 12]. Consequently, a natural next step is to investigate whether or not it can be checked if the plants are fulfilling the requirements using any of these approaches.

The papers [3, 12] use the ARX and ARMAX model structure to perform the identification whereas [6] use time domain vector fitting. The papers [3, 6, 12] validated their approaches by comparing the performance of the identified models with measured data. In [7] it was proven, given some technical conditions, that the use of PMU data would indeed result in a consistent estimate of transfer function used for checking a plant's performance in the new requirements.

An important contribution in [4], which lays the theoretical foundation for the new draft requirements, is to state stability and performance requirements for hydro power plants in terms of the plants' sensitivity function and disturbance rejection. This a good step towards basing the requirements on well established control system principles. We will use the stability and performance requirements from [4] to show that these requirements can also be checked using PMU measurements. This will be demonstrated using simulations and data from a PMU and from tests performed at a power plant in the Norwegian power system. In the simulations we will investigate how the proposed PMU approach performs under the presence of deadband at the input of the governor and with bakclash after the governor servo. The importance of the electrical distance between the PMU and the generator is also investigated.

In [5] they describe the identification from the governor input to the electrical power in open loop. This is a similar approach as [3, 6] where the transfer function from the electrical frequency to the electrical power is estimated using phasor measurements. In [12] it was proposed to estimate the transfer function from the power to the frequency. Similarly, [7] also looked at the identification from the electrical power to the frequency. In this paper we will clear up this confusion by providing precise description of both these transfer functions. We will also show when the different descriptions are valid by considering the fact that the plant can be operated in either closed or open loop during the identification. For the closed loop case we will also investigate what role it plays for the identification whether or not the plant is operated using speed or frequency feedback.

In addition to the discussion on what to use as the input and output signals for the identification we will extend upon the work presented in [9]. In [9] it is shown how the new draft requirements can be checked using PMU measurements while the plant is in normal operation. In this paper we will strengthen the conclusions from [9] by performing Monte Carlo simulations (MCS) using SIMULINK and PSS/E to test the approach from [9]. In the MCS we will investigate the effect of nonlinearities and the assumption that the power system frequency is a good estimate of the machine's speed. This assumption was first presented in [7] and is necessary for performing the identification using PMU measurements.

The outline of the paper is as follows. In Section 2 the modelling used for a hydro power plant is presented. A brief description of the new draft requirements and our proposal are presented in Section 3. In Section 4 we present the different identification experiments proposed for the identification of hydro power plant dynamics. We also shortly describe the proposed methodology for identifying the plants in Section 5. Results from both simulations and real system data is presented in Section 6 and 7. Finally conclusions and further work are presented in 8.

## 2 Power plant model

For the power plant model we will assume the structure depicted in Fig. 1. The transfer function $G_p(s)$ represents the governor, servo and turbine dynamics and $G_J(s)$ represents the swing dynamics of the plant. The swing dynamics are given by the swing equation. A linear version of the swing equation often used is:

$$G_J(s) = \frac{1}{2Hs + K_d} \tag{1}$$

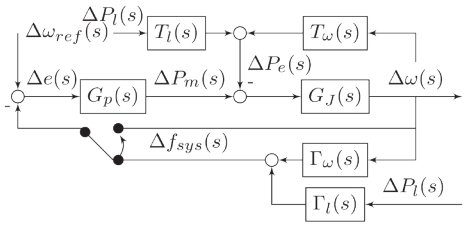


**Fig. 1**: Block diagram of power plant

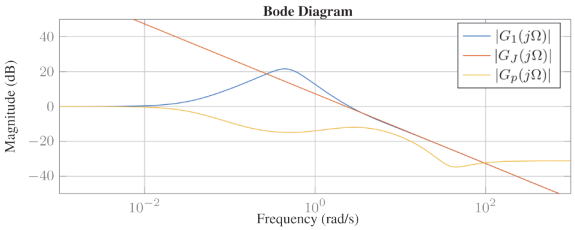


**Fig. 2**: Comparison of transfer functions

Here, $H$ is the inertia constant of the machine and $K_d$ is the speed damping of the generator.

To be able to analyze whether or not one can identify any dynamics at the power plant one needs to analyze how the dynamics are excited. From Fig. 1 one can see that the electric power at the generator bus bar consists of two parts. One which is dependent on the electrical angular rotor speed $\Delta\omega(s)$ through the transfer function $T_\omega(s)$ and one which is dependent on the random load changes in the system $\Delta P_l(s)$ through the transfer function $T_l(s)$. The part generated by the random load changes is the part that provides the external excitation to the system. Without it one would need to add some other external excitation to enable the identification. In addition if the plant is operated with the power system frequency $\Delta f_{sys}(s)$ as the feedback signal instead of $\Delta\omega(s)$ the random load changes will also excite the plant through the transfer function $\Gamma_l(s)$.

To understand some of the transfer functions that are defined one needs to know the equation for the electric power at the generator's bus bar, which is approximated by the following expression [1]

$$P_e(t) = \frac{3V_t(t)E_a(t)\sin\delta_{Ev}(t)}{X_s} \tag{2}$$

where $V_t(t)$ is the terminal voltage of the machine, $E_a(t)$ is the internal voltage, $\delta_{EV}(t)$ is the angle between the internal voltage and the terminal voltage and $X_s$ is the synchronous reactance. If we linearise (2) assuming the voltages to be constant we get the following equation:

$$\Delta P_e(s) = K_{11}(\frac{\Delta\delta(s)}{s} - \Delta\delta_V(s)) \tag{3}$$

where $K_{11}$ is a linearization constant $\delta$ is the electrical rotor angle and $\delta_V$ is the voltage angle at the terminal of the generator. We will now rewrite (3) as a function of the random load changes in the system and the angular electrical speed of the machine's rotor.

$$\Delta P_e(s) = T_l(s)\Delta P_l(s) + T_\omega(s)\Delta\omega(s) \tag{4}$$

Where $T_l(s)$ is the transfer function from the random load changes to the voltage angle $\Delta\delta_V(s)$ at the generator terminal and $T_\omega(s)$ is the transfer function from the electrical angular speed of the machine's rotor $\Delta\omega(s)$ to the electrical angle of the rotor $\Delta\delta(s)$ and the voltage angle of the $\Delta\delta_V(s)$ at the generator terminal. In practice the angular speed of the machine's rotor will not greatly influence the voltage angle of the generator terminal and one can therefore normally write $T_\omega(s)$ as:

$$T_\omega(s) = \frac{K_{11}}{s} \tag{5}$$

From Fig. 1 one can see that whether or not one uses the power system frequency or the angular speed of the machine's rotor as the feedback signal will affect what one is identifying in closed loop. If one is using the power system frequency as the feedback signal one will typical measure it as the derivative of the voltage angle at the generator terminal. The electrical angular speed of the machine's rotor can instead be approximated from the mechanical speed of the rotor using the following relation.

$$\Delta\omega_1(s) \triangleq \frac{p}{2}\Delta\omega_{m1}(s) \tag{6}$$

where $\omega_{m1}(s)$ is the mechanical speed of the rotor and $p$ is the number of pole pairs. One common method for estimating the electrical speed of the rotor is thus to measure the mechanical speed and calculate it using the number of poles.

The change in $\Delta\omega(s)$ due to a change in electrical load is determined by the swing equation and $\Delta\omega(s)$ is therefore a good candidate for a feedback signal to the governor to change the mechanical output and to contain the change in $\Delta\omega(s)$. Moreover, since the hydro power plants investigated are synchronous generators we have that $\Delta f_{sys}(j\Omega < \Omega_c) = 2\pi\Delta\omega(j\Omega < \Omega_c)$ and it will therefore be the same to use the power system frequency as the feedback for dynamics slower than $\Delta\Omega_c$.

## 3 The new requirement

The theoretical background behind the new requirements is presented in [4]. In short they perform a stability and performance analysis on an aggregated system model and then they use a per unit system to formulate the requirement for each plant. The per unit system and aggregated system model used in the draft requirements are presented in the appendix. We will instead present the requirements for the model depicted in Fig. 1. The stability margin of the closed loop consisting of the transfer functions $G_p(s)$ and $G_J(s)$ can be estimated using the sensitivity function $S(s)$ as follows:

$$|S(s)| = \frac{1}{|1 + G_p(s)G_J(s)|} < M_s \tag{7}$$

The performance requirement is stated in terms of the system's disturbance rejection. It uses the idea that the power system frequency should fulfill the following constraint $|\Delta f_{sys}(s)| < 0.1Hz$. Since the machines are synchronous we can write this constraint as a constraint on the change in the machine's electrical angular rotor speed due to a change in electrical power as.

$$\Delta\omega(s) = G_J(s)S(s)\Delta P_e(s) = G_{1_{sys}}(s)\Delta P_e(s) \tag{8}$$

We now see that if we know the power of $\Delta P_e(s)$ we can put requirements on the plant's disturbance rejection given by $G_1(s)$ to try to keep the frequency deviation below $0.1Hz$.

$$|G_1(j\Omega)| < \frac{\sigma_{\omega_{req}}}{\sqrt{\phi_{P_e}(j\Omega)}} \tag{9}$$

where $\sigma_{\omega_{req}}$ is the variance of the change in electrical rotor speed when it is assumed white and subjected to $|\omega(j\Omega)| < 0.2\pi$.

In the new draft requirement they propose to find $G_1(s)$ and $S(s)$ by identifying $G_p(s)$ and then to use the estimate together with an estimate of $G_J(s)$, which has been derived from an estimate for the total system inertia of the Nordic Synchronous area. When checking

the stability requirements they use an estimate from a low inertia operating state. We will refer to the sensitivity function obtained using the minimum system inertia as $S_{\min}(s)$. Similarly, they use the average system inertia when finding $G_1(s)$ and we will refer to this estimate as $G_{avg}(s)$.

We will, instead of using a system based estimate for the machine's inertia for the estimate of $G_J(s)$, estimate both $S(s)$ and $G_1(s)$ based on measurements obtained locally at the plant. As was shown in [7] $G_1(s)$ can easily be identified by measuring electrical power and frequency. We will now show how $S(s)$ can be approximated from an estimate of $G_1(s)$. In Fig. 2 we have plotted $G_1(s)$, $G_J(s)$, and $G_p(s)$ for a hydro power plant. The transfer functions are plotted per unit where the base for $G_p(s)$ is $G_p(0)$ and the base for the two other transfer functions are $G_1(0)$. In the rest of this paper transfer functions will be plotted using this per unit system if not stated otherwise. From the figure one see that the dynamics of $G_1(s)$ are completely determined by the swing dynamics for faster dynamics. Due to the physics of the system this will always be the case. If we now assume the speed damping of the machine to be negligible we can use (1) and interpolation* to obtain the following expression for the machine's inertia

$$H \approx \frac{\Omega_2 - \Omega_1}{2\Omega_1\Omega_2(|G_1(j\Omega_1)| - |G_1(j\Omega_2)|)} \tag{10}$$

We can now find $S(s)$ as follows

$$S(s) \approx 2HsG_1(s) \tag{11}$$

## 4 Tests for validating the plants

In the draft requirements [5] they require the power plant owners to estimate the transfer function from the input of the governor to the electrical power at the generator bus bar. However, in [7] we identify the transfer function from the electrical power at the generator bus bar to the machine speed. Clearly, both approaches cannot simultaneously be correct. To investigate which approach is correct we will present both transfer functions and look at whether or not they can be identified for the following cases:

**Case 1**: The plant is operating under normal conditions with speed feedback and we have access to the control system signals.
**Case 2**: The plant is still operating under speed feedback, but we don't have access to the control system signals for the identification and therefore use frequency as an estimate for the speed.
**Case 3**: The plant is operating with frequency feedback and we have access to the frequency measurements.
**Case 4**: In this case we have disconnected the input to the governor and replaced it with our own signal.

### 4.1 Transfer function from the electrical power to the machine speed $G_1(s)$

We start by looking at the transfer function from the electrical power to the machine speed $G_1(s)$.

$$G_1(s) = -G_J(s)S(s) \tag{12}$$

In [7] **Case 1** was investigated and the result from this investigation is stated in the following proposition.

**Proposition 1.** *A consistent estimate of $G_1(s)$ can be identified for* **Case 1** *if the following conditions are met:*

**Condition C1.** *$P_l(s)$ is persistently exciting.*

**Condition C2.** *There is a delay in either $G_1(s)$ or $T_\omega(s)$*

Under normal power system operation Condition C1 should hold as there are constant load changes and switching events in the power system. In case Condition C2 does not hold, we can still get a good estimate if the effect of the plant's process noise on the electrical power is small compared to the effect of the random load changes.

For **Case 2** and **Case 3** we will assume the following

**Assumption A1.** *The measured electrical frequency is a good estimate of rotor speed for slow dynamics if we measure sufficiently close to the generator.*

With Assumption A1 in place we state the following:

**Proposition 2.** *$G_1(s)$ can be identified for the cases* **Case 2** *and* **Case 3** *if assumption* A1 *holds and conditions* C1 *and* C2 *are met.*

In **Case 4** we are operating in open loop and it will therefore not be possible to identify $G_1(s)$.

### 4.2 Transfer function from the governor input to the electrical power

According to [5] the power plant owners have to identify the transfer function from the governor's input to the electrical power. This transfer function is given by:

$$G_{req}(s) = \frac{G_p(s)G_J(s)T_\omega(s)}{1 + G_J(s)T_\omega(s)} \tag{13}$$

From (13) we see that the power plant owners will not be required to identify the transfer function used for testing the new requirements. However, it can easily be shown that $G_{req}(\Omega < \Omega_c) \approx G_p(\Omega < \Omega_c)$. We do this by inserting (1) and (5) into (13) to get:

$$G_{req}(s) = \frac{G_p(s)K_{11}}{K_{11} + s(K_d + 2Hs)} \tag{14}$$

From (14) we see that the transfer function one can identify using the measurements as proposed in [5] is the plant transfer function filtered by a second order low pass filter with a resonance frequency of:

$$\Omega_r = \sqrt{\frac{K_{11}}{2H}} \tag{15}$$

Normally, $K_d$ is quite small and one can therefore expect the low pass filter to be underdamped and have a clear resonance peak. Moreover, we will assume $\Omega_c < \Omega_r$.

Since the tests described in [5] are described for open loop operation we will first investigate this case. From [10] we know that an open loop experiment is informative if the input is persistently exciting. From this we have the following proposition.

**Proposition 3.** *$G_{req}(\Omega < \Omega_c)$ is a good estimate of $G_p(\Omega < \Omega_c)$ and can be identified for* **Case 4** *if the following condition is met*

**Condition C3.** *$u(s)$ is persistently exciting*

For the three other cases we can in general not expect to identify $G_{req}(s)$. The reason for this is that the main source of frequency deviations for slow dynamics are due to load changes resulting in the change of generator speeds due to the swing mechanics. In other words, the main excitation to the plant is $\Delta P_e(s)$ not $\Delta f_{sys}(s)$.

**Proposition 4.** *$G_{req}(s)$ is not possible to identify for* **Case 1**, **Case 2**, *and* **Case 3**.

*One does not actually need to interpolate, but it is done to average out errors

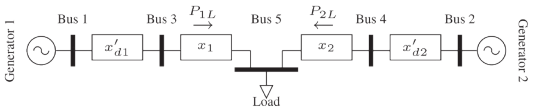


**Fig. 3**: Small test system

## 5 Methodology

Our proposed methodology for testing whether or not a power plant fulfills the requirements for stability and disturbance rejection uses prediction identification[10]. In this technique we assume that we after the application of an antialiasing filter have collected a data set $Z^N = \{u[n], y[n] | n = 1 \cdots N\}$. The signals in the dataset are assumed generated by

$$\mathcal{S} : y[n] = G_1(z, \theta_0)u[n] + H_1(z, \theta_0)e_1[n] \tag{16}$$

where $G_1(z, \theta_0)$ is the transfer function we want to identify $e_1[n]$ is white noise, $H_1(z, \theta_0)$ is monic, $z^{-1}$ is the time delay operator and $\theta_0$ is the parameter vector parametrizing the true system $\mathcal{S}$. With this in place we move on to the aim of prediction error identification, which is to find the parameter vector $\hat{\theta}_N$ such that [10]:

$$\hat{\theta}_N = \arg\min_{\theta} \frac{1}{N} \sum_{t=1}^{N} \epsilon[n, \theta] \tag{17}$$

with

$$\epsilon[n, \theta] = H_1^{-1}(z, \theta)(y[n] - G_1(z, \theta)u[n]) \tag{18}$$

The identification approach used in the methodology consists of the following steps:

1. The data set $Z^N$ has to be collected while the plant is operating at the desired operating point. Preferably the plant should be operated with speed feedback and the rotor speed should be used as the output signal $y[n]$. If one does not have access to measurements of the rotor speed, a measurement of the frequency can be used instead. For the input signal $u[n]$ one should always use the electrical power of the generator.
2. The next step is to preprocess the data. First one should remove the mean of the collected signals and send them through a low pass filter. For the estimation of the plant's inertia the sample frequency should be chosen such that one can clearly see the slope of the bode plot for the faster dynamics.
3. After the preprocessing the correct model order should be chosen. To do this we suggest to use the box-Jenkins model structure. One easy approach is to start with a high model order and then reduce the model order until one finds the lowest possible model order passing predefined sanity tests for the model.
4. The last step is to estimate the plant's inertia. This can be done by inspecting the slope of the identified bode plot to find where the slope is constant and then apply (10).

## 6 Simulation results

To test the theory the power system depicted in Fig. 3 was implemented in Simulink. For the modelling of the turbine the non-linear model assuming a non-elastic water column described in [17] was used. For the governor the proportional controller with transient droop described in [17] was used. This combination of turbine and governor is referred to as HYGOV in several simulation softwares. The governor and turbine used the tuning from [13]. Except for the droop at plant 1 which was set to 8% and the droop at plant 2, which was set to 10%. For a complete set of simulation parameters please refer to the appendix. The frequency at the non generator buses were modeled using the FD equation described in [11].

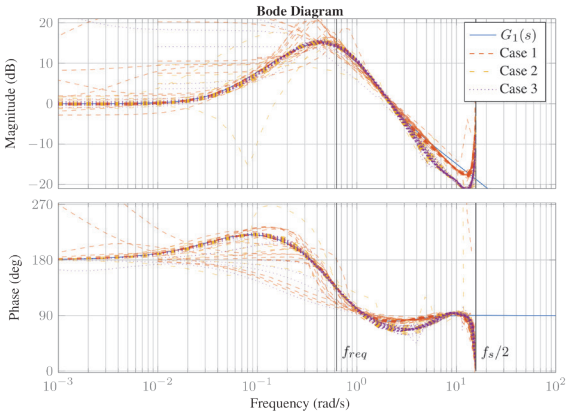


**Fig. 4**: 100 attempts of identifying $G_1(s)$ for the different cases

To excite the system the load was modelled as a wiener process with a standard deviation of $0.4\%[p.u.]$ on system base and a time step of $0.02s$. This choice was made since it resulted in a system where the frequency stayed within the allowed range of $\pm 0.1Hz$. Noise was also added to the generator speed of the two plants. This noise was modelled as white noise processes with standard deviations of $0.004\%[p.u.]$ and $0.04\%[p.u.]$ for plant 1 and 2 respectively. When performing the open loop test for identifying $G_{req}(s)$ white noise with a standard deviation of $0.2\%[p.u.]$ was injected to the governor input. A white noise processes was chosen just for simplicity and other choices are possible. The system base was $30.3GW$ and the machine bases for generator 1 and 2 were $0.3GW$ and $30GW$ respectively. The sampling rate for the data set was set to $2Hz$ and the Nyquist frequency is marked in the figure as $f_s/2$.

For all presented simulation results we have performed a simple Monte Carlo Simulation (MCS). That is the Simulink simulations have been run 1000 times. For each run the different noise signals exciting the system have been regenerated to make the run differ from each other. In all the plots we compare all the MCS runs with one analytical representation of the transfer function we are estimating. The analytical transfer function was calculated using the linearization described in [17].

### 6.1 Testing of the different cases

To check the identification of $G_1(s)$ we tested **Case 1**, **Case 2** and **Case 3**. The results from these tests are plotted in Fig. 4, as expected all cases follow the analytical transfer function closely up to a certain frequency. However, one can see that one obtains a small error for the faster dynamics in the cases were we don't have speed feedback and access to the speed measurement. Moreover, **Case 1** and **Case 2** shows some more variation for slower dynamics. This may be since **Case 3** is more added excitation. The results are also good for faster dynamics than $f_{req,\max} = 0.1Hz$, which corresponds to the sine wave with the shortest wave length specified in [5].

The results from the identification of $G_{req}(s)$ are provided in Fig. 5. In the figure one can see how the transfer functions $G_p(s)$ and $G_{req}(s)$ follow each other closely until right before the resonance peak, given by (15), as stated in Proposition 3. The identification experiment performed in open loop also follows $G_p(s)$ closely up to the Nyquist frequency, so well beyond what's in the draft requirements. However, it has more trouble converging than the other cases. For the three other cases one see as expected that we don't identify $G_{req}(s)$. It is also interesting to see that the identified transfer function resembles the inverse of $G_1(s)$. Another point worth mentioning is that the result we see in Fig. 5 is the same function presented in the previous papers [3, 6]. These do, however, deviate

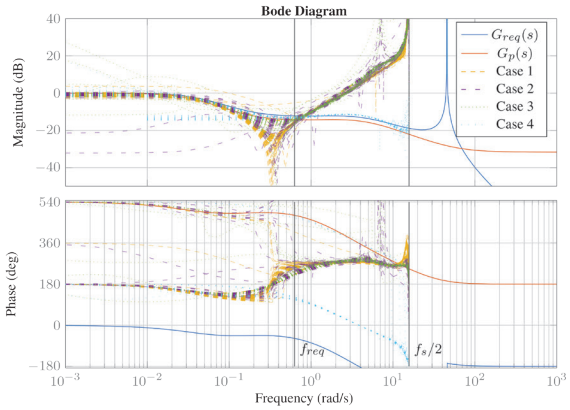


**Fig. 5**: 100 attempts of identifying $G_{req}(s)$ for the different cases

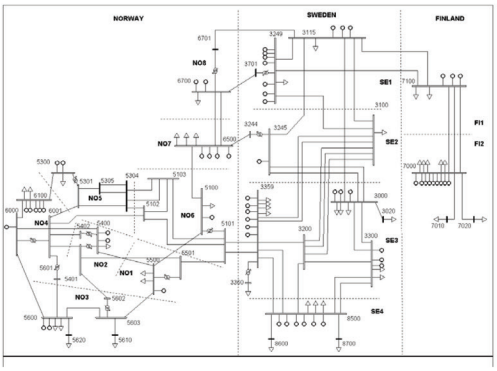


**Fig. 6**: The Nordic 44 test network from [15]

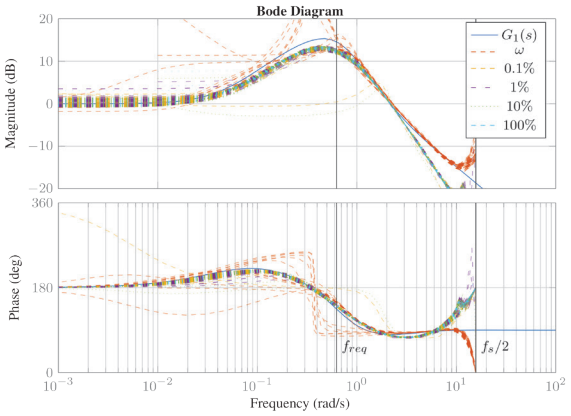


**Fig. 7**: Identification with different reactances

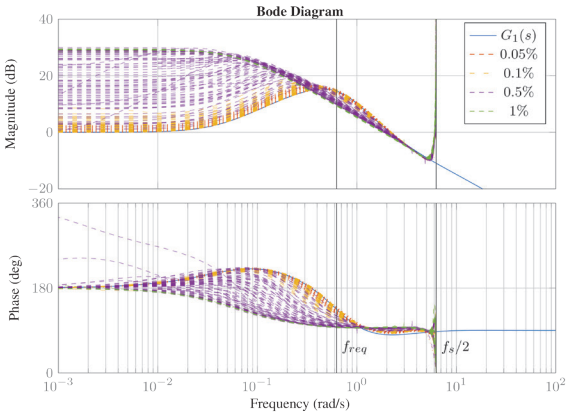


**Fig. 8**: Testing different deadbands

from $G_p(s)$ before $f_{req}$ and can therefore not be used to check the requirements.

### 6.2 *Testing of Assumption* A1 *and effect of nonlinearities*

Since the FD equation provides a rather simplified representation of the power system frequency we also tested **Case 1** and **Case 2** using the commercial power system simulator PSS/E. We used the Nordic 44 power system model depicted in Fig. 6 and described in [16] with the tuning from [13], except for changing the droop of the generator we investigated to $8\%$. The model was modified by moving one of the plants from its original bus to a new bus connected to the original by a new line modelled as a reactance. This version of the test network can be found at [8]. The identification was then performed using the speed of the machine and the frequency of the original bus with an increasing line reactance.The simulation was run $100$ times. The result of this is plotted in Fig. 7, where one can see that using the frequency instead of the speed gives an incorrect estimate of the swing dynamics. This corresponds with the findings in Fig. 4.

The effect of different deadbands are presented in Fig. 8. In [2] the maximum allowed deadband for certain power plants are given to be $0.5Hz$, which corresponds to $1\%p.u.$. From the figure one can see that with this value no identification is possible as long as the frequency stays in its allowed range. With a value of $0.05\%p.u.$ the results are quite good. For all the other cases the results are not really reliable. However, with a deadband of $0.1\%p.u.$ one should be careful as the shape of the plot still remains reasonable.

How the backlash affects the results are presented in Fig. 9. For the test of the backlash we start with a value at one tenth of what is reported in [14], which doesn't give any problems. The next value corresponds to the value reported in [14] and with this value one can see that the identification is incorrect for higher frequency dynamics. When the backlash is further increased by a factor of $10$ the results are not anywhere near correct.

### 6.3 *Comparison of our approach and the one in the draft requirements*

To compare our proposal for testing the requirements with the one proposed in [4] we have in Fig. 10 plotted the amplitude of the sensitivity function calculated, analytically, with our approach denoted $|S(e^{j\Omega}, \hat{\theta})|$, and the approach from [4] denoted $|S_{\min}(e^{j\Omega}, \hat{\theta})|$. From the figure one can see that $S(z, \hat{\theta})$ is a better estimate than $S_{\min}(z, \hat{\theta})$ around the peak of the sensitivity function, which is the value we want to check. The peak value of the sensitivity functions are reported in TABLE 1. From the table one can see that the method proposed in the draft requirements overestimates the stability margin. The approaches where one does not have the speed measurements on the other hand underestimates the stability margin. A comparison of the estimated inertia constants for the three first cases are presented in TABLE 2. As one would expect **Case 1** is clearly the best.

The function $G_1(s)$ is also plotted together with two estimates in Fig. 11. In this case the estimate obtained using $G_{J_{\min}}(s)$ clearly shows a better performance in terms of disturbance rejection than what's actually the case.

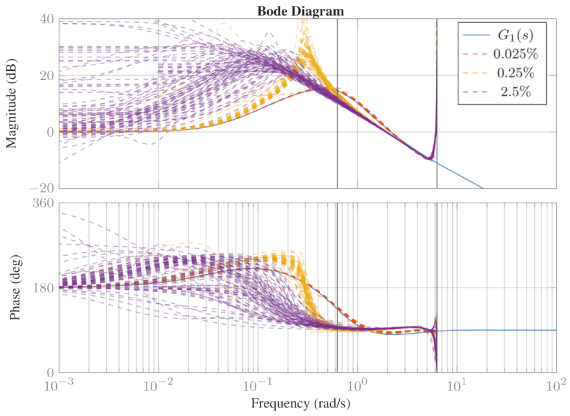


**Fig. 9**: Testing different backlasch

**Table 1** Maximum values of sensitivity functions

| Method | Median | Root mean square error (RMSE) |
|---|---|---|
| $\max\|S(j\Omega)\|$ | 1.84 | 0 |
| $\max\|S(e^{j\Omega},\hat{\theta})\|$, **Case 1** | 1.84 | 0.25 |
| $\max\|S(e^{j\Omega},\hat{\theta})\|$, **Case 2** | 1.75 | 0.34 |
| $\max\|S(e^{j\Omega},\hat{\theta})\|$, **Case 3** | 1.74 | 0.39 |
| $\max\|S_{\min}(e^{j\Omega},\hat{\theta})\|$ | 1.66 | 0.25 |

**Table 2** Estimated inertias

| Case | Median | RMSE |
|---|---|---|
| Actual | 3.5 | 0 |
| **Case 1** | 3.40 | 0.46 |
| **Case 2** | 3.33 | 0.40 |
| **Case 3** | 3.27 | 0.43 |

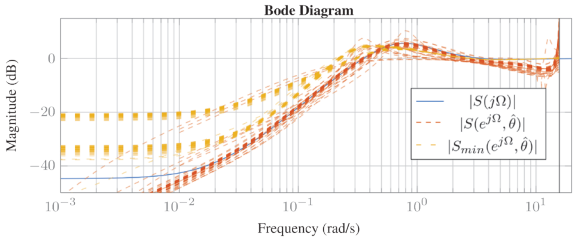


**Fig. 10**: The sensitivity function calculated using our approach and the one from [4]

## 7 Results from power plants in the Norwegian system

### *7.1 Comparison of PMU approach and draft requirements*

To test the methodology on real data we will use data from a test run by Statkraft on one of their power plants and PMU measurements from the same plant. The turbines in the plant are Pelton turbines. This is an advantage as the servos for such turbines are not expected to have any considerable backlash. The one line diagram of the relevant part of the plant is shown in Fig. 12. The PMU data was collected from the high voltage side of the step up transformer in February 2016, while the plant was in normal operation. Since the generators are very close to each other we assume they can be treated as one. The signals collected using the PMU and the ones provided

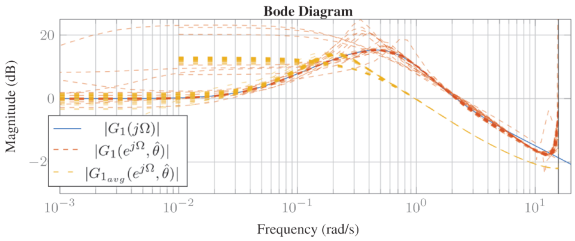


**Fig. 11**: The disturbance rejection function calculated using our approach and the one from [4]

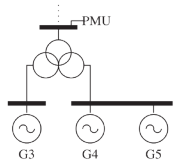


**Fig. 12**: One line diagram of the plant

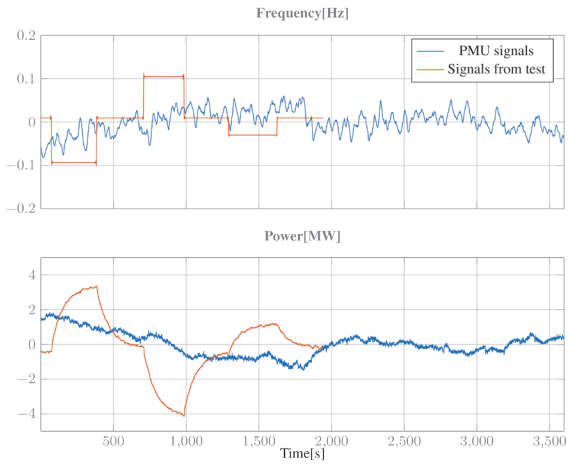


**Fig. 13**: Dataset collected using PMU and test at the plant

by Statkraft after it has been filtered and detrended are presented in Fig. 13.

The bode plot of the identified plant using PMU data is presented in Fig. 14, together with its 95% confidence interval. From the plot one can see that it resembles that of $G_1(s)$ presented from the simulations, and that it has low variance. In this case the bode plot is not plotted using per unit.

To check the identification of the transfer function $G_{req}(s)$ we will use data from a test performed by Statkraft at the same plant. During the test all the generators at the plant were operated with speed feedback except $G4$, and $G5$, which were fed a signal from a signal generator. During the tests both sinusoids and step signals were injected to the governor. Since a step contains all frequencies we will use one of the step tests for the identification.

In Fig. 15 attempts of identifying $G_{req}(s)$ during both open and closed loop operation are presented. The data for the closed loop operation comes from the PMU and the data for open loop operation comes from the step test. One can observe that the result obtained for the closed loop operation resembles that of Fig. 5, which further supports the statement that the plant should be operated in open loop to be able to identify $G_{req}(s)$. The results obtained from the open loop

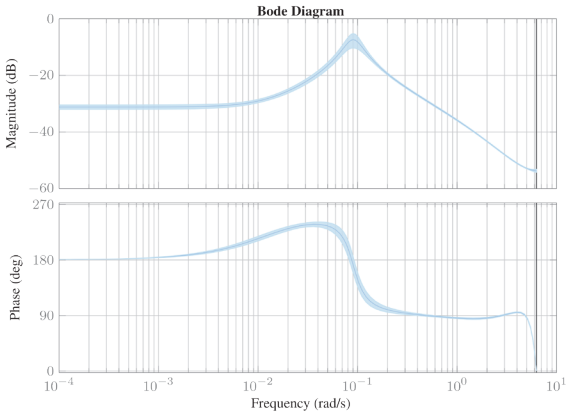


**Fig. 14**: $G_1(s)$ identified using PMU measurements

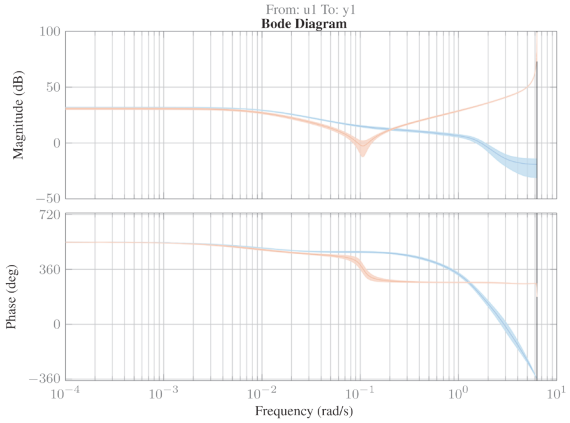


**Fig. 15**: Attempts of identifying $G_{req}(s)$ in closed and open loop operation

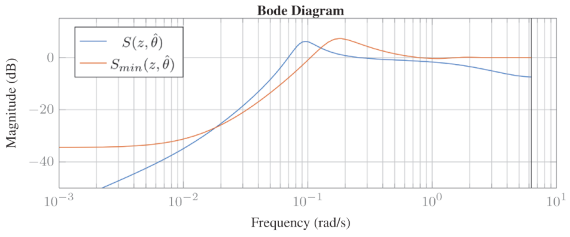


**Fig. 16**: The sensitivity function calculated using our approach and the approach from [4]

operation on the other hand looks reasonable, however, the variance is increasing significantly for the faster dynamics. As in the previous plot this plot is not in per unit.

We also compared the estimate for the sensitivity function and $G_1(s)$ in Fig. 16 and Fig. 17. In this case both estimates are much closer to each other than the case was for the simulations. This is obviously something that can happen since some plants may have similar swing dynamics as the average system. The main point, however, remains that one may as well check the requirements using PMU measurements instead of using the approach proposed in [5].

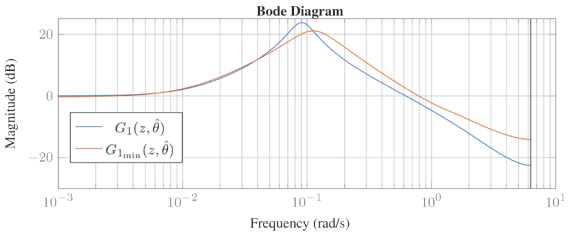


**Fig. 17**: The sensitivity function calculated using our approach and the one from [4]

**Table 3** Droop setting and $G_1(0)$

| Droop | $60min$ | $45min$ | $30min$ | $15min$ |
|---|---|---|---|---|
| 10% | 9.5% | 9.5% | 9.5% | 9.5% |
| 6% | 6.2% | 6.0% | 5.9% | 6.1% |
| 5% | 4.9% | 4.9% | 5.0% | 5.1% |
| 3% | 3.1% | 3.1% | 3.1% | 2.9% |
| 2% | 2.0% | 1.8% | 1.8% | 1.7% |

### *7.2 Results from a plant operating in closed loop and using control system measurements instead of PMU*

When using PMU measurements for obtaining the estimate one have to keep in mind that there may be some losses in the active power of the plant, which are not accounted for. In addition the closer to the generator one measures the power system frequency the better we can assume it to estimate the electrical angular speed of the machine's rotor. It is therefore of interest to see how our approach performs when one uses measurements obtained as close as possible to the generator. This can be achieved if one has access to the control signals of a modern hydro turbine governor. For the purpose we are using the PMUs this is essentially the same as placing a PMU on the generator terminal.

Another advantage of having access to the control system of a hydro power plant is that it allows us to test if the method is able to capture changes in the governor parameters. We therefore did a test at one of Statkraft's power plants where we connected a computer to the control system of the governor. The tests consisted of letting the plant run for one hour, before we changed the governor parameters. The plant was also set to operate with a constant load during the tests. While the parameters where changed we did not record anything, which means that the datasets may be a few minutes shorter than one hour. An example of a dataset is presented in Figure 18. This dataset was obtained with a droop setting of 2%.

Based on the tests performed on the other power plant, new parameters for the PID part of the governor was calculated. Although, these parameters were calculated for another plant we compared these new parameters with the old parameters for this plant. A result of this is shown in Figure 19, where one can see that the proposed approach can indeed detect the parameter change. One can also see that the new parameters give a better disturbance rejection than the old parameters.

We also tested several different droop settings. The result of this is given in Figure 20. All the estimates in this figure is performed while the plant is operated using the new PID parameters. However, for the droop setting of 10% and 6% a smaller proportional gain is used than for the other cases. One can clearly see that the approach captures both the change in the droop and the proportional gain. The approach's sensitivity to different lengths of the dataset is demonstrated in Figure 21, where one can see that the results are quite reasonable for all lengths except for the 15 minutes dataset. The steady state gain for the transfer functions in Figure 20 is presented together with the droop setting in table 3 for different lengths of the datasets. As expected the values are quite close.

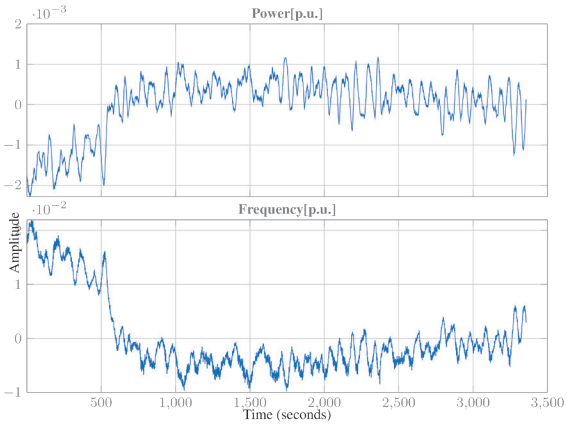


**Fig. 18**: Signals from control system

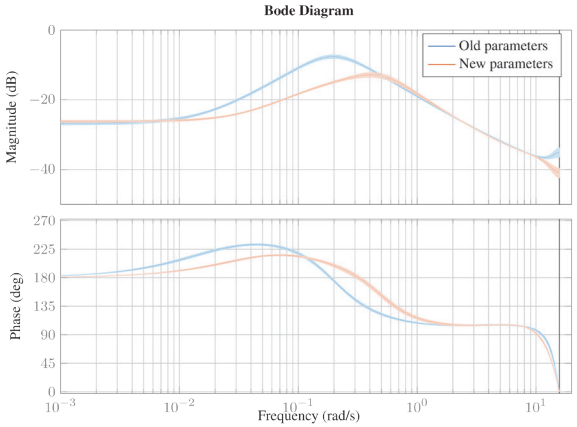


**Fig. 19**: Estimate of $G_1(s)$ new and old tuning

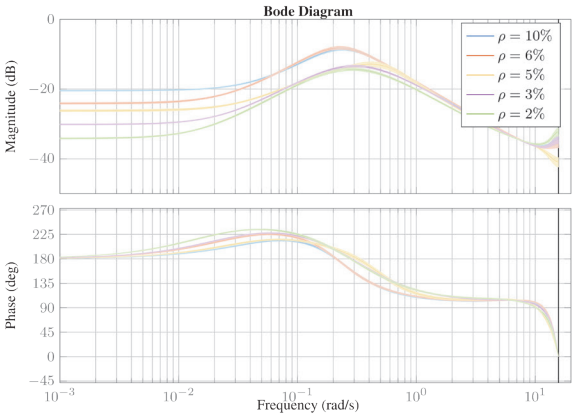


**Fig. 20**: $G_1(s)$ with different droop settings

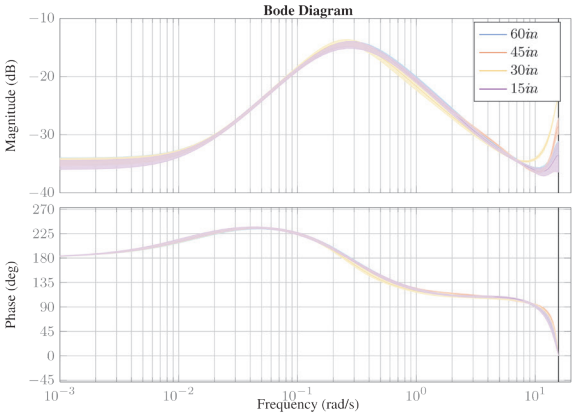


**Fig. 21**: $G_1(s)$ obtained using different signal length

## 8 Conclusions and further work

In this paper we have presented a method for testing a hydro power plant's stability margin and disturbance rejection using PMU and control system measurements. The main advantage of the proposed method is that it is almost non-intrusive. That is the tests can be performed while the power plant is in normal operation, with the only restrictions that the scheduled power production of the plant should remain constant during the test. Furthermore, the best results are obtained if one has access to measurements of the rotor's speed, since this allows for obtaining a good estimate of the plant's inertia. Otherwise, one can use measurements of frequency and one should get an estimate which is not any worse than what one would get using the method proposed in the recent draft requirements for FCR providers in the Nordic synchronous area.

We also discussed the different input output combinations that have been attempted in the literature for identification of hydro power plant dynamics using PMUs. In the discussion we argued that one should use the electrical power as the input signal and the power system frequency as the output signal. This was also demonstrated through simulations.

The method is most applicable to power plants, which does not have a significant input deadband or backlash. Input deadband can be set intentionally to prevent wear and tear of the power plant components and may in some cases be avoided. The backlash on the other hand is mostly dependent on the type of turbine. Generally one can expect a significant backlash in kaplan turbines and high pressure francis turbines. For these type of turbines further research should be put into determining the best way of checking the requirements.

## 9 References


1 Stephen J. Chapman. *Electric machinery and power system fundamentals*, volume 3. McGraw-Hill New York, 2002.

2 European Commission. Network Code on Requirements for Grid Connection Applicable to all Generators, April 2016.

3 Dinh Thuc Duong, Kjetil Uhlen, Stig Løvlund, and Erik Alexander Jansson. Estimation of Hydro Turbine-Governors Transfer Function from PMU Measurements. Boston, July 2016. IEEE.

4 Robert Eriksson, Niklas Modig, and Andreas Westberg. FCR-N DESIGN OF REQUIREMENTS. ENTSO-E report, July 2017.

5 Prequalification Working Group. Technical Requirements for Frequency Containment Reserve Provision in the Nordic Synchronous Area. Draft, June 2017.

6 S. H. Jakobsen and K. Uhlen. Vector fitting for estimation of turbine governing system parameters. In *2017 IEEE Manchester PowerTech*, pages 1–6, June 2017.

7 S. H. Jakobsen, K. Uhlen, and X. Bombois. Identification of hydro turbine governors using PMU data. In *2018 IEEE International Conference on Probabilistic Methods Applied to Power Systems (PMAPS)*, pages 1–6, June 2018.

8 Sigurd Hofsmo Jakobsen. N44 test network. 2018.

9 Sigurd Hofsmo Jakobsen, Kjetil Uhlen, and Petter Lie. System identification techniques for validating hydro power plants FCR performance. Aalborg, June 2019. Cigre.

10 Lennart Ljung. *System identification*. Springer, 1998.

11 F. Milano and Á Ortega. Frequency Divider. *IEEE Transactions on Power Systems*, 32(2):1493–1501, March 2017.

12 B. Mogharbel, L. Fan, and Z. Miao. Least squares estimation-based synchronous generator parameter estimation using PMU data. In *2015 IEEE Power Energy Society General Meeting*, pages 1–5, July 2015.

13 T. J. M. A. Parreiras, S. Gomes, G. N. Taranto, and K. Uhlen. Closest security boundary for improving oscillation damping through generation redispatch

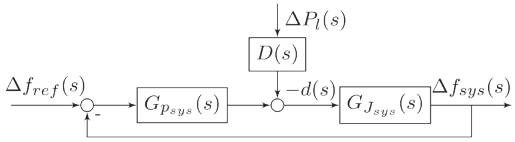


**Fig. 22**: Model used in [4]

using eigenvalue sensitivities. *Electric Power Systems Research*, 160:119–127, July 2018.

14 L. Saarinen, P. Norrlund, and U. Lundin. Field Measurements and System Identification of Three Frequency Controlling Hydropower Plants. *IEEE Transactions on Energy Conversion*, 30(3):1061–1068, September 2015.

15 Silje Mork Hamre. Inertia and FCR in the Present and Future Nordic Power System. Master's thesis, Norwegian University of Science and Technology, Trondheim, June 2015.

16 Luigi Vanfretti, Svein H. Olsen, V. S. Narasimham Arava, Giuseppe Laera, Ali Bidadfar, Tin Rabuzin, Sigurd H. Jakobsen, Jan Lavenius, Maxime Baudette, and Francisco J. Gómez-López. An open data repository and a data processing software toolset of an equivalent Nordic grid model matched to historical electricity market data. *Data in Brief*, 11:349–357, April 2017.

17 Working Group on Prime Mover and Energy Supply Models for System Dynamic Performance Studies. Hydraulic turbine and turbine control models for system dynamic studies. *IEEE Transactions on Power Systems*, 7(1):167–179, February 1992.

## Appendix

### *per unit system used in the requirements*

In the draft requirements they assume the system model depicted in Fig. 22, where $G_{p_{sys}}(s)$ is the aggregated response of all the turbines, servos and governors in the system and $G_{J_{sys}}(s)$ is the aggregated swing dynamics of the system. The transfer function $D(s)$ represents the transfer function from the aggregated load to the aggregated swing dynamics. The stability requirements are then expressed in terms of the norm of the sensitivity function of the aggregated system.

$$|S_{sys}(s)| < M_s \tag{19}$$

where

$$S_{sys}(s) = \frac{1}{1 + G_{J_{sys}}(s)G_{p_{sys}}(s)} \tag{20}$$

and $M_s$ is a constant.

The performance requirement is stated in terms of the system's disturbance rejection. It uses the idea that the power system frequency should fulfill the following constraint $|\Delta f_{sys}(s)| < 0.1Hz$. The change in the power system frequency is given by the following equation

$$\Delta f_{sys}(s) = -2\pi G_{J_{sys}}(s)S_{sys}(s)d(s) = G_{1_{sys}}(s)d(s) \tag{21}$$

We can now write the power spectral relation between the random load changes and the change in power system frequency as:

$$|S_{sys}(j\Omega)|^2\phi_{P_l}(j\Omega) = \frac{1}{2\pi|D(j\Omega)G_{J_{sys}}(j\omega)|^2}\phi_f(j\Omega) \tag{22}$$

where $\phi_{P_l}(j\Omega)$ is white noise with power spectral density (PSD) equal to one and $\phi_f(j\Omega)$ is the psd of the power system frequency with the value $\sigma_f^2$. The performance requirement is thus stated as:

$$|S_{sys}| < \frac{\sigma_f}{|D(s)G_{J_{sys}}(s)|} \tag{23}$$

To test whether or not the plants fulfill the requirements [4] suggests that the power plants owners estimate the transfer function $G_p^{(p.u.)}(s)$ for their plant. This function is to be multiplied with $G_{J_{sys}}^{(p.u.)}(s)$ to check the requirements. To explain the rational behind this we start by defining the per unit base for a plant as it's static gain

$$G_p^{base} = G_p(0) \tag{24}$$

For the system base we will use the sum of all the static gains of the plants in the system, that is

$$G_{J_{sys}}^{base} = \frac{1}{\sum_i^{N_g} G_{p_i}(0)} \tag{25}$$

If we now look at the sensitivity for the whole system we get.

$$S_{sys}(s) = G_{J_{sys}}(s)G_{p_{sys}}(s) = G_{J_{sys}}(s)\sum_i^{N_g} G_{p_i}(s)$$

$$G_{J_{sys}}(s)\sum_i^{N_g} G_{p_i}(s)\frac{G_{p_i}(0)}{G_{p_i}(0)} \approx G_{J_{sys}}^{(p.u.)}(s)G_p^{(p.u.)}(s) \tag{26}$$

In the last step of (26) we have assumed all plants $G_{p_i}(s)$ to be approximately equal to each other. We will now introduce two different versions of $G_{sys}(p.u.)$. Namely, $G_{J_{\min}}^{(p.u.)}$ and $G_{J_{avg}}^{(p.u.)}$ these are the system transfer functions for the system with the minimum amount of inertia and with the average amount of inertia. From now on we will assume everything to be in per unit if not stated otherwise. The requirement for stability and performance are thus stated as follows

$$|S_{\min}(s)| = \frac{1}{|1 + G_p(s)G_{J_{\min}}|} < M_s \tag{27}$$

$$|S_{avg}| < \frac{\sigma_f}{|D(s)G_{J_{avg}}(s)|} \tag{28}$$

Where $G_{\min}(s)$ and $G_{avg}(s)$ are assumed to be given by

$$G_{sys}(s) = \frac{600MW}{0.1Hz}\frac{f_0}{S_{sys}}\frac{1}{2H_{sys}s + K_{d_{sys}}f_0} \tag{29}$$

### *Simulation parameters*

**Table 4** The parameters used for Fig. 3

| Variable | Explanation | Value | |
|---|---|---|---|
| $S_1$ | Machine 1 base power | $300MW$ | - |
| $S_2$ | Machine 2 base power | $3GW$ | - |
| $S_{base}$ | System base power | $3.3GW$ | - |
| $U_{base}$ | Base voltage for the transmission system | $400kV$ | - |
| $U_M$ | base voltage for the machines | $20kV$ | - |
| $D$ | Proportional load frequency dependency | 50 | $S_{base}$ |
| $H_1$ | Generator 1 inertia constant | 3.5 | |
| $H_2$ | Generator 2 inertia constant | $9.68s$ | |
| $K_{d1}$ | Damping constant | 0.1 | - |
| $k_{d2}$ | Damping constant | 0.1 | - |
| $x_1$ | Reactance between bus 3 and 5 | 0.5 | $S_{base}$ |
| $x_2$ | Reactance between bus 4 and 5 | 0.5 | $S_{base}$ |
| $x_{d1}$ | Sub transient reactance generator 1 | 0.15 | $S_1$ |
| $x_{d2}$ | Sub transient reactance generator 2 | 0.15 | $S_1$ |

**Table 5** Hydro turbine governor parameters

| Variable | Explanation | Value |
|---|---|---|
| $T_f$ | Low pass filter time constant | $0.2s$ |
| $T_r$ | Droop time constant | $5s$ |
| $r$ | Temporary droop | $0.3$ |
| $\rho_1$ | Droop | $0.08$ |
| $\rho_2$ | Droop | $0.1$ |
| $T_y$ | Servo time constant | $0.2s$ |
| $T_w$ | Water starting time | $1.01s$ |
| $q_{nl}$ | No load flow | $0.1$ |
| $h_s$ Static head of water column | | $1$ |
| $A_t$ Turbine gain | | $1$ |

## Paper VI

# Checking hydro power plants' FCR performance using system identification in closed loop

# Checking hydro power plants' FCR performance using system identification in closed loop

Sigurd Hofsmo Jakobsen*†, Xavier Bombois‡, Kjetil Uhlen*
Department of Electric Power Engineering, Norwegian University of Science and Technology, Trondheim, Norway*
sigurd.h.jakobsen@ntnu.no†
Laboratoire Ampère, Ecole Centrale de Lyon, Université de Lyon, Ecully, France‡

***Abstract*—In the Nordic power system draft requirements for the FCR providers have been developed. In these a set of open loop tests are proposed to check the requirements. As a response to this we have investigated whether or not the draft requirements can be checked for hydro power plants, while they are operating in closed loop, using only one test and system identification. We show under which conditions this approach will lead to consistent results. Although, these conditions may not hold in general, we argue that the introduced bias in the estimation should be small. Moreover, it is shown that parts of the requirements can be checked without adding external excitation.**

**The presented theoretical insight is demonstrated using a simple test network and results from a hydro power plant in the Norwegian power system, which show good correspondence with the presented theory.**

## I. Introduction

The Nordic transmissions system operators (TSOs) are developing new requirements for the frequency containment reserve (FCR) providers [1]. One part of the new requirements is to perform a series of open loop tests for estimating the transfer function of the FCR. This is an intrusive and time consuming approach, and other approaches should therefore be investigated. Some alternatives have already been investigated, where the least intrusive approaches use measurements from PMUs during normal operation and the most intrusive do open loop tests at the plant.

Among the papers using measurements from normal operation we have [2]–[5]. In [2], [4] they use ARX and ARMAX model structures to perform the identification whereas [3] used time domain vector fitting. A disadvantage of these approaches is that they can only be used for checking parts of the requirements.

Another common method for doing the identification using PMU measurements is to use disturbance[1] recordings, an approach used in the papers [6]–[9]. In [6], [9] an unscented Kalman filter is used for the identification. Another paper using measurements from disturbance recordings is [7] who uses constrained optimization to perform the identification. An example on how to tune simulation models by comparing simulation results with disturbance recordings can be found in [8].

[1]In this context disturbance refers to a larger power system event, i.e. load or generation tripping and not normal load variations

Traditionally, before the wide spread installation of PMUs in the power system, model validation was done by performing field tests at the power plants. This approach is described in [10]–[12]. In [10] they tune parameters in simulation models based on load rejection tests and steady state measurements. The paper [11] describes how a model of the turbine can be obtained using a gradient based non linear search algorithm fitting measured frequency responses from injection of sine and square waves to the governor. A similar approach was used in [12] where the servo and turbine dynamics were identified from field test at a power plant. For the system identification they used different techniques such as visual inspection grey box identification and analysis of the plant's response in the frequency domain. In addition it was demonstrated how the backlash, which can be found in some servos, can be identified.

None of the aforementioned papers show how to identify the transfer functions needed to check the requirements directly. Moreover, the PMU based methods may lack in accuracy since the PMU measures at some distance from the plant and the external excitation cannot be controlled. To overcome these issues we propose to use, for the identification, measurements from the plant's control system, while the plant is operating in closed loop. In addition we will investigate if parts of the requirements can be checked without adding external excitation, and the consistency of the results.

The outline of the paper is as follows. In Section II a model of a power plant is presented, together with the signals that will have to be measured to perform the identification. All the different systems, which we are interested in identifying and the signals needed for each system are explained in Section III. In Section IV two technical theorems are presented, and used in Section V for analysing the identifiability of the different systems. Section VI discusses the results from the analysis and provides some simulation examples to illustrate the main points of the analysis. The results from a real power plant is presented in Section VII. Finally, the conclusions and further work are outline in VIII.

## II. Model of the power plant

To be able to analyse whether or not the requirements for a power plant can be checked using system identification, we need a model of the power plant. For this purpose we will use the model depicted in Fig. 1. Other models and structures

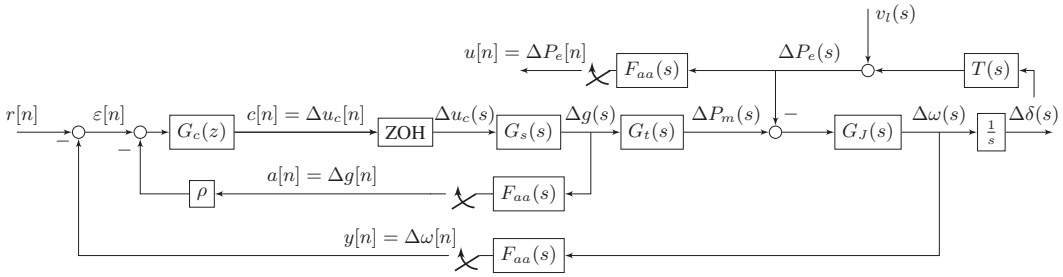


Fig. 1: Block diagram of a hydro power plant in a power system

are possible, however, the same analysis performed in this paper could easily be done for others structures as well. It is important to notice that we in our analysis assume the plant to be operating within a confined region, such that its behavior can be described by linear models.

In the figure, we use classical notation. The Laplace transform of a continuous-time signal $x(t)$ is denoted by $x(s)$ and the shift operator for a discrete time signal $x[n]$ is denoted by $z$ ($n$ is the sample number).

In Fig. 1, the (first-order) continuous-time transfer function $G_J(s)$ represents the swing dynamics of the power plant. This transfer function is of crucial importance as it determines the initial change in the electrical angular speed of the machine's rotor $\Delta\omega(t)$ due to changes in the electric power $\Delta P_e(t)$. Further change in the speed of the machine is contained by the controller $G_c$. This controller is here assumed to be a digital PID controller and is therefore represented by a discrete-time transfer function $G_c(z)$. Since the controller is digital, the continuous-time speed $\Delta\omega(t)$ needs to be discretized via a sampling mechanism preceded by an anti-aliasing filter $F_{aa}(s)$. The corresponding discrete-time signal is denoted $y[n]$. The signal $r[n]$ is an excitation signal that can be added for identification purposes, this signal is thus equal to zero in normal operation. The discrete-time output $c[n]$ of the controller is transformed into a continuous-time signal via a zero-order hold (ZOH) mechanism. The resulting continuous-time signal $\Delta u_c(t)$ is applied to the servo $G_s(s)$ which changes the water flow to the turbine by changing the opening of the guide vanes $\Delta g(t)$. The parameter $\rho$ in the model is referred to as the droop and determines the steady state gain of the governor.

In Fig. 1, we also assume that we have a discrete-time measurement $u[n]$ of the (continuous-time) electric power $\Delta P_e(t)$. As shown in Fig.1, this measurement is done in the same way as the one of $\Delta\omega(t)$.

In our modelling we assume the feedback to the controller to be the rotor's electrical angular speed. Other choices are possible and one common choice is to use the power system electrical frequency as the feedback signal. Since the machines are synchronous machines the power system frequency will be very close to the rotor's electrical angular frequency. However, it may vary for faster dynamics and we will therefore restrict our analysis to having the rotor's electrical speed as the feedback signal. The speed is measured by measuring how fast the rotor is rotating and the relation between the rotor's mechanical speed and electrical speed is given by:

$$\Delta\omega(t) \triangleq \frac{p}{2}\Delta\omega_m(t) \tag{1}$$

where $\Delta\omega_m(t)$ is the mechanical speed of the rotor and $p$ is the number of poles in the machine.

For the identification it is very important how the systems we want to identify are excited. Since the plant is assumed to use the rotor's electrical angular speed as the feedback signal, the main external excitation will be changes in the electric power at the bus bar. For the active power at the bus bar of a synchronous machine we have the following approximate expression [13]

$$P_e(t) = \frac{3V_t(t)E_a(t)\sin\delta_{Ev}(t)}{X_s} \tag{2}$$

where $V_t(t)$ is the terminal voltage of the machine, $E_a(t)$ is the internal voltage, $\delta_{EV}(t)$ is the angle between the internal voltage and the terminal voltage and $X_s$ is the synchronous reactance. If we linearise (2) assuming the voltages to be constant we get the following equation

$$\Delta P_e(s) = \beta(\frac{\Delta\omega(s)}{s} - \Delta\delta_V(s)) \tag{3}$$

where $\beta$ is a linearization constant, $\Delta\omega(s)/s = \delta(s)$ is the angle of the internal voltage as a function of the machine's electrical speed and $\Delta\delta_V(s)$ is the angle of the terminal voltage. The angle of the terminal voltage will be a function of both random load changes and the angle of the machine's internal voltage. We will therefore split these two contributions to get the expression for the electric power used in Fig. 1

$$\Delta P_e(s) = v_l(s) + \frac{T(s)}{s}\Delta\omega(s) \tag{4}$$

where $v_l(s)$ is a signal incorporating the effects of all random events in the power systems. It will be modeled as a stochastic process generated by a white noise $e_l$ filtered by a stable transfer function $H_l$. The transfer function $T(s)$ is the transfer function from the rotor angle of the machine to the electrical power at the bus bar. This transfer function includes both the influence the angle has directly on the power and its influence on the terminal voltage angle through the network. Although, we have done our analysis assuming constant voltages, time dependent voltages would not change the conclusion of the

analysis. The reason for this is that there should still exist a transfer function from the load and rotor angle to the electric power of the generator.

## III. Description of systems to be identified

In this section we will present the transfer functions used to check the draft requirements and the datasets that can be used for obtaining these functions.

In [14] the theory and idea behind the draft requirements are presented. In short they put requirements on the plants' sensitivity function and disturbance rejection function. If we denote by $G_c(s)$ the continuous-time equivalent of the digital controller $G_c(z)$, the sensitivity function is defined as

$$S(s) = \frac{1}{1 + G_p(s)G_J(s)} \tag{5}$$

with

$$G_p(s) = \frac{G_c(s)G_s(s)G_t(s)}{1 + \rho G_c(s)G_s(s)} \tag{6}$$

and the plant's disturbance rejection function is defined as

$$G_1(s) = G_J(s)S(s) \tag{7}$$

In the requirements it is proposed to estimate the function $S(s)$ and $G_1(s)$ by estimating $G_p(s)$ while the plant is operated in open loop, that is the input signal $\varepsilon[n]$ to the controller is generated by a signal generator. The estimate of $G_p(s)$ is then to be used together with an estimate of $G_J(s)$ derived from the sum of the inertia of all the machines in the power system. We will instead let the plant continue to operate in closed loop and identify both, $G_1(s)$, and $S(s)$ directly. We will also show how $G_p(s)$ and $G_J(s)$ can be identified separately while the plant is operating in closed loop.

Since the identification of the transfer functions is performed using a computer, the measured signals will have to be sampled. We will therefore use the discrete version of the signals and transfer functions from now on.

### A. Description of the signals relevant for $S(z)$ and $G_1(z)$

By inspecting Fig. 1, we observe that the discrete-time signals $r[n]$, $u[n]$ and $\varepsilon[n] = r[n] - y[n]$ are related by discrete-time versions $S(z)$ and $G_1(z)$ of the continuous-time transfer functions $S(s)$ and $G_1(s)$:

$$\varepsilon[n] = G_1(z)u[n] + S(z)r[n] \tag{8}$$

From this we conclude that if we have collected the dataset $Z_{ur}^N = \{u[n], r[n], \varepsilon[n] | n = 1 \dots N\}$ we can identify $S(z)$ and $G_1(z)$ if the systems are identifiable using this dataset (the identifiability will be the purpose of the next sections). The subscript $ur$ in $Z_{ur}$ denotes the input signals to the multi input single output (MISO) system described by (8).

Notice that if we set $r[n] = 0$, we get the following relation

$$\varepsilon[n] = G_1(z)u[n] \tag{9}$$

In this configuration, it will no longer be possible to identify $S(z)$. However, it could still be possible to identify $G_1(z)$ using the dataset $Z_u^N = \{u[n], \varepsilon[n] | n = 1 \dots N\}$

### B. Description of the signals relevant for identifying $G_p(z)$, $G_J(z)$

The FCR is delivered by the process described by the transfer function $G_p(z)$ and the TSOs will, therefore, in many cases be interested in obtaining this transfer function first before estimating $S(z)$ and $G_1(z)$. Indeed this is what is proposed in [1]. Moreover, it is of interest to know the swing dynamics $G_J(z)$ of the plant. In fact [15] reviews methods for estimating system inertia both in the literature and in use by the TSOs. We will therefore, demonstrate how these transfer functions can also be identified.

For the purpose of identifying $G_p(z)$ and $G_J(z)$, one can observe in Fig.1 that the signals $c[n]$, $u[n]$ and $y[n]$ are related as follows:

$$y[n] = G_{Jp}(z)c[n] - G_J(z)u[n] \tag{10}$$

where $G_J(z)$ is a discretized version of $G_J(s)$ and $G_{Jp}$ is a discretized version of the product $G_s(s)G_t(s)G_J(s)$ (combined with the ZOH and the antia-aliasing filter). We therefore conclude that we could estimate $G_J(z)$ and $G_{Jp}(z)$ using the dataset $Z_{cu}^N = \{c[n], u[n], y[n] | n = 1 \dots N\}$ if the systems are identifiable using this dataset. To find $G_p(z)$ we also need to know the transfer function of the servo $G_s(z)$ and of the controller $G_c(z)$. We will assume the controller to be known and we see that the signals $c[n]$ and $a[n]$ are related by:

$$a[n] = G_s(z)c[n] \tag{11}$$

We therefore conclude that we could estimate $G_s(z)$ using the dataset $Z_c^N = \{c[n], a[n] | n = 1 \dots N\}$ if the system is identifiable using this dataset. An estimate of $G_p(z)$ can then be deduced from the models of $G_J(z)$, $G_{Jp}(z)$, and $G_s(z)$ using the following relation:

$$G_p(z) = \frac{G_{Jp}(z)G_c(z)}{G_J(z)(1 + \rho G_c(z)G_s(z))} \tag{12}$$

**Remark 1.** *For the sequel, it is important to note that the transfer function $G_{Jp}(z)$ will generally contain a delay (due to the presence of the ZOH) while the other transfer functions $G_J(z)$, $S(z)$ and $G_1(z)$ will generally not contain any delay.*

## IV. System identification theory

To prove the identifiability of the systems presented in the previous section we will present two technical theorems. One relevant for (MISO) systems and one relevant for single input single output (SISO) systems. In the next section we will then discuss the identifiability of the systems using these theorems.

### A. MISO theorem

We suppose the dataset $Z_{miso}^N = \{u_1[n], u_2[n], y[n] | n = 1 \dots N\}$ generated by:

$$\mathcal{S}_{miso} : y[n] = \boldsymbol{G}(z, \theta_0)\boldsymbol{u}[n] + v[n] \tag{13}$$

where $\boldsymbol{G}(z, \theta_0) = \begin{bmatrix} G_1(z, \theta_0) & G_2(z, \theta_0) \end{bmatrix}$ and $\boldsymbol{u} = \begin{bmatrix} u_1[n] & u_2[n] \end{bmatrix}^T$. The term $v[n]$ models process noise and is assumed generated by $v[n] = H(z, \theta_0)e[n]$, where $H(z, \theta_0)$ is assumed monic and $e[n]$ is white noise with variance $\sigma_e^2$.

As we can see in (13) the true system $\mathcal{S}_{miso}$ is parametrized by the parameter vector $\theta_0$. In the sequel, we will suppose that this parameter vector $\theta_0$ is unknown, but that the model structure $\mathcal{M}_{miso} = \{G_1(z,\theta), G_2(z,\theta), H(z,\theta)\}$ is known. Consequently, the identification boils down to the determination of a consistent estimate of $\theta_0$.

The input signals $\boldsymbol{u}^T[n] = \begin{bmatrix} u_1[n] & u_2[n] \end{bmatrix}$ are assumed to be generated with two external excitation signals $w_1[n]$ and $w_2[n]$ and may also be influenced (via some feedback) by the noise $e[n]$ generating $v[n]$ in (13):

$$\boldsymbol{u}[n] = \boldsymbol{K}(z)\boldsymbol{w}[n] + \boldsymbol{\Gamma}(z)e[n] \tag{14}$$

where $w[n] = \begin{bmatrix} w_1[n] & w_2[n] \end{bmatrix}^T$ and where $\boldsymbol{K}(z)$ and $\boldsymbol{\Gamma}(z)$ are a matrix of transfer functions and a vector of transfer functions, respectively. In this paper, we only suppose knowledge of $\boldsymbol{u}[n]$. Consequently, $\boldsymbol{w}[n]$, $\boldsymbol{K}(z)$ and $\boldsymbol{\Gamma}(z)$ are not necessarily known quantities. Using prediction error identification [16] and the dataset $Z^N_{miso}$ an estimate $\hat{\theta}_N$ of $\theta_0$ can be deduced as follows:

$$\hat{\theta}_N = \arg\min_{\theta} \frac{1}{N} \sum_{n=1}^{N} \epsilon^2_{miso}[n,\theta] \tag{15}$$

with the prediction error defined as:

$$\epsilon_{miso}[n,\theta] = H^{-1}(z,\theta)(y[n] - \boldsymbol{G}(z,\theta)\boldsymbol{u}[n]) \tag{16}$$

In order to validate our identification setting it is important to verify whether or not (15)-(16) will lead to a consistent estimate of $\theta_0$ when $\boldsymbol{u}[n]$ is generated as in (14). To do this we need to verify that the true parameter vector $\theta_0$ is the unique solution to the asymptotic prediction criterion:

$$\theta^* = \arg\min_{\theta} \bar{E}\epsilon^2_{miso}[n,\theta] \tag{17}$$

with

$$\bar{E}\epsilon^2_{miso}[n,\theta] = \lim_{N\to\infty} \frac{1}{N} \sum_{n=1}^{N} E\epsilon^2_{miso}[n,\theta] \tag{18}$$

The operator $E$ denotes the expectation operator.

Before we investigate whether or not the estimate (15) is consistent we will make some assumptions.

**Assumption A1.** *The external excitations $w_1[n]$ and $w_2[n]$ are assumed to be uncorrelated white noises with variance $\sigma_1^2$ and $\sigma_2^2$ respectively. Moreover, they are assumed uncorrelated to the white noise $e[n]$.*

**Remark 2.** *Other $\boldsymbol{w}[n]$ than white noise could also work, such as multisine and filtered white noise.*

**Assumption A2.** *The determinant $\det(\boldsymbol{K}(e^{j\Omega}))$ is nonzero for all $\Omega$.*

In addition we have the following condition

**Condition C1.** *If we denote $\boldsymbol{\Gamma}(z) = \begin{bmatrix} \Gamma_1(z) & \Gamma_2(z) \end{bmatrix}^T$, there must be a delay in $G_1(z,\theta_0)\Gamma_1(z)$ and in $G_2(z,\theta_0)\Gamma_2(z)$ whenever these transfer functions are nonzero.*

The identifiability of the system $\mathcal{S}_{miso}$ is now stated in the following theorem.

**Theorem 1.** *Consider the dataset $Z^N_{miso} = \{u_1[n], u_2[n], y[n] | n = 1 \dots N\}$ where $Z^N_{miso}$ is generated by* (13)-(14)*. Moreover, consider Assumptions A1-A2 and Condition C1 Then the prediction error criterion* (15) *with* (16) *yields a consistent estimate of $\theta_0$.*

*Proof:* We start by inserting (13) into (16) to obtain.

$$\epsilon_{miso}[n,\theta] = e[n] + \frac{\boldsymbol{\Delta G}(z,\theta)\boldsymbol{u}[n] + \Delta H(z,\theta)e[n]}{H(z,\theta)} \tag{19}$$

with $\boldsymbol{\Delta G}(z,\theta) = \boldsymbol{G}(z,\theta_0) - \boldsymbol{G}(z,\theta)$ and $\Delta H(z,\theta) = H(z,\theta_0) - H(z,\theta)$. We now insert (14) into (19).

$$\epsilon_{miso}[n,\theta] = e[n] + \nu(z,\theta)e[n] + \boldsymbol{\chi}(z,\theta)\boldsymbol{K}(z)\boldsymbol{w}[n] \tag{20}$$

with

$$\boldsymbol{\chi}(z,\theta) = \frac{\boldsymbol{\Delta G}(z,\theta)}{H(z,\theta)} \tag{21}$$

, and

$$\nu(z,\theta) = \boldsymbol{\chi}(z,\theta) \begin{bmatrix} \Gamma_1(z) \\ \Gamma_2(z) \end{bmatrix} + \frac{\Delta H(z,\theta)}{H(z,\theta)} \tag{22}$$

Due to the monicity of $H(z,\theta_0)$ and the combination of Assumption A1 and Condition C1,

$$\begin{aligned} \bar{E}\epsilon^2_{miso}[n,\theta] = \sigma_e^2 \\ + \frac{1}{2\pi}\int_{-\pi}^{\pi} \nu(e^{j\Omega},\theta)\sigma_e^2\nu(e^{-j\Omega},\theta)d\Omega \\ + \frac{1}{2\pi}\int_{-\pi}^{\pi} \boldsymbol{\chi}(e^{j\Omega},\theta)\boldsymbol{\phi_{Kw}}(\Omega)\boldsymbol{\chi}^T(e^{-j\Omega},\theta)d\Omega \end{aligned} \tag{23}$$

with

$$\boldsymbol{\phi_{Kw}}(\Omega) = \boldsymbol{K}(e^{j\Omega})\boldsymbol{\phi_w}(\Omega)\boldsymbol{K}^T(e^{-j\Omega}) \tag{24}$$

Where $\boldsymbol{\phi_w}(\Omega) = diag(\sigma_1^2, \sigma_2^2)$. Let us first observe that (24) is a strictly positive definite matrix at each $\Omega$ by Assumption A2. To prove the consistency, we will show that $\theta_0$ is the unique minimizer of (23). That is, it is the unique parameter vector $\theta^*$ yielding $\bar{E}\epsilon^2_{miso}[n,\theta^*] = \sigma_e^2$. Since (24) is strictly positive definite, we observe that this only holds if $\boldsymbol{\chi}(\theta^*) = \nu(\theta^*) = 0$ for all $\Omega$. From (21) and (22), this implies that $\boldsymbol{\Delta G}(\theta^*) = \Delta H(\theta^*) = 0$ for all $\Omega$; which in turn implies $\theta^* = \theta_0$. ■

### *B. SISO theorem*

We now consider the dataset $Z^N_{siso} = \{u[n], y[n] | n = 1 \dots N\}$ generated by:

$$\mathcal{S}_{siso} : y[n] = G(z,\theta_0)u[n] + v[n] \tag{25}$$

where the term $v[n]$ models process noise and is assumed generated by $v[n] = H(z,\theta_0)e[n]$, where $H(z,\theta_0)$ is assumed monic and $e[n]$ is white noise with variance $\sigma_e^2$ and the input signal $u[n]$ is given by:

$$u[n] = \sum_{i=1}^{q} K_i(z)w_i[n] + \Gamma(z)e[n] \tag{26}$$

where $q$ is the number of external excitation signals $w_i[n] (i = 1 \dots q)$. We observe that $u[n]$ may also be influenced by $e[n]$ via some feedback. As in the previous section, we do not

suppose $w_i[n]$, $K_i(z)$ $(i = 1 \dots q)$ and $\Gamma(z)$ to be known. We will nevertheless assume the following:

**Assumption A3.** *The signals $w_i[n]$ $(i = 1 \dots q)$ and $e[n]$ are all uncorrelated white noise with variances $\sigma_i^2 (i = 1 \dots q)$.*

For this system the prediction error is given by:

$$\epsilon_{siso}[n, \theta] = H^{-1}(z, \theta)(y[n] - G(z, \theta)u[n]) \tag{27}$$

Similarly as for the MISO-system we will verify whether or not (27) in (15) will lead to a consistent estimate of $\theta_0$, given the following technical condition.

**Condition C2.** *If this transfer function is nonzero, there is a delay in $G(z, \theta_0)\Gamma(z)$.*

**Theorem 2.** *Consider the dataset $Z_{siso}^N = \{u[n], y[n] | n = 1 \dots N\}$ where $Z_{siso}^N$ is generated by* (25) *and* (26) *with $q \geq 1$. Moreover, consider Assumption A3 and Condition C2. Then the prediction error criterion* (15) *with* (27) *yields a consistent estimate of $\theta_0$.*

*Proof:* We start by inserting (25) into (27) to obtain.

$$\begin{aligned}\epsilon_{siso}[n, \theta] = e[n] \\ + \frac{\Delta G(z, \theta)u[n] + \Delta H(z, \theta)e[n]}{H(z, \theta)}\end{aligned} \tag{28}$$

with $\Delta G(z, \theta) = G(z, \theta_0) - G(z, \theta)$, and $\Delta H(z, \theta) = H(z, \theta_0) - H(z, \theta)$

Due to the monicity of $H(z, \theta_0)$ combined with Assumption A3 and Condition C2,

$$\begin{aligned}\bar{E}\epsilon_{siso}^2[n, \theta] = \sigma_e^2 + \frac{1}{2\pi}\int_{-\pi}^{\pi} \zeta(e^{j\Omega}, \theta)\sigma_e^2\zeta(e^{-j\Omega}, \theta)d\Omega \\ + \frac{1}{2\pi}\sum_{i=1}^{q}\int_{-\pi}^{\pi} \chi_i(e^{j\Omega}, \theta)\sigma_i^2\chi_i(e^{-j\Omega}, \theta)d\Omega\end{aligned} \tag{29}$$

with

$$\zeta(z, \theta) = \frac{\Delta G(z, \theta)\Gamma(z) + \Delta H(z, \theta)}{H(z, \theta)} \tag{30}$$

and

$$\chi_i(z, \theta) = \frac{\Delta G(z, \theta)}{H(z, \theta)}K_i(z) \tag{31}$$

To prove the consistency, we will show that $\theta_0$ is the unique minimizer of (29), that is it is the unique parameter vector $\theta^*$ yielding $\bar{E}\epsilon_{siso}^2[n, \theta^*] = \sigma_e^2$. We observe that this only holds if $\zeta(z, \theta^*) = \chi_i(z, \theta^*) = 0 (i = 1 \dots q)$. Since $q \geq 1$ it follows from (30) and (31) that the latter statement implies that $\Delta G(z, \theta^*) = \Delta H(z, \theta^*) = 0$. This in turn implies $\theta^* = \theta_0$. ∎

**Remark 3.** *For SISO identification, a single external excitation (i.e. $q = 1$) will be sufficient to ensure the consistency. The advantage of having multiple external excitation $(q > 1)$ is the reduction of the variance of the estimate $\hat{\theta}$.*

## V. Validation of the system identification experiments

### A. Identifiability of $S(z)$ and $G_1(z)$ using the dataset $Z_{ur}^N$

We will now proceed to investigate whether or not the sensitivity function $S(z)$ and the disturbance rejection function $G_1(z)$ can be identified using the dataset $Z_{ur}^N = \{u[n], r[n], \varepsilon[n] | n = 1 \dots N\}$. We assume the system can be parametrized by a parameter vector $\theta_0$ in a known model structure.

$$\mathcal{S}_{ur} : \varepsilon[n] = G_1(z, \theta_0)u[n] + S(z, \theta_0)r[n] + v[n] \tag{32}$$

where $v[n] = H(z, \theta_0)e[n]$, $e[n]$ is white noise with variance $\sigma_e^2$ and $H(z, \theta_0)$ is assumed monic. The term $v[n]$ represents process noise. It is not included in Fig. 1, however, in general it is very unlikely that $\varepsilon[n]$ is perfectly described by (8).

We see that this situation corresponds to the one of Section IV-A Indeed, by denoting $\boldsymbol{u}^T[n] = [u[n]\ r[n]]$, $\boldsymbol{w}^T[n] = [e_l[n]\ r[n]]$ and by using Fig. 1, we can write the following for some transfer functions $K_{11}(z)$, $K_{12}(z)$ and $\Gamma_1(z)$:

$$\begin{aligned}\begin{bmatrix} u[n] \\ r[n] \end{bmatrix} &= \begin{bmatrix} K_{11}(z) & K_{12}(z) \\ 0 & 1 \end{bmatrix}\begin{bmatrix} e_l[n] \\ r[n] \end{bmatrix} + \begin{bmatrix} \Gamma_1(z) \\ 0 \end{bmatrix} e[n] \\ &= \boldsymbol{K}(z)\boldsymbol{w}[n] + \boldsymbol{\Gamma}(z)\end{aligned} \tag{33}$$

We observe that, if we apply an excitation signal $r[n]$, we have two external excitation signals generating $\boldsymbol{u}[n] = \begin{bmatrix} u[n] & r[n] \end{bmatrix}^T$ (i.e. $e_l[n]$ and $r[n]$). Consequently, using Theorem 1, the estimate of $\theta_0$ obtained with prediction error identification using the dataset $Z_{ur}^N$ will be consistent if Assumptions A1, A2 and Condition C1 are fulfilled. Let us discuss this matter in the following remarks:

**Remark 4.** *That Assumption A1 does not hold would imply that at least two of the following signals, the aggregated stochastic load behavior $e_l[n]$, the added perturbation $r[n]$ and the process noise $e[n]$ are correlated. This is highly unlikely.*

**Remark 5.** *As shown in* (33)*, it is clear that Assumption A2 will always be respected in practice.*

**Remark 6.** *In this case, Condition C1 boils down to the presence of a delay in $G_1(z, \theta_0)\Gamma_1(z)$. This delay condition does not cause any problem when the feedback mechanism is realized via a digital controller and a ZOH. However, in our case, the feedback mechanism which is at stake in Theorem 1 is the one pertaining to the link between $\Delta\omega(t)$ and $\Delta P_e(t)$. In general, there will be no delay in $G_1(z, \theta_0)\Gamma_1(z)$. Consequently, we will not be able to guarantee the consistency, and the estimate* (15) *will therefore be biased. However, the bias will remain limited if the contribution of the process noise $v[n]$ in $u[n]$ is negligible. Indeed, in this case, $\nu(z, \theta)$ in* (22) *reduces to $\Delta H(z, \theta)/H(z, \theta)$ and* (23) *holds even if there is no delay in $G_1(z, \theta_0)\Gamma_1(z)$. That the contribution of the process noise $v[n]$ in $u[n]$ is negligible should normally be met in practice as one can expect the contribution of random fluctuations in the rotor angle to influence the power at the bus bar less than the contribution of all other random changes in the power system.*

### B. Identifiability of $G_{Jp}(z)$ and $G_J(z)$ using the dataset $Z_{cu}^N$

We will now investigate whether or not we can identify consistent models of $G_{Jp}(z)$ and $G_J(z)$ using the dataset $Z_{cu}^N = \{c[n], u[n], y[n] | n = 1 \dots N\}$, as for the previous system we assume that the system can be parametrized by a parameter vector $\theta_0$ in a known model structure:

$$\mathcal{S}_{cu} : y[n] = \boldsymbol{G}(z, \theta_0)\boldsymbol{u}[n] + v_1[n] \tag{34}$$

where $\boldsymbol{G}(z, \theta_0) = \begin{bmatrix} G_{Jp}(z, \theta_0) & -G_J(z, \theta_0) \end{bmatrix}$. The term $v_1[n]$ models process noise and is assumed generated by $v_1[n] = H_1(z, \theta_0)e[n]$, where $H_1(z, \theta_0)$ is assumed monic. Using Fig. 1, the input signal $\boldsymbol{u}^T[n] = \begin{bmatrix} c[n] & u[n] \end{bmatrix}$ can thus be rewritten as:

$$\begin{bmatrix} c[n] \\ u[n] \end{bmatrix} = \begin{bmatrix} K_{cl}(z) & K_{cr}(z) \\ K_{ul}(z) & K_{ur}(z) \end{bmatrix} \begin{bmatrix} e_l[n] \\ r[n] \end{bmatrix} + \begin{bmatrix} \Gamma_{ce}(z) \\ \Gamma_{ue}(z) \end{bmatrix} e[n]$$
$$\boldsymbol{u}[n] = \boldsymbol{K}(z)\boldsymbol{w}[n] + \boldsymbol{\Gamma}(z)e[n] \tag{35}$$

If an external signal $r[n]$ is applied to the system, we are thus here also in a situation corresponding to Section IV-A and, using Theorem 1, the estimate of $\theta_0$ obtained with the data set $Z_{cu}^N$ will be consistent if Assumption A1, A2 and Condition C1 are fulfilled. Assumption A1 and A2 are generically fulfilled in this case too. However, we have a similar problem with Condition C1, which requires a delay in both $G_{Jp}(z, \theta_0)\Gamma ce(z)$ and $G_J(z)\Gamma_{ue}(z)$, as discussed in the following remark

**Remark 7.** *The delay condition will generally hold for $G_{Jp}(z, \theta_0)\Gamma_{ce}(z)$ due to the presence of the ZOH (see Remark 1). However, for the same reason as in Remark 6, this will not be the case for $G_J(z, \theta_0)\Gamma_{ue}(z)$. The undesired bias will however be limited under the same condition as in Remark 6.*

### C. Identifiability of $G_1(z)$ without external excitation

We will now investigate whether or not $G_1(z)$ can be identified without adding external excitation, that is $r[n] = 0$. This possibility was mentioned in Section III-A (see (9)). Note that we analyzed this particular case in a previous paper[5], but it will also be included here for completeness with extra attention to the delay condition. As for the previous system we assume that $G_1(z)$ can be parametrized by a parameter vector $\theta_0$ in a known model structure. The relevant dataset for this analysis is $Z_u^N = \{u[n], \varepsilon[n] | n = 1 \dots N\}$, which we suppose is generated by:

$$\mathcal{S}_u : \varepsilon[n] = G_1(z, \theta_0)u[n] + v[n] \tag{36}$$

and using (33) with $r[n] = 0$. We are thus now in the situation described in Section IV-B with $q = 1$. Consequently, using Theorem 2, the estimate of $\theta_0$ obtained with the dataset $Z_u^N$ when $r[n] = 0$ will be consistent if $e_l[n]$ is independent of $e[n]$ (Assumption A3) and if Condition C2 holds. This latter condition here entails the presence of a delay in $G_1(z, \theta_0)\Gamma_1(z)$. As already mentioned in Remark 6, this will not be the case in practice, but the bias will be limited under the same condition as the one mentioned in Remark 6.

**Remark 8.** *If we are only interested by $G_1(z, \theta_0)$, it is thus not necessary to add the external excitation $r[n]$. However, as pointed out in Remark 3 adding this external excitation $r[n]$ and following the procedure in Section V-A will generally yield an estimate with lower variance. The addition of an external excitation $r[n]$ will also make it more likely that the contribution of $v[n]$ in $u[n]$ is negligible, reducing in this way the bias due to the absence of delay in $G_1(z, \theta_0)\Gamma_1(z)$ (see Remark 6)*

### D. Identifiability of $G_s(z)$ using the dataset $Z_c^N$

We will now investigate whether or not we can identify $G_s(z)$. For this purpose, we assume that the system can be parametrized by a parameter vector $\theta_0$. The relevant dataset in this case $Z_c^N = \{c[n], a[n] | n = 1 \dots N\}$ is supposed generated by:

$$\mathcal{S}_c : a[n] = G_s(z, \theta_0)c[n] + v_2[n] \tag{37}$$

$v_2[n]$ models process noise and is assumed generated by $v_2[n] = H_2(z, \theta_0)e_2[n]$, where $H_2(z, \theta_0)$ is assumed monic. It is arguable whether there will be significant process noise in the servo, however, it is included for completeness and it will be supposed that this signal $v_2$ is uncorrelated with $e_l[n]$ and $v[n]$. The signal $v_2[n]$ will generally be negligible in practice with respect to $e_l[n]$ and $v[n]$. That is the reason why it was not considered as an extra external excitation in the previous subsection. The signal $c[n]$ in (37) will be made up of a contribution of the random load changes $e_l[n]$, the process noise $e[n]$ and possibly of a contribution of the external excitation $r[n]$.

This situation corresponds to the case discussed in Section IV-B. Using Theorem 2, this identification will therefore yield a consistent estimate since all conditions/assumptions are here respected. In particular, note that, here, Condition C2 will hold since the to be identified transfer function $G_s(z, \theta_0)$ will generally contains a delay (due the presence of the ZOH between $c[n]$ and $a[n]$).

Note also that, due to the presence of $e_l[n]$, we will necessarily have $q \geq 1$ and the external excitation $r[n]$ is thus not required for the consistency.

## VI. Simulation results and discussion

This far we have shown under which conditions the transfer functions $S(z)$, $G_1(z)$, $G_p(z)$ and $G_J(z)$ can be identified. We will now proceed with a numerical example. For this purpose, the simple test system depicted in Fig. 2 was implemented in Simulink. The power plants at bus 1 and 2 are modeled using their synchronous reactance, the swing equation, the first turbine model from [18] and a PID regulator. A DC power flow was used for modelling the power flow. The stochastic load at bus 5 was modelled as white noise through an integrator. Its power was chosen such that the power system frequency stayed within its allows band of $0.1Hz$. Process noise was added to the angular speed $\Delta\omega[n]$ of the power plant at bus 1. For a more detailed derivation of the test system please refer to [17]. When $r[n] = 0$ the only external excitations are $e[n]$ and $e_l[n]$, that means no process noise is added to the

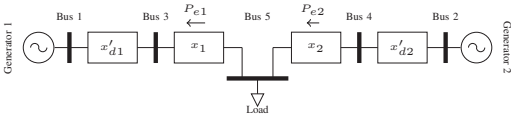


Fig. 2: Small test system used for the simulations

power plant at bus 2. In this section, the excitation signal $r[n]$ will always be applied and will be given by a white noise of standard deviation $\frac{0.1}{50\cdot 3}$. This standard deviation was chosen to keep the per unit value of $r[n]$ within $0.1[Hz]$ with a $99.7\%$ probability, where $0.1/50[p.u.]$ is the allowed band of the power system frequency in normal operation[2].

To strengthen the conclusions from the simulations a Monte Carlo Simulation (MCS) approach was used. The approach consisted of running the test system for a simulation time of $1200s$ to generate the different datasets. The transfer functions $S(z,\hat{\theta}_N)$, $G_1(z,\hat{\theta}_N)$, $G_p(z,\hat{\theta}_N)$ and $G_J(z,\hat{\theta}_N)$ were then identified using these datasets and the functions provided by the system identification MATLAB toolbox [19]. For the SISO systems a box-Jenkins model structure was used and for the MISO systems a high order ARX model structure was preferred. This simulations and identification were repeated a $1000$ times, and stochasticity was added by regenerating the process noise $e[n]$, and the stochastic load $e_l[n]$ after each simulation. Since $r[n]$ is a signal generated for the purpose of the identification it is only generated once.

As mentioned in Remarks 6, 7 and 8, the absence of a delay in certain transfer functions leads to a bias that will be smaller for smaller values of the SNR (by SNR, we here mean the ratio of the contribution of $e_l[n]$ $r[n]$ to $u[n]$ and of the contribution of $e[n]$ to $u[n]$). To check this, we ran multiple MCS for different values of the SNR. Different SNR values can be obtained by changing the variance of $e[n]$ in the process noise.

Let us first consider the procedure of Section III-B and let us apply this procedure $1000$ times and for different values of the SNR to derive models for $G_p(z)$ and $G_J(z)$. These models of $G_p(z)$ and $G_J(z)$ can subsequently be used to derive models for $G_1(z)$ and $S(z)$ using (5) and (7). In Fig. 3, we represent the means of the frequency responses of the models $G_p(z)$ and $G_J(z)$ obtained in this way and we observe that the bias remains limited even for small values of the SNR. The same can also be said for the means of the models for $G_1(z)$ and $S(z)$ (see Fig.4 and 5).

The procedure of Section III-A based on the data set $Z_{ur}^N$ has also been tested using a MCS for different values of the SNR. This procedure yields the mean values represented in red in Fig. 3 and 4. We observe a small bias for high SNR, but a larger bias than in the case of the procedure in Section III.B for lower values of the SNR. The procedure in Section III.A seems thus more sensitive (at least in in this example) to the bias introduced by the absence of delay. Note also that, since $S(z)$ is identified directly in this procedure, the low gain in low frequencies is more difficult to identify (see Fig. 4).

[2]In practice the power system will sometimes leave this band

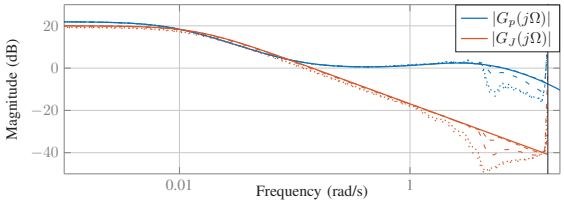


Fig. 3: The mean value of $|G_p(e^{j\Omega},\hat{\theta}_N)|$ and $|G_J(e^{j\Omega},\hat{\theta}_N)|$ calculated from the MCS. The solid lines are the analytical calculated versions and the dashed loosely dashed dotted and loosely dotted lines represent an SNR of $50dB$, $26dB$, $6dB$, and $3dB$ respectively

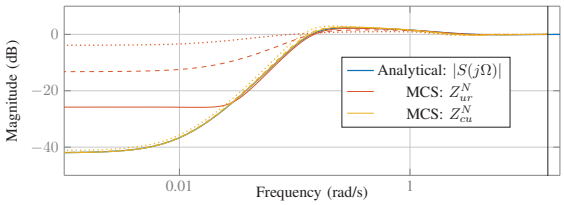


Fig. 4: The mean value of $|S(e^{j\Omega},\hat{\theta}_N)|$ calculated analytical and from the MCS. The solid, dashed and dotted lines represent an SNR of $50dB$, $26dB$, and $6dB$ respectively

In the next section, the procedure discussed in Section V.C (i.e. a procedure with $r[n]=0$) will be used on real-life data.

## VII. Results from a real power plant

A test was performed on a power plant in the Norwegian power system. For the test the dataset $Z_u^N$ was collected with a small adjustment with respect to Fig. 1: the plant plant was operating with the power system frequency as the feedback signal. It would be possible to operate with the angular speed of the rotor as the feedback signal. However, to change to this operation the plant would have to be shut down. Since the difference between these two signals is negligible for slow dynamics, we decided to not change the feedback signal.

Results obtained from five different datasets are depicted in Fig. 6. The droop constant $\rho$ was chosen differently in each of these datasets. Moreover, the proportional constant of

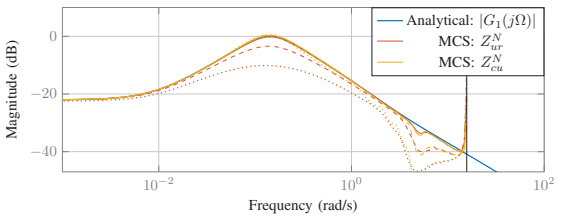


Fig. 5: The mean value of $|G_1(e^{j\Omega},\hat{\theta}_N)|$ calculated analytical and from the MCS. The solid, dashed and dotted lines represent an SNR of $50dB$, $26dB$, and $6dB$ respectively

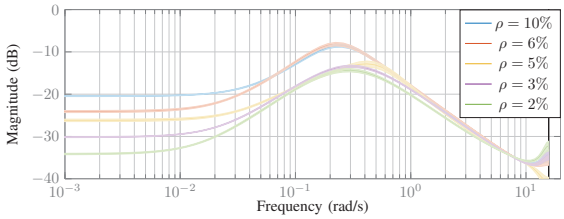


Fig. 6: Identification of $G_1(z, \hat{\theta}_N)$ with different droop

TABLE I: Droop setting and $G_1(0)$

| Droop | Data set lenght | | | |
|---|---|---|---|---|
| | $60min$ | $45min$ | $30min$ | $15min$ |
| 10% | 9.5% | 9.5% | 9.5% | 9.5% |
| 6% | 6.2% | 6.0% | 5.9% | 6.1% |
| 5% | 4.9% | 4.9% | 5.0% | 5.1% |
| 3% | 3.1% | 3.1% | 3.1% | 2.9% |
| 2% | 2.0% | 1.8% | 1.8% | 1.7% |

the PID regulator was changed from 2.5 to 5 for the datasets where the droop was below 6%. The datasets were recorded between the changing of the parameters, so they are about an hour long. In the figure one can see that the static gain of the disturbance rejection is changed when the droop is changed. Similarly, one can clearly see a change in the peak of the transfer function when the proportional constant of the PID regulator is changed. The legend of Fig. 6 shows the value of the droop the plant owner used for the dataset.

To check how good the obtained estimate is the droop setting was compared with the one calculated from the steady state gain of the estimated transfer function. The results are presented in TABLE I. As can be seen from the table there is a good correspondence even when only a part of the full data set (of 60 min) is used for the identification.

## VIII. Conclusions and Further Work

We have shown that both the stability requirements and the performance requirements for FCR providers can be checked in closed loop operation if extra excitation is added. Although, consistency cannot in general be guaranteed, we expect the bias due to this to be negligible. Moreover, the performance requirements ($G_1(z)$) can be checked without adding extra excitation. However, extra excitation will reduce the bias introduced by the lack of consistency.

The best results were obtained by first estimating the transfer function for the FCR and the swing dynamics instead of estimating the transfer functions for checking the stability and performance requirements directly. This is promising as these are transfer function the TSOs normally are interested in addition to the ones used for checking the requirements.

In comparison to what is proposed in the new draft requirements our proposal is much less intrusive as only one test is needed and the plant can continue to operate in closed loop. We therefore recommend that the proposed approach should be considered for checking the new requirements in case they are enforced.

The analytical insight was confirmed using a simple test system and tests from a real power plant. However, the power plants were Pelton turbines, where one expects no backlash. In case one wants to attempt the approach for high pressure Francis turbines or Kaplan turbines the approach will have to be modified to account for backlash.

There are also room for improvements in the current proposed approach. In particular it should be investigated whether or not the bias introduced by the lack of the delay can be mitigated and how large bias one can expect from an actual power plant. Moreover, if one wants to add extra excitation one should look into how to best design the excitation signal.

## References


[1] P. W. Group, "Technical requirements for frequency containment reserve provision in the nordic synchronous area," Draft, Jun. 26, 2017.

[2] Dinh Thuc Duong, Kjetil Uhlen, Stig Løvlund, and Erik Alexander Jansson, "Estimation of hydro turbine-governor's transfer function from PMU measurements," presented at the IEEE PES General Meeting, Boston: IEEE, Jul. 2016.

[3] S. H. Jakobsen and K. Uhlen, "Vector fitting for estimation of turbine governing system parameters," in *2017 IEEE Manchester PowerTech*, Jun. 2017, pp. 1–6. DOI: 10.1109/PTC.2017.7980855.

[4] B. Mogharbel, L. Fan, and Z. Miao, "Least squares estimation-based synchronous generator parameter estimation using PMU data," in *2015 IEEE Power Energy Society General Meeting*, Jul. 2015, pp. 1–5. DOI: 10.1109/PESGM.2015.7286559.

[5] S. H. Jakobsen, K. Uhlen, and X. Bombois, "Identification of hydro turbine governors using PMU data," in *2018 IEEE International Conference on Probabilistic Methods Applied to Power Systems (PMAPS)*, Jun. 2018, pp. 1–6. DOI: 10.1109/PMAPS.2018.8440273.

[6] H. G. Aghamolki, Z. Miao, L. Fan, W. Jiang, and D. Manjure, "Identification of synchronous generator model with frequency control using unscented kalman filter," *Electric Power Systems Research*, vol. 126, pp. 45–55, Sep. 2015, ISSN: 0378-7796. DOI: 10.1016/j.epsr.2015.04.016.

[7] N. D. Hatziargyriou, E. S. Karapidakis, G. S. Stavrakakis, I. F. Dimopoulos, and K. Kalaitzakis, "Identification of synchronous machine parameters using constrained optimization," in *Power Tech Proceedings, 2001 IEEE Porto*, vol. 4, 2001, 5 pp. vol.4–. DOI: 10.1109/PTC.2001.964812.

[8] D. Kosterev, "Hydro turbine-governor model validation in pacific northwest," *IEEE Transactions on Power Systems*, vol. 19, no. 2, pp. 1144–1149, May 2004, ISSN: 0885-8950. DOI: 10.1109/TPWRS.2003.821464.

[9] J. C. N. Pantoja, A. Olarte, and H. Díaz, "Simultaneous estimation of exciter, governor and synchronous generator parameters using phasor measurements," in *2014 Electric Power Quality and Supply Reliability Conference (PQ)*, Jun. 2014, pp. 43–49. DOI: 10.1109/PQ.2014.6866781.

[10] L. N. Hannett, J. W. Feltes, and B. Fardanesh, "Field tests to validate hydro turbine-governor model structure and parameters," *IEEE Transactions on Power Systems*, vol. 9, no. 4, pp. 1744–1751, Nov. 1994, ISSN: 0885-8950. DOI: 10.1109/59.331426.

[11] D. J. Trudnowski and J. C. Agee, "Identifying a hydraulic-turbine model from measured field data," *IEEE Transactions on Energy Conversion*, vol. 10, no. 4, pp. 768–773, Dec. 1995, ISSN: 0885-8969. DOI: 10.1109/60.475851.

[12] L. Saarinen, P. Norrlund, and U. Lundin, "Field measurements and system identification of three frequency controlling hydropower plants," *IEEE Transactions on Energy Conversion*, vol. 30, no. 3, pp. 1061–1068, Sep. 2015, ISSN: 0885-8969. DOI: 10.1109/TEC.2015.2425915.

[13] S. J. Chapman, *Electric machinery and power system fundamentals*. McGraw-Hill New York, 2002, vol. 3.

[14] R. Eriksson, N. Modig, and A. Westberg, "FCR-n DESIGN OF REQUIREMENTS," ENTSO-E report, Jul. 4, 2017.

[15] ENTSO-E, "Future system inertia," 2015.

[16] L. Ljung, *System identification*. Springer, 1998.

[17] S. H. Jakobsen and K. Uhlen, "Development of a test system for identification of turbine dynamics using the dc power flow," presented at the Mathmod, Feb. 2018.

[18] Working Group on Prime Mover and Energy Supply Models for System Dynamic Performance Studies, "Hydraulic turbine and turbine control models for system dynamic studies," *IEEE Transactions on Power Systems*, vol. 7, no. 1, pp. 167–179, Feb. 1992, ISSN: 0885-8950. DOI: 10.1109/59.141700.

[19] Mathworks. (2018). System identification toolbox, [Online]. Available: https://se.mathworks.com/products/sysid.html.

# Appendix

# Appendix A

# An open data repository and a data processing software toolset of an equivalent Nordic grid model matched to historical electricity market data

Data in Brief 11 (2017) 349–357

Contents lists available at ScienceDirect

Data in Brief

journal homepage: www.elsevier.com/locate/dib

Data Article

# An open data repository and a data processing software toolset of an equivalent Nordic grid model matched to historical electricity market data

Luigi Vanfretti [a,*], Svein H. Olsen [b], V.S. Narasimham Arava [a], Giuseppe Laera [a], Ali Bidadfar [c], Tin Rabuzin [d], Sigurd H. Jakobsen [d], Jan Lavenius [a], Maxime Baudette [a], Francisco J. Gómez-López [a]

[a] SmarTS Lab, KTH Royal Institute of Technology, Stockholm, Sweden
[b] Statnett SF, Oslo, Norway
[c] Technical University of Denmark, Risø, Denmark
[d] Norwegian University of Science and Technology, Trondheim, Norway

ARTICLE INFO

*Article history:*
Received 7 November 2016
Received in revised form
27 January 2017
Accepted 9 February 2017
Available online 13 February 2017

*Keywords:*
Electrical power systems
Electric power transmission
Smart grid
Power system modeling and simulation
Power system dynamics
Dynamic simulations
Power flow
Common Information Model (CIM)
Modelica
Historical market data
Modeling
Simulation

ABSTRACT

This article presents an open data repository, the methodology to generate it and the associated data processing software developed to consolidate an hourly snapshot historical data set for the year 2015 to an equivalent Nordic power grid model (aka Nordic 44), the consolidation was achieved by matching the model's physical response w.r.t historical power flow records in the bidding regions of the Nordic grid that are available from the Nordic electricity market agent, Nord Pool.

The model is made available in the form of CIM v14, Modelica and PSS/E (Siemens PTI) files. The Nordic 44 model in Modelica and PSS/E were first presented in the paper titled "iTesla Power Systems Library (iPSL): A Modelica library for phasor time-domain simulations" (Vanfretti et al., 2016) [1] for a single snapshot. In the digital repository being made available with the submission of this paper (SmarTSLab_Nordic44 Repository at Github, 2016) [2], a total of 8760 snapshots (for the year 2015) that can be used to initialize and execute dynamic simulations using tools compatible with CIM v14, the Modelica language and the proprietary PSS/E tool are provided. The Python scripts to generate the snapshots (processed data) are also available with all the data in the

* Corresponding author.
*E-mail address:* luigiv@kth.se (L. Vanfretti).

http://dx.doi.org/10.1016/j.dib.2017.02.021

GitHub repository (SmarTSLab_Nordic44 Repository at Github, 2016) [2].

This Nordic 44 equivalent model was also used in iTesla project (iTesla) [3] to carry out simulations within a dynamic security assessment toolset (iTesla, 2016) [4], and has been further enhanced during the ITEA3 OpenCPS project (iTEA3) [5]. The raw, processed data and output models utilized within the iTesla platform (iTesla, 2016) [4] are also available in the repository. The CIM and Modelica snapshots of the "Nordic 44" model for the year 2015 are available in a Zenodo repository.



## Specifications Table

| | |
|---|---|
| Subject area | *Electric Power Systems* |
| More specific subject area | *Power system dynamics and simulation* |
| Type of data | *Excel files, Tables, Figures* |
| How data was acquired | *Historical Data Records: Nord Pool;*<br>*Source Model Parameter Data: Literature* [6,7] |
| Data format | *Raw, Processed* |
| Experimental factors | *Power flows were obtained for the Nordic 44 model in PSS/E for every one hour for the year 2015 and were consolidated by matching the model's physical response with data records available from Nord Pool.* |
| Experimental features | *CIM v14 files and Modelica records were generated from the consolidated/matched PSS/E snapshots of the Nordic 44 model.* |
| Data source location | *Electric market data for the Nordic grid*<br>*Nord Pool webpage (*http://www.nordpoolspot.com*) (for historical power flow data), model structure data from* [6,7] *and modifications documented in this article.* |
| Data accessibility | *The processed data is archived in a Zenodo repository at:*<br>- https://doi.org/10.5281/zenodo.162907 (2015 data)<br>*The data processing software is made available in a GitHub repository:*<br>Nordic44-Nordpool http://dx.doi.org/github.com/SmarTS-Lab/Nordic44-Nordpool |

## Value of the data

- The raw Nord Pool data of the power flow records matched with the model's response (processed data) yield thousands of representations of the Nordic 44 model that can be useful to understand the power flow patterns and the electricity market's operation in the Nordic synchronous electric power system during 2015.
- The Nordic 44 model can be used as a test system for power system studies, including static and dynamic analysis under realistic operation conditions for 2015. For example, it can be used to train and test Machine Learning techniques (e.g. Decision Trees) and other computational techniques that are essential in the work flows used for dynamic security assessment of electrical power systems.
- The processed data and models can be used to test and validate the functionalities of power system security assessment software both offline and online dynamic assessment tools, e.g. iTesla [3,4], DSAT [8], SIGAURD [9].

- The data provided using the CIM v14 standard can be used to test the functional layer of applications in Smart Grid Architectures and most importantly, to quantitatively assess the interoperability of power system simulation tools that adopt CIM.
- The data and models provided in Modelica can be used with any Modelica compliant software tool to perform power system dynamic simulations and studies. When using OpenModelica [10], this provides researchers with a fully open source software environment for dynamic simulation.

## 1. Data

### 1.1. Matching historical market data

Raw data from Nord Pool was consolidated with a physical model representation of the Nordic grid by matching the measurement records to the model's power flow results (processed data). This has resulted in thousands of representations of the "Nordic 44" model for the year 2015 that are made available in the GitHub repository with the submission of this article.

These snapshots are provided in the form of CIM v14, Modelica and PSS/E (Siemens PTI) files. The Python scripts (i.e. software toolset) used to generate these snapshots (CIM v14, Modelica and PSS/E) are also made available in the repository.

### 1.2. Historical market data

The pre-processed (raw) data was downloaded from Nord Pool webpage. For each hour, the records contain the active power production and consumption data in the bidding regions of the Nordic grid and the active power exchange between them. These records were matched to an electrical grid model steady-state response, as explained next.

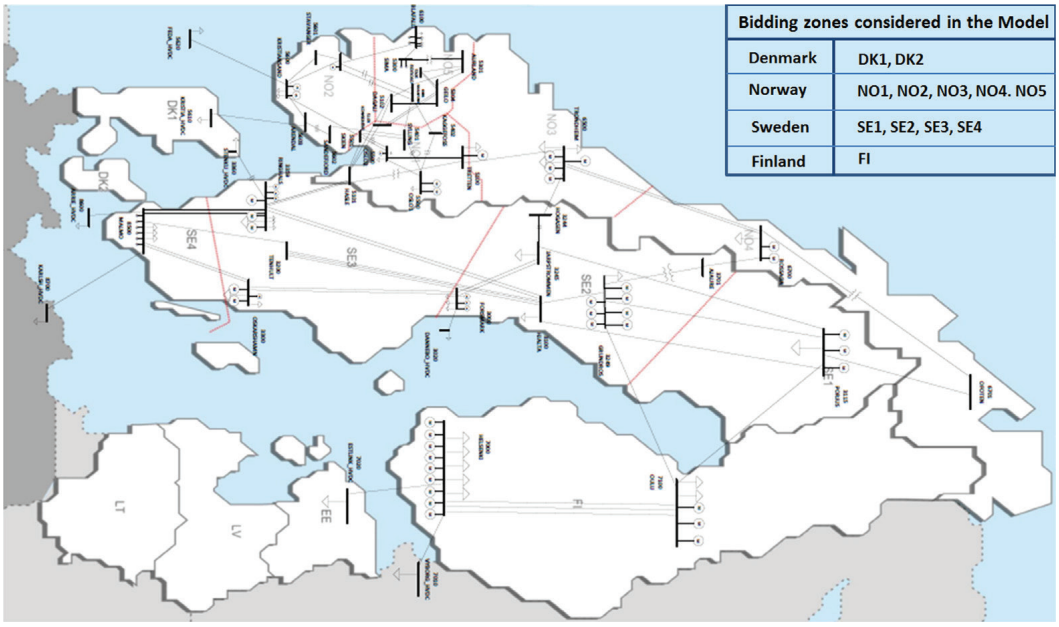


**Fig. 1.** SmarTS Lab Nordic 44 Equivalent Model Mapped to the bidding zones of the Nordic grid used in Nord Pool for 2015.

### 1.3. Model parameter and structure data

To match and consolidate the historical market data to a physical description of the power network, the Nordic 44 model was developed. Note that the aim here was to set a "base case", from which multiple snapshots of actual measurements records could be mapped to the quantitative response from computations on a physical model of the grid that included both steady-state and dynamic analysis features.

The development of this source model/"data" consisted of (a) obtaining editable files in the PSS/E form to, (b) extend the model to represent better the Norwegian portions of the Nordic grid and to adapt it to modeling limitations in both the iTesla platform and the iPSL library (i.e. lack of HVDC link models).

*Step (a)* used source files which was stripped from user defined models and other equipment, and other additional modifications carried out by Emil Hillberg of STRI on behalf of Statnett SF. The resulting model of this step is archived in Models.zip in respective Zenodo repositories.
Note that the starting model is an extension itself of the Nordic 23 bus model developed at SINTEF Energy Research in several steps [6]. The Nordic 23 bus model was developed from a 15 bus Nordic power system model developed at NTNU and the details of this model are explained in [7].
*Step (b)* included the assignment of bus bar names, grouping of busses according to the actual bidding region, and numerous other changes as described in the documentation available in./…/SmarTSLab_Nordic44/00_Documentation/N44_changes.docx.

The model developed in Step (b) is used throughout the historical data matching and consolidation process to create snapshots of the actual operational conditions of the Nordic Grid for 2015. This base case can be found in the repository in the GitHub repository at./nordic44/models/ and archived in Models.zip in respective Zenodo repositories.

## 2. Experimental design, materials and methods

### 2.1. Pre-processed data

The pre-processed (raw) data was downloaded from Nord Pool webpage as MS-Excel files (Consumption_xx.xlsx, Exchange_xx.xlsx, and Production_xx.xlsx) were saved in a folder with

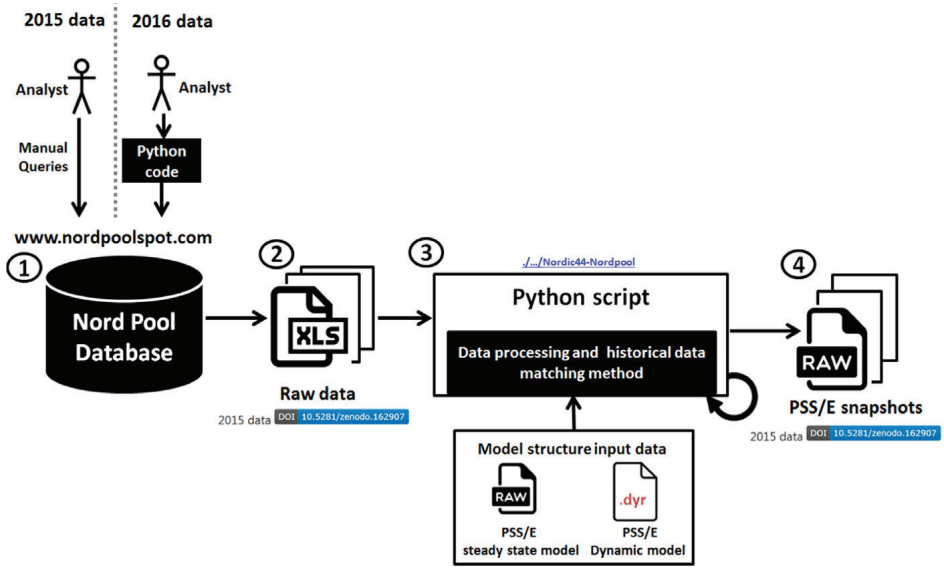


**Fig. 2.** Matching and consolidation of historical data with the Nordic 44 grid model.

corresponding date (e.g. N44_20150401 refers to the folder containing the hourly snapshots of the 1st April 2015). The MS-Excel files (Production_xx.xlsx and Consumption_xx.xlsx) contain the active power production and consumption data in the bidding regions of the Nordic grid for every hour as shown in Fig. 1. The MS-Excel file (Exchange_xx.xlsx) contains the active power exchange data between the bidding regions of the Nordic grid for every hour. Now, the toolset was updated to automatically download the data from the Nord Pool ftp server, inspired by the work in [11]. The raw data is stored in a Python dictionary allowing for easy data manipulation in Python and integration with PSS/e through psspy. It is still possible to save the data to excel and to load in excel files to the dictionary ensuring both forward and backward compatibility.

### 2.2. Data processing method

For each hour, an equivalent Nordic power system model (Nordic 44) was created, matched and consolidated with the load generation balance in the bidding regions and the active power exchange between the bidding regions. The buses in the Nordic 44 model were named according to the closest city or town corresponding to both the geographical location and the detailed grid structure available to Statnett SF. The work flow used to create the PSS/E snapshots is shown below in Fig. 2.

The major steps of the data processing workflow include:

(1) The raw data for the year 2015 was downloaded from Nord Pool (http://www.nordpoolspot.com) to MS-Excel files through manual queries to the Nord Pool database. This procedure was automated by implementing a Python class for connecting to the Nord Pool ftp server and handling the Nord Pool data. An example on how to use the Python code to generate the cases is

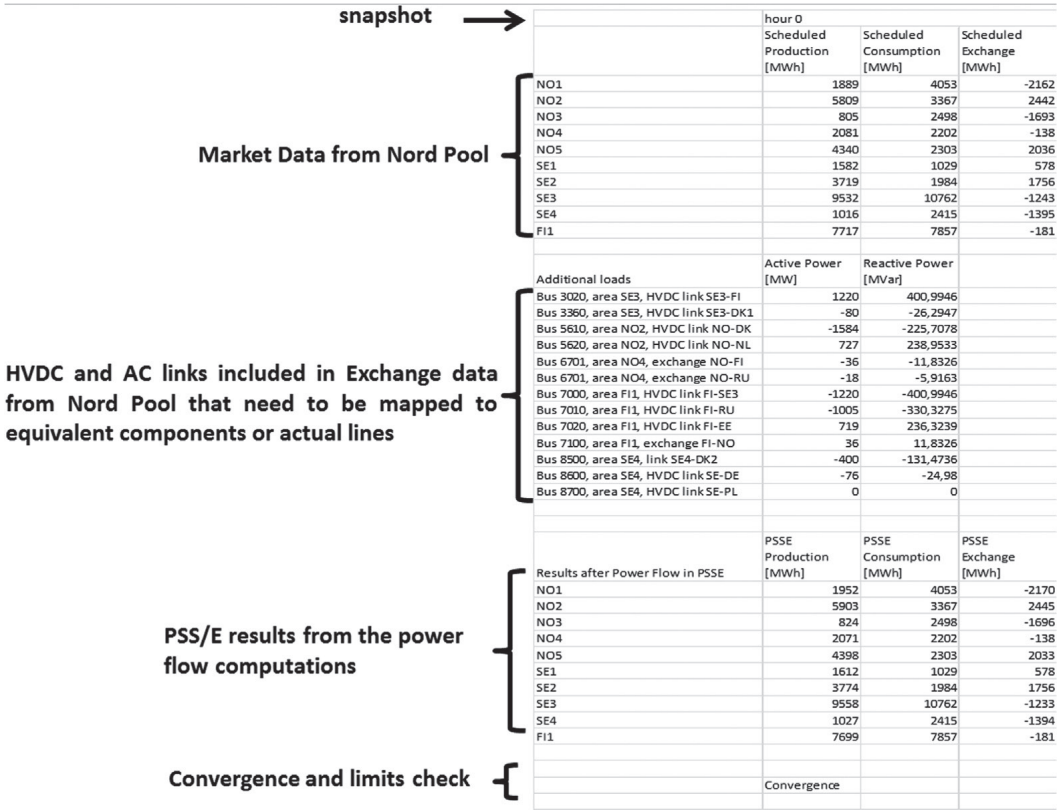


| | hour 0 | | |
|---|---|---|---|
| | Scheduled Production [MWh] | Scheduled Consumption [MWh] | Scheduled Exchange [MWh] |
| NO1 | 1889 | 4053 | -2162 |
| NO2 | 5809 | 3367 | 2442 |
| NO3 | 805 | 2498 | -1693 |
| NO4 | 2081 | 2202 | -138 |
| NO5 | 4340 | 2303 | 2036 |
| SE1 | 1582 | 1029 | 578 |
| SE2 | 3719 | 1984 | 1756 |
| SE3 | 9532 | 10762 | -1243 |
| SE4 | 1016 | 2415 | -1395 |
| FI1 | 7717 | 7857 | -181 |

| Additional loads | Active Power [MW] | Reactive Power [MVar] |
|---|---|---|
| Bus 3020, area SE3, HVDC link SE3-FI | 1220 | 400,9946 |
| Bus 3360, area SE3, HVDC link SE3-DK1 | -80 | -26,2947 |
| Bus 5610, area NO2, HVDC link NO-DK | -1584 | -225,7078 |
| Bus 5620, area NO2, HVDC link NO-NL | 727 | 238,9533 |
| Bus 6701, area NO4, exchange NO-FI | -36 | -11,8326 |
| Bus 6701, area NO4, exchange NO-RU | -18 | -5,9163 |
| Bus 7000, area FI1, HVDC link FI-SE3 | -1220 | -400,9946 |
| Bus 7010, area FI1, HVDC link FI-RU | -1005 | -330,3275 |
| Bus 7020, area FI1, HVDC link FI-EE | 719 | 236,3239 |
| Bus 7100, area FI1, exchange FI-NO | 36 | 11,8326 |
| Bus 8500, area SE4, link SE4-DK2 | -400 | -131,4736 |
| Bus 8600, area SE4, HVDC link SE-DE | -76 | -24,98 |
| Bus 8700, area SE4, HVDC link SE-PL | 0 | 0 |

| Results after Power Flow in PSSE | PSSE Production [MWh] | PSSE Consumption [MWh] | PSSE Exchange [MWh] |
|---|---|---|---|
| NO1 | 1952 | 4053 | -2170 |
| NO2 | 5903 | 3367 | 2445 |
| NO3 | 824 | 2498 | -1696 |
| NO4 | 2071 | 2202 | -138 |
| NO5 | 4398 | 2303 | 2033 |
| SE1 | 1612 | 1029 | 578 |
| SE2 | 3774 | 1984 | 1756 |
| SE3 | 9558 | 10762 | -1233 |
| SE4 | 1027 | 2415 | -1394 |
| FI1 | 7699 | 7857 | -181 |

| | |
|---|---|
| Convergence | |

**Fig. 3.** Screenshot of the MS-Excel file PSSE_in_out.xlsx.

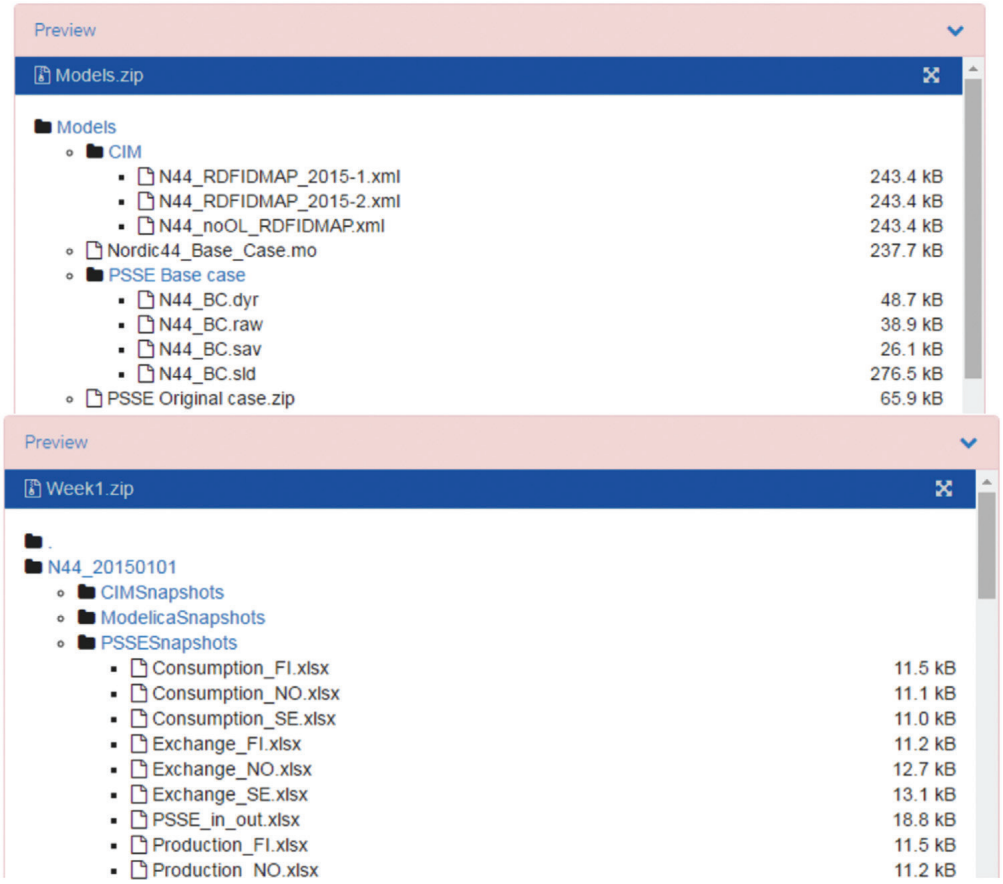


**Fig. 4.** Screenshot of the Zenodo repository showing the Nordic 44 model and PSS/E snapshots.

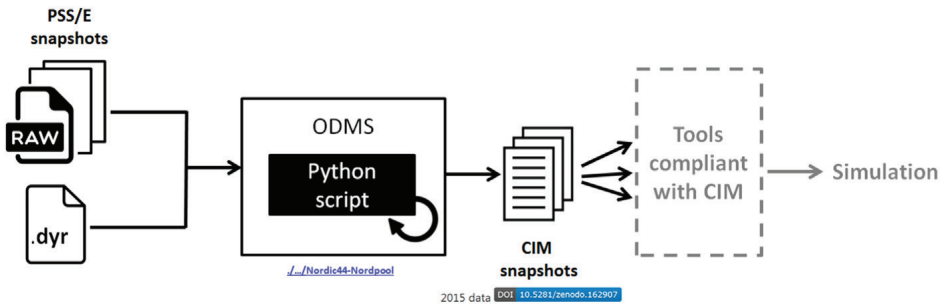


**Fig. 5.** Generation of CIM v14 snapshots.

provided in the GitHub repository (./examples/multiple_data_sets_from_nordpool.py /data_set_-from_nordpool.py)

(2) The raw data from Nord Pool contains only active power flow measurements (generation, consumption and exchange) within the bidding regions and between the bidding regions, for every hour.

(3) Another Python script simulates/computes the power flow with the constraint of minimizing the error between the power through the lines between the bidding regions. The method implemented in the Python script performs several checks (e.g. convergence, limits etc.), and after

completing these tasks, it computes the error between the Nord Pool measurement records and those obtained from the Python script computations on the Nordic 44 model. A summary of results is written in an MS-Excel file for each snapshot and named PSSE_in_out.xlsx.

(4) The obtained PSS/E snapshots (processed data) contain the power flow solutions that give the best match to the historical data from Nord Pool. These are necessary to initialize simulations, especially those needed for DSA.

At the end of this work flow, MS-Excel files (PSSE_in_out.xlsx) are generated by the Python script for every snapshot with raw data from Nord Pool and the results from PSS/E. These MS-Excel files (PSSE_in_out.xlsx) include limit checking messages (branch overloading, bus voltage out of limits and generator overloading). A screenshot of the created Excel file is shown in Fig. 3.

The PSS/E snapshots for each hour before solving the power flow (hx_before_PF.raw, unmatched processed data) and after solving the power flow (hx_after_PF.raw, matched processed data) were also made available in the repository. The Nordic 44 model and the PSS/E snapshots can be accessed from the repository as shown in Fig. 4.

### 2.3. Processed data and post-processing

CIM v14 and Modelica snapshots were generated from the matched PSS/E solved power flow snapshots (processed data). The PSS/E snapshots and PSS/E dynamic model parameters data (.dyr) files were used by the Python script to generate the CIM v14 snapshots as shown in Fig. 5. The Python script uses the Application Programming Interface (API) of the Operational Database Management System (PSS/ODMS) software [12] to generate the snapshots. These generated CIM snapshots can be used for information exchange according to CIM and to perform analysis in CIM compliant tools [13,14].

The generated CIM snapshots were placed in the folder corresponding to the day they refer to (e.g. N44_20150401 refers to the 1st of April 2015). In each folder there are three files that define individual CIM snapshots for each hour (N44_hx_EQ.xml, N44_hx_SV.xml and N44_hx_TP.xml). N44_noOL_RDFIDMAP.xml is the file with IDs mapping of those cases with fixed overloading problems. N44_RDFIDMAP_2015-1.xml and N44_RDFIDMAP_2015-2.xml are the files with IDs mapping of the remaining snapshots from 2015. The screenshot of the generated CIM snapshots in the GitHub repository is shown in Fig. 6.

PSS/E snapshots and PSS/E dynamic model parameters data (.dyr) files were used by the Python script "*Raw2Record*" (./…/SmarTS-Lab/Raw2Record) to generate the associated Modelica snapshots as

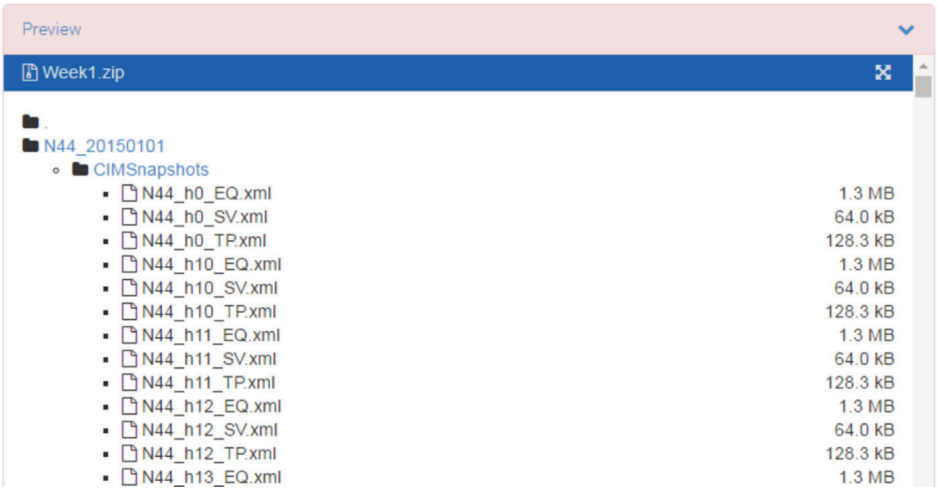


**Fig. 6.** Screenshot showing the CIM v14 snapshots.

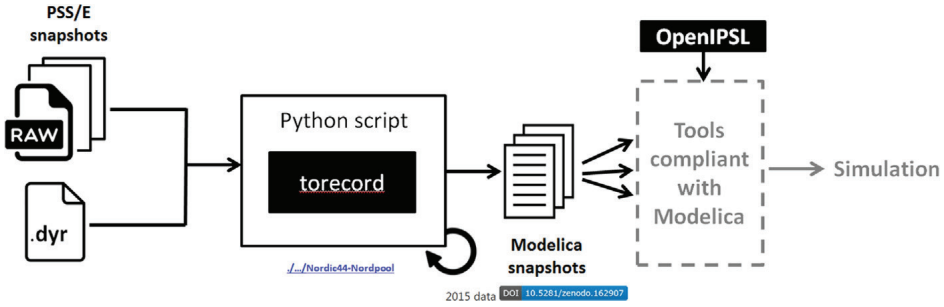


**Fig. 7.** Generating Modelica snapshots.

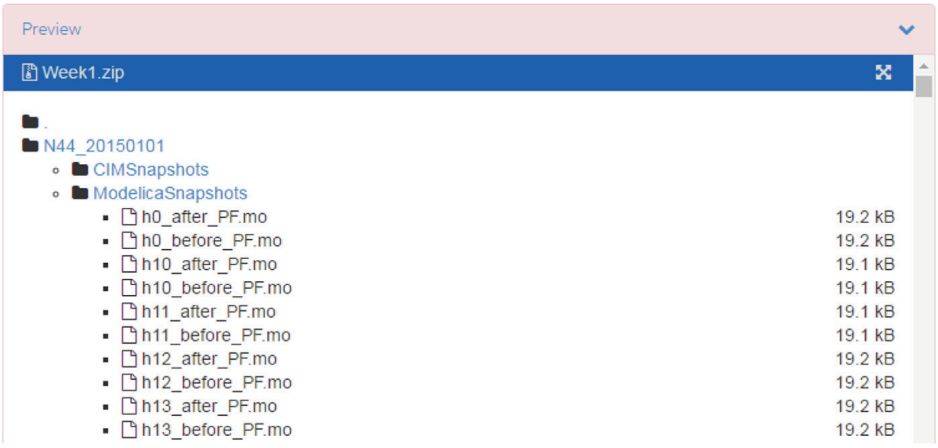


**Fig. 8.** Screenshot to access Modelica snapshots.

shown in Fig. 7. These generated Modelica snapshots together with the OpenIPSL library can be used for simulation in the Modelica compliant tools. The generation of the record files using the python script is illustrated with an example (./examples/multiple_data_sets_from_nordpool.py /data_set_-from_nordpool.py) and is provided in the GitHub repository.

During the iTesla project, another methodology to generate Modelica model snapshots using the iTesla platform [3] was attempted. Note that these snapshots were created using a different methodology reported in [15]. The resulting snapshots available for this approach cover only from April 1, 2015 to July 31, 2015 and are archived in iTesla_Platform.zip in the Zenodo repository. This archive contains both the snapshot models together with the appropriate version of the iPSL library.

The data records are stored in the /ModelicaSnapshots/ sub-folder of the Zenodo archive. They require the Modelica model that was manually implemented for Nordic 44 reported in [1] with the record structures corresponding to the PSS/E snapshots. The Python script ("torecord") used to generate Modelica snapshots from PSS/E snapshots as described in Fig. 7. The OpenIPSL library used in generation of these snapshots can be found in./…/SmarTS-Lab/OpenIPSL (Fig. 8).

The CIM and Modelica snapshots (processed data) of the "Nordic 44" model for the year 2015 are available the aforementioned Zenodo repository (see [2]).

## Acknowledgements

The Nordic44 data and model reported in this paper were used in the iTesla project (iTesla) [3] to carry out simulations within a dynamic security assessment toolset (iTesla, 2016) [4]. The raw, processed data and output models utilized within the iTesla platform [4]. The Modelica modeling has

been further enhanced during the ITEA3 OpenCPS project (iTEA3) [5]. iTesla (2016) [4] are also available in the repository. The CIM and Modelica snapshots of the "Nordic 44" model for the year 2015 are available in a Zenodo repository (see [2]).

Therefore, the authors would like to acknowledge the contributions of Emil Hillberg of STRI that during the FP7 iTesla project by provided the source files for the Nordic 44 model and his suggested modifications to it as described in Section 1.2, step (a). The financial support from following funding bodies and projects is gratefully acknowledged:

- Vinnova through the funding supporting KTH SmarTS Lab in the ITEA 3 Project 14018 – OPENCPS [5],
- STandUP for Energy Collaboration Initiative, supporting the first author.
- Statnett SF, the Norwegian electrical power transmission system operator, supporting the second author, and
- The European commission through the FP7 iTesla Project [3].

## Transparency document. Supplementary material

Transparency data associated with this article can be found in the online version at http://dx.doi.org/10.1016/j.dib.2017.02.021.

## References

[1] L. Vanfretti, T. Rabuzin, M. Baudette, M. Murad, iTesla Power Systems Library (iPSL): A Modelica Library for Phasor Time-Domain Simulations, Elsevier Software X (2016) http://dx.doi.org/10.1016/j.softx.2016.05.001 (URL: ⟨https://github.com/SmarTS-Lab/OpenIPSL⟩).
[2] SmarTSLab_Nordic44 Repository at Github, URL: ⟨https://www.github.com/SmarTS-Lab/Nordic44-Nordpool⟩, 2016.
[3] iTesla: Innovative Tools for Electrical System Security within Large Areas. URL: ⟨http://www.itesla-project.eu/⟩.
[4] iTesla, iTesla Power System Toolbox (iPST). URL: ⟨https://www.github.com/itesla/ipst⟩, 2016.
[5] ITEA3, OpenCPS: Open Cyber-Physical System Model-Driven Certified Development. URL: ⟨http://www.itea3.org/project/opencps.html⟩.
[6] WILMAR WP5, Deliverable D5.1 System Stability Analysis, November. URL: ⟨http://www.wilmar.risoe.dk/Deliverables/WP5%20Deliverable%20D5-1%20final.pdf⟩, 2005.
[7] B.H. Bakken, Technical and Economic Aspects of Operation of Thermal and Hydro Power Systems, Doctoral Dissertation at the Norwegian University of Science and Technology. ⟨https://inis.iaea.org/search/search.aspx?orig_q=RN:30035980⟩, 1997.
[8] Powertech, DSATools. URL: ⟨http://www.dsatools.com⟩.
[9] Siemens, SIGUARD. URL: ⟨http://w3.siemens.com/smartgrid/global/en/products-systems-solutions/control-center-solutions/grid-control-platform/solutions/transmission-management/grid-stability/pages/online-dynamic-security-assessment.aspx⟩.
[10] P. Fritzson, Introduction to Modeling and Simulation of Technical and Physical Systems with Modelica, John Wiley & Sons, Inc, Hoboken, NJ, USA, 2011, URL: ⟨https://www.openmodelica.org⟩.
[11] Knut Bjørsvik, A Scheme for Creating an Small-Signal On-line Dynamic Security Assessment Tool (MSc Thesis), Norwegian University of Science and Technology, 2016, Available online: ⟨https://brage.bibsys.no/xmlui/handle/11250/2400486⟩.
[12] PSS®ODMS-CIM based Network Modelling and Analysis Software, URL: ⟨http://w3.siemens.com/smartgrid/global/en/products-systems-solutions/software-solutions/planning-data-management-software/model-data-management/pages/pss-odms.aspx⟩.
[13] CIM: Common Information Model. URL: ⟨https://www.entsoe.eu/major-projects/common-information-model-cim/Pages/default.aspx⟩.
[14] Common Grid Exchange Model Specification (CGEMS), version 2.5, Draft IEC 61970-600 Part 1. (Edition-2). URL: ⟨https://www.entsoe.eu/Documents/CIM_documents/IOP/CGMES_2_5_TechnicalSpecification_61970-600_Part%201_Ed2.pdf⟩.
[15] L. Vanfretti, M. Murad, J.F. Gómez-López, G. Leon, S. Machado, J.B. Heyberger, S. Petitrenaud, Towards Automated Power System Model Transformation for Multi-TSO Phasor Time Domain Simulations using Modelica, in: Proceedings of IEEE PES Innovative Smart Grid Technologies Europe, October 9–12, 2016, Ljubljana, Slovenia.

# Appendix B

# The Nordic 44 test network

# The Nordic 44 test network

Sigurd Hofsmo Jakobsen
Lester Kalemba
Espen Hafstad Solvang

December 13, 2018

## 1 Introduction

Power systems are among the largest, most complex systems ever constructed. Consequently, analysis of these systems often involve computer simulations, since it would be too complicated to analyse them analytically. However, for the purpose of education and understanding certain phenomena, small test networks specifically tailored for capturing the interesting phenomena, while still being small enough to be analysed analytically, are in use. Similarly, even with the computational power available today, small test networks are often used for studying specific phenomena during computer simulations. One such test network is the Nordic 44 (or N44) test network.

N44 is an aggregated dynamic power system simulation model designed for analysis of dynamic phenomena in the Nordic power grid. This network was initially developed at The Norwegian University of Science and Technology (NTNU) and has gone through many iterations before reaching its present state. In this short memo, the different stages of development of the network will be described along with a brief overview of how the multiple variations of N44 have been used and how they differ. Although, this is a task not necessary for the continued use and development of the network, it can hopefully be of interest for present and future users.

## 2 Historical background

As mentioned in the introduction, the test network went through many iterations before reaching its current state. In this section, the different versions known to the authors will be briefly presented and explained.

### 2.1 Nordic 15

The first iteration of the test network was developed during Bjørn Bakken's PhD study [1] at NTNU. It was used for studying a proposed concept for automatic generation control (AGC) with the introduction of more HVDC connections to

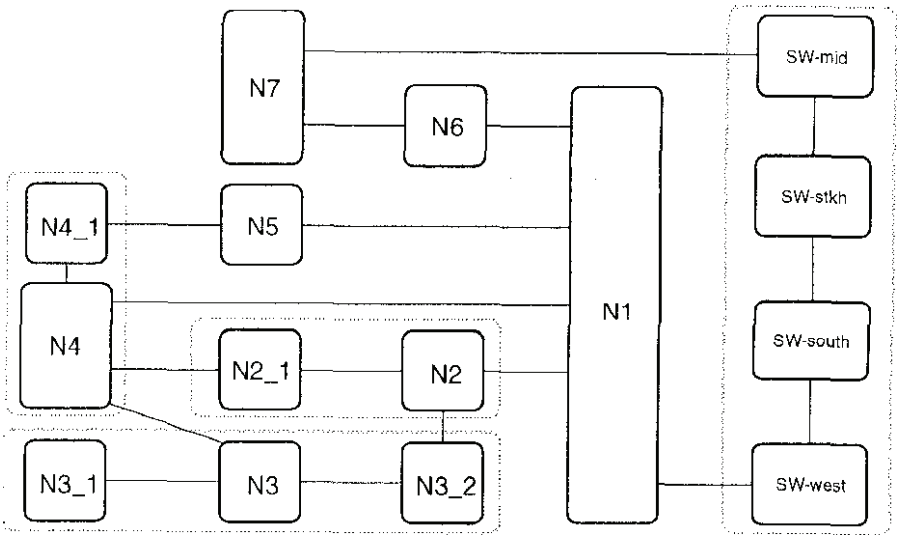


Figure 1: The 15 bus network from [1]

the Nordic power system. When the system was created only the HVDC connection to Denmark was present. In the model, three additional connections are added - one to the Netherlands and two to Germany. The network and proposed control concept was published in a journal article [2]. The Nordic 15 model was tuned using measurements from generator outages in the Norwegian power system and the methodology used is described in [1]. It is not an aggregated model of the whole Nordic system as it only includes buses in Norway and Sweden.

## 2.2 Nordic 18

The Nordic 15 bus system was later extended to an 18 bus system in [3]. The model was developed in PSS/E and has two major load situations for which it is tuned for both stationary and dynamic analysis. The model is used for long-term simulations of secondary control and AGC, and has modelled the large generation and load areas as well as tie-line interfaces of the Nordic system. The model is shown in Fig. 2.

## 2.3 Nordic 23

The test network was further developed and buses were added to create a 23 bus network. The network was used for investigating stability problems arising from the large-scale integration of variable renewable generation into the Nordic power system [4].

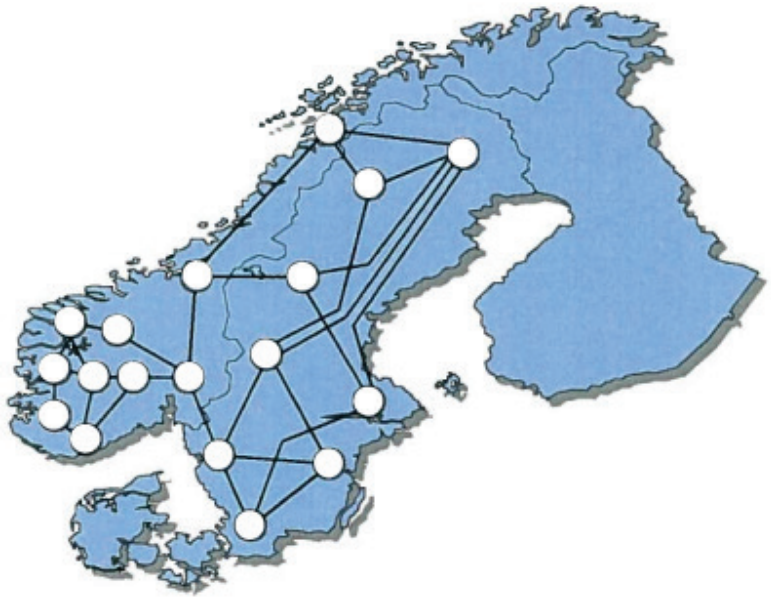

Figure 2: The 18 bus network from [3]

## 2.4 Relation to the Swedish (Nordic 32) test system

A perhaps better known test system than the Nordic 44 system is the Swedish test system. Normally, the system is referred to as the Nordic 32 system, a name very similar to the Nordic 23 bus system. It is, therefore, not surprising that there has been some confusion whether or not the Nordic 44 system originated from the Nordic 32 system. To avoid confusion we will refer to the Nordic 32 system as the Swedish test system.

This system was first described in [5] and referred to as the Swedish system. It was also adopted by the IEEE Power System Dynamic Performance Committee as a test system for voltage security [6]. By this committee, the network is referred to as the Nordic test system, a name that should be used with care, since the network originally was intended to represent Sweden and also to avoid confusion.

To further add to the confusion on the origins of the Nordic 44 system, the Swedish test system was merged with the Norwegian and Finnish part of the Nordic 23 system [7].

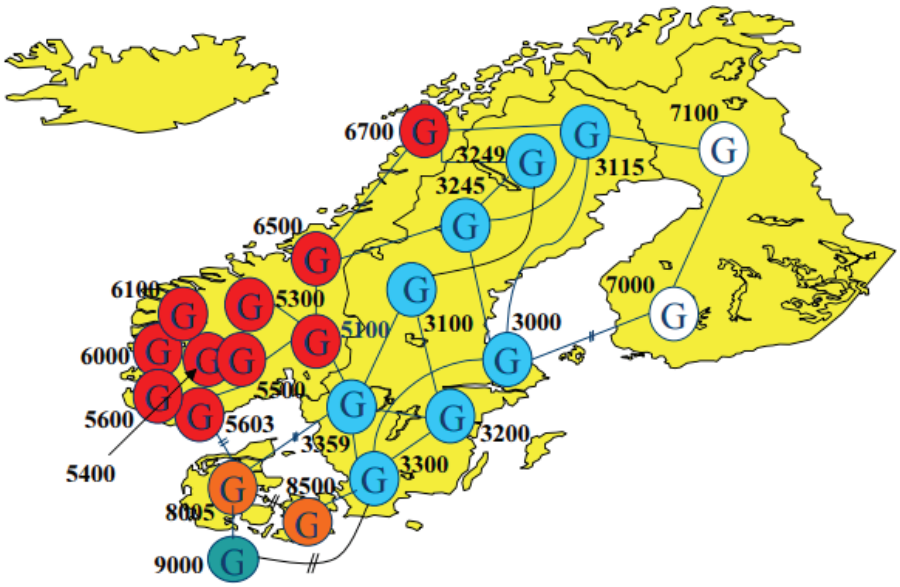


Figure 3: The 23 bus network from [4]

# 3 The Nordic 44 test network

In this section, it is briefly described how the Nordic 44 test network was developed from the Nordic 23 test network and some applications it has been used for.

## 3.1 Intial development of the Nordic 44 test network

Development of the Nordic 44 test system started following the initial development of a 66 bus network (Nordic 66) proposed by STRI. However, following consultations between STRI and NTNU, development of the Nordic 66 test system was discontinued. It was decided instead that an earlier version, the Nordic 23, be used and extended to capture the system state at the time. Subsequently, the Nordic 44 was created based on the Nordic 23. The initial model was mapped to real EMS data from Statnett by STRI in collaboration with NTNU. This work was done for Statnett in the iTesla project (EU FP7, 2012-2016).

## 3.2 Branching of N44

The N44 model has been used for different purposes and the model has been adjusted in a variety of ways to suit these purposes. The N44 model name, however, has not been changed for any of the model adjustments and an overview of the multitude of N44-variations is thus necessary. Primarily, there are two

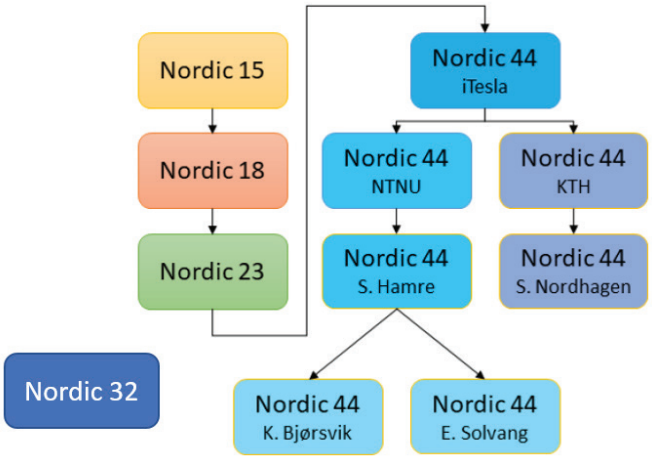


Figure 4: Overview of N44 development along with historical background pre-N44

model branches that are commonly referred to. These are the KTH-branch, and the NTNU-branch. For each of these branches, N44 has been used by several authors to achieve different goals. An overview of this development, along with historical background previously given, is shown in Fig. 4. The NTNU-branch has at NTNU been used extensively for dynamic analysis, which was the original intended purpose of the Nordic 44 model.

### 3.2.1 The KTH-branch

The KTH branch stems from continued development of N44 at KTH (Royal Institute of Technology in Stockholm) for the iTesla project. Their work includes mapping buses to market areas, giving buses geographical names, implementing the network in the Modelica language as well as mapping Nord Pool market data to the model. In KTH's first publication using the Nordic 44 test network, it was used to demonstrate the iTesla power system library [8]. The next publication documents the work on mapping Nord Pool market data to the test network together with data sets for 2015 and 2016. Links to the data sets and the code used for creating them are free and links can be found in the publication [9]. The KTH branch was utilized for reliability studies in [10] using MATPOWER/MATLAB, where the modelling of corrective actions in reliability analysis was studied. For this study, the version developed at KTH was used since it was deemed to have the most correct power flow between the Nord Pool market areas. A modified version of the KTH-branch Nordic 44 model was also used by [11] to study possible adverse interactions among independently tuned power system stabilizers.

### 3.2.2 The NTNU branch

NTNU's version of the Nordic 44 was based on a version given by STRI and not the version developed at KTH. It is available in PSS/E as well as DIgSILENT Powerfactory. The initial mapping of the buses to the market areas was improved by [12], who used the model for analyzing inertia and frequency containment reserves in the Norwegian power system. The model was also tuned for frequency response against a recent (2013) scheduled generator outage in Sweden. Although, the frequency response was tuned to have a response similar to the actual system this model is not stable. It is not evident from the system response during short simulations, but if the system is simulated for a longer time one will observe large oscillations in power and frequency. A closer investigation of the tuning of the governor revealed the governors to be tuned incorrectly.

Building on the work in [12], a further mapping of the buses to the market areas was performed in [13], where the model was used to create a small-signal online dynamic security assessment tool. To acquire operating states for this tool, a Python script for automatically downloading historical power exchange data from Nord Pool was developed. Small-signal stability was achieved using the stability analysis and control system design software PacDyn. The problem with the governors causing instability was also fixed in this version. Also building on the work in [12], simultaneous HVDC contingencies were simulated in [14] with the intention of observing frequency deviations and voltage dips following large loss of power import as well as investigating the ability of System Integrity Protection Schemes (such as HVDC Emergency Power) and corrective actions (such as generators' primary response) to hinder critical consequences.

## 3.3 Ongoing and future use of Nordic 44

Ongoing works involving the Nordic 44 model include stability assessment of future scenarios of the Nordic/European interconnected power system, being undertaken as part of the CloudGrid project. So far, several future load flow scenarios involving variations of generation from wind power plants and HVDC connections are under consideration.

# References


[1] B. H. Bakken, "Technical and economic aspects of operation of thermal and hydro power systems," Norges Teknisk-Naturvitenskapelige Univ., 1997. [Online]. Available: `https://inis.iaea.org/search/search.aspx?orig_q=RN:30035980` (visited on 06/13/2017).

[2] B. H. Bakken and O. S. Grande, "Automatic generation control in a deregulated power system," *IEEE Transactions on Power Systems*, vol. 13, no. 4, pp. 1401–1406, Nov. 1998, ISSN: 0885-8950. DOI: `10.1109/59.736283`.

[3] O. S. Grande, K. Uhlen, B. H. Bakken, M. Hernes, and O. B. Fosso, "Operational security assessment - planning and control," SINTEF Energy Research, Technical Report TR A5294, Oct. 17, 2000.

[4] W. WP5, "System stability analysis," SINTEF Energy Research, Deliverable TR F6212, Mar. 9, 2005. [Online]. Available: http://www.wilmar.risoe.dk/Results.htm.

[5] C. T. F. 38.02.08, "Long-term dynamics - phase II," Jun. 1995.

[6] IEEE PES Task Force on Test Systems for Voltage Stability Analysis and Security Assessment, "Test systems for voltage stability analysis and security assessment," PES - TR 19, Aug. 25, 2015.

[7] M. Seyedi and M. Bollen, "The utilization of synthetic inertia from wind farms and its impact on existing speed governors and system performance," Elforsk rapport 13:02, Jan. 2013. [Online]. Available: http://www.elforsk.se/Rapporter/?download=report&rid=13_02_.

[8] L. Vanfretti, T. Rabuzin, M. Baudette, and M. Murad, "iTesla power systems library (iPSL): A modelica library for phasor time-domain simulations," *SoftwareX*, vol. 5, pp. 84–88, 2016, ISSN: 2352-7110. DOI: 10.1016/j.softx.2016.05.001. [Online]. Available: http://www.sciencedirect.com/science/article/pii/S2352711016300097 (visited on 06/13/2017).

[9] L. Vanfretti, S. H. Olsen, V. S. N. Arava, G. Laera, A. Bidadfar, T. Rabuzin, S. H. Jakobsen, J. Lavenius, M. Baudette, and F. J. Gómez-López, "An open data repository and a data processing software toolset of an equivalent nordic grid model matched to historical electricity market data," *Data in Brief*, vol. 11, pp. 349–357, Apr. 2017, ISSN: 2352-3409. DOI: 10.1016/j.dib.2017.02.021. [Online]. Available: http://www.sciencedirect.com/science/article/pii/S2352340917300409 (visited on 06/13/2017).

[10] S. W. Nordhagen, "Reliability analysis of the nordic44 model and modelling of corrective actions in OPAL," 2017. [Online]. Available: https://brage.bibsys.no/xmlui/handle/11250/2440582 (visited on 06/13/2017).

[11] L. Kalemba, K. Uhlen, and M. Hovd, "Two-tier Approach for the Design of Multiple Power Oscillation Damping Controllers," *2016 IEEE EnergyCon*, Apr. 2016.

[12] S. M. Hamre, "Inertia and FCR in the present and future nordic power system," Master thesis, Norwegian University of Science and Technology, Trondheim, Jun. 2015.

[13] K. Bjørsvik, "A scheme for creating an small-signal on-line dynamic security assessment tool - using PSS/e and PacDyn," *138*, 2016. [Online]. Available: https://brage.bibsys.no/xmlui/handle/11250/2400486 (visited on 06/13/2017).

[14] E. H. Solvang, "Dynamic simulations of simultaneous hvdc contingencies in the nordic power system considering system integrity protection schemes," Master thesis, Norwegian University of Science and Technology, Trondheim, Jun. 2018.

[15] I. B. Sperstad, S. H. Jakobsen, and O. Gjerde, "Modelling of corrective actions in power system reliability analysis," in *POWERTECH 2015*, Eindhoven, Jun. 2015. DOI: 10.1109/PTC.2015.7232453. [Online]. Available: http://ieeexplore.ieee.org/ielx7/7210291/7232233/07232453.pdf?tp=&arnumber=7232453&isnumber=7232233.

[16] O. Gjerde, G. Kjølle, S. H. Jakobsen, and V. V. Vadlamudi, "Enhanced method for reliability of supply assessment - an integrated approach," in *2016 Power Systems Computation Conference (PSCC)*, Genoa, Jun. 2016, pp. 1–7. DOI: 10.1109/PSCC.2016.7540989. [Online]. Available: http://ieeexplore.ieee.org/document/7540989/.

[17] T. K. Vrana, E. S. Aas, T. I. Reigstad, and O. Mo, "Impact of Present and Future HVDC Links on the Nordic Power Grid," Manchester, UK, 2017. DOI: 10.1049/cp.2017.0056. [Online]. Available: http://ieeexplore.ieee.org/document/7934985/.

[18] E. Hagstrøm, I. Norheim, and K. Uhlen, "Large-scale wind power integration in norway and impact on damping in the nordic grid," *Wind Energy*, vol. 8, no. 3, pp. 375–384, DOI: 10.1002/we.168. eprint: https://onlinelibrary.wiley.com/doi/pdf/10.1002/we.168. [Online]. Available: https://onlinelibrary.wiley.com/doi/abs/10.1002/we.168.

# A Appendix: NTNU master thesis versions

This appendix attempts to summarize some of the changes made to the Nordic 44 model and how it has been used by graduates at NTNU. For further details, the reader is referred to the original works.

## A.1 Thesis of S. Nordhagen

All changes in this subsection refer to [10]. No changes made to PSS/E-model. Changes are made in MATLAB, by adjusting an mpc-struct in MATPOWER format. In this work, a MATLAB script adds three new buses after a power flow simulation. The three buses added are:

- 7030 FennoScan, a load bus for HVDC-cable from Finland to Norway. Corresponds to internal exchange in the Nordic power grid, with bus 3020 FennoScan. The power consumption at this bus is set to the negative of bus 3020 FennoScan, as, disregarding losses, the load consumed will be the negative of consumption at 3020 FennoScan.
- 6702 Exchange NO-FIN, exchange from Norway to Finland. A load bus in Norway which models power flow between Norway and Finland. The

exchange is set to 0 MW (interestingly, when setting the power exchange to zero, neither the load at this bus nor 7130 are directly set to zero. They are set equal to the load at 6701 Ofoten, where the load is zero).

- 7130 Exchange NO-FIN, exchange from Finland to Norway. A load bus in Finland which models power flow between Finland and Norway. The power consumption is, like bus 6702, set to zero.

Corrective actions related to reactive compensation were also implemented in the OPAL prototype contingency analysis module [15], [16] in the thesis of [10], but these corrective actions are not discussed here.

## A.2 Thesis of S. M. Hamre

Changes refer to the work of [12]. The generator and load count is reduced from 80 to 61, and 48 to 43 respectively. Some of the key model changes are:

- Moving power production from SE3 to SE1 and SE2 in order to obtain the right amount of hydropower with regards to FCR and inertia. This is because SE3 has thermal power plants, while SE2 and SE1 has hydropower plants, with different dynamic responses. This change will likely lead to increased deviation of power exchanges from NordPool data (cf. p. 50). To move power, MBase and PMax generator parameters changed in many cases when moving capacity around. In these cases, the ratio between the two parameters was maintained (cf. Ch. 7 for more details). Inertia constant $H$ is not changed, as it is related to the base MVA rating.

- The ZIP load model was changed from an initial 60/40/0 (I/Y/P, given in percentages) to 10/10/80. This was necessary to tune the frequency response from dynamic simulations to the measured frequency response in the real system for a generator outage that occurred in 2013. To achieve the right frequency nadir, HYGOV parameters were adjusted for each ZIP load case and are displayed in Table 20, pp. 51-52.

- Line impedances were reduced by 40% in order to circumvent line overloads, as lower impedances will lead to higher line ratings. (How a lower impedance leads to higher line ratings in the model is not understood; the line rating tabular values are certainly the same, but physically the heat generation would be different.) Reduction of impedance also improved the damping of the system, ref. p. 51.

- Branches that connect to HVDC buses all have their line ratings set to 0.

- PSS model STAB2A replaced by STAB1 in PSS/E.

Details of reducing the generator and load count as well as moving generation capacity around is omitted as it is performed through a trial-and-error approach.

### A.3 Thesis of K. Bjørsvik

Changes refer to the work of [13]. The generator and load count is reduced from 61 to 18, and 43 to 25 respectively. Some of the key changes made to the model are:

- Aggregating every generator at the same bus into an equivalent generator. Data describing one original generator was saved into a spreadsheet to be able to recalculate the aggregated generator data depending on how many generators that should be turned on.
- Aggregating every load at the same bus into an equivalent load.

See chapter 4.5 for details about how the aggregated generators and loads are changed in Python in dynamic simulations according to different cases from Nord Pool market data, and how losses are taken into account by 718 MW reduction of loads.

### A.4 Thesis of E. H. Solvang

Changes refer to the work of [14]. Used for dynamic simulation in PSS/E of simultaneous outages of HVDC interconnectors connecting the Nordic (Norway, Sweden and Finland) synchronous area to Continental Europe. Many case studies were performed and different adjustments were made to the generation and load. The goal of the adjustment was to retain the tuning for response in grid frequency achieved in [12] while adjusting HVDC power import. The simultaneous outages are studied in the context of high-impact low-probability (HILP) events and the disturbance should therefore be very large. The import of HVDC interconnectors is set to the maximum power transmission capacity of the modelled links. Adjusting the import alters the power flow of the system. Attempts are thus made to reduce the generation in proximity to the HVDC link so that the interregional power flow remains similar to before adjusting HVDC import. HVDC links exporting power are not considered. The thesis highlights a need for tuning of the dynamic voltage response of the N44 model. Contributions to the model are found in Python code using the PSSPY-API in PSS/E. Contributions include

- Added PV-buses representing the HVDC interconnectors North Sea Link and NordLink
- Added Under-Frequency Load Shedding by use of the Protection Relay Model DLSHBL

## B Appendix: The GridBalance model

The GridBalance model is dynamic power system simulation model with an aggregated representation of the grid expected in the Nordic power system in

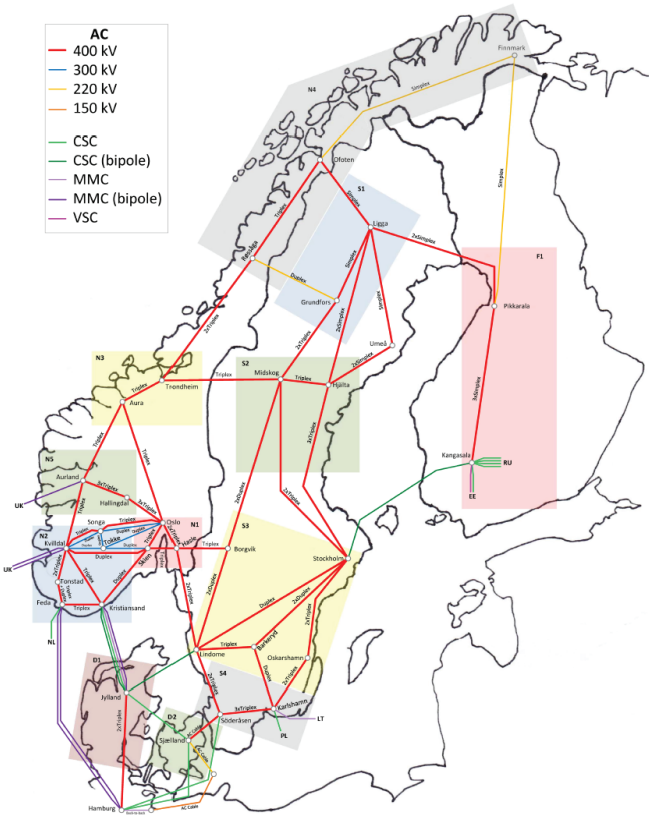


Figure 5: The GridBalance model, from [17].

2030. A presentation of the model is given in [17]. A graphical depiction of the grid model from [17] is reproduced in Fig. 5.

The model for the Nordic power system has 33 nodes, each comprising one or more AC buses. That grid equivalent was developed based in part on the 23-bus model used in [18], which in turn was based on [1], and implemented in DIgSILENT PowerFactory. Since the N44 model was also developed based on [1], the GridBalance model is in this sense related to the N44 model. In contrast to the N44 model, the GridBalance model also includes buses representing Denmark: one bus for Eastern Denmark (Zeeland, belonging to the Nordic synchronous area) and one bus for Western Denmark (Jutland, belonging to the Continental European system). In addition there is a bus in Northern Germany and an equivalent external grid model (from the PowerFactory library) connected to this bus to represent the Continental European power system.

Compared to the present-day (as of 2017) Nordic power system, the following HVDC links were added to the model: 4 HVDC interconnections under construction (KriegersFlak, NordLink, NSN-Link) or under development (NorthConnect) as well as 3 hypothetical HVDC links. As one of the objectives of the development of the GridBalance model is to study the impact of the increasing number of HVDC links in the Nordic power grid, HVDC converters are modelled with greater detail than for the N44 model. Furthermore, as stated in [17], the idea behind the work with the GridBalance model was to develop the model for use in different national and international research projects, as well as for educational purposes (PhD) without any restrictions due to intellectual property rights.

# Appendix C

# An alternative derivation of the frequency divider formula using the dc power flow

# An alternative derivation of the frequency divider formula using the dc power flow

Sigurd Hofsmo Jakobsen,
Kjetil Uhlen, Member, IEEE
Department of Electric Power Engineering
Norwegian University of Science and Technology,
Trondheim, Norway,
sigurd.h.jakobsen@ntnu.no

***Abstract*—The frequency divider is a simple yet reliable formula for estimating bus frequencies in dynamic power system simulation. In the original paper a thorough mathematical derivation of the formula is given. We will in this letter show that one will arrive at the same formula by applying a standard dc power flow description of the network. The assumptions behind the dc power flow are well known to all power system engineers and most students and should therefore be a good starting point for deriving the formula.**

## I. Introduction

Simple and reliable formulas explaining the workings of the power system are useful not only for simulation purposes, but also for the sake of analytical analyses of fundamental power system problems and teaching purposes. In this regard formulas such as the frequency divider [1] (FD) formula are powerful tools. The FD formula provides an easy yet reliable way to calculate bus frequencies as a function of generator speeds and the reactances in the system. It is an approach relevant for large scale dynamic power system simulations where the generator speeds and rotor angles are state variables. The advantage of the FD formula is that it is more precise than the often used centre of inertia (COI) equation, and more numerical stable than the use of a washout and filter as demonstrated in [1].

In [1] a thorough derivation of the FD formula is presented. However, as will be shown in this letter it is possible to arrive at the same formula if one starts with a standard dc power flow. The assumptions and rationale behind the dc power flow is assumed to be known, which makes it a good starting point for the derivation of the formula. It should be noted that, although, [1] starts out with a current injection model they make a number of assumptions. In fact through their assumptions they implicitly assume a dc power flow to end up with the final formula.

## II. Derivation of the frequency divider formula

The idea behind the derivation is that the fundamental frequency of the voltage at a certain bus can be calculated as the time derivative of the voltage angle at the same bus. We therefore only need to find an expression for the voltage bus angles as a function of the generator rotor angles.

The power flowing on the lines in a power system is related to the power injections at the buses through the power flow equations. The power flow equation for active power neglecting the terms related to ohmic losses and shunt elements is.

$$P_k = U_k \sum_{m \in \Omega_k} U_m x_{km}^{-1} \sin \theta_{km} \tag{1}$$

where:
$P_k$**:** is the power injection at node $k$,
$\theta_{km}$**:** is the voltage angle difference between node $k$ and $m$,
$x_{km}$**:** is the reactance between node $k$ and $m$,
$\Omega_k$**:** is the buses adjacent to bus $k$.
$U_k$**:** is the voltage at bus $k$.
$U_m$**:** is the voltage at bus $m$.

In real power systems the voltages are normally close to $1(p.u.)$ and the angles are small. Using these observations the DC power flow approximation is written as follows:

$$P_k \approx \sum_{m \in \Omega_k} x_{km}^{-1} \theta_{km} \tag{2}$$

To arrive at the same equation as in [1] we rewrite (3) in terms of the change in power due to change in angles.

$$\Delta P_k \approx \sum_{m \in \Omega_k} x_{km}^{-1} \Delta \theta_{km} \tag{3}$$

Written on matrix form this becomes:

$$\mathbf{\Delta P} = \mathbf{B} \mathbf{\Delta} \theta \tag{4}$$

where:
$\mathbf{\Delta P}$**:** is the vector of change in power injections,
$\mathbf{B}$**:** is the nodal susceptance matrix,
$\mathbf{\Delta}\theta$**:** is the vector of change in voltage bus angles.

It is important to note that the transient reactances of the generators are included in the nodal susceptance matrix $\mathbf{B}$. To arrive at the FD formula we write (4) as follows.

$$\begin{bmatrix} \mathbf{\Delta P}_e \\ \mathbf{\Delta P}_l \end{bmatrix} = \begin{bmatrix} \mathbf{B}_{11} & \mathbf{B}_{12} \\ \mathbf{B}_{21} & \mathbf{B}_{22} \end{bmatrix} \begin{bmatrix} \mathbf{\Delta}\theta_e \\ \mathbf{\Delta}\theta_l \end{bmatrix} \tag{5}$$

where:
$\mathbf{\Delta P}_e$**:** is the change in power injection at the generator buses
$\mathbf{\Delta P}_l$**:** is the change in power injection at the loads
$\mathbf{\Delta}\theta_e$**:** is the change in rotor angle at the generator buses
$\mathbf{\Delta}\theta_l$**:** is the change in voltage angle at the non generator buses

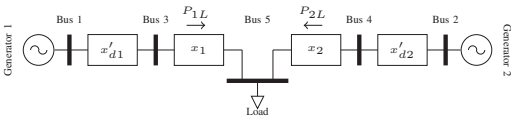


Fig. 1: Single line diagram of the system

In [1] a current injection formulation is used and the current injected at the load buses is assumed negligible. Similarly, we assume the change in power injection at the load buses $\mathbf{\Delta P}_l$ to be negligible The angle of the non generator buses can now be calculated as:

$$\mathbf{\Delta}\theta_l = -\mathbf{B}_{22}^{-1}(\mathbf{B}_{21}\mathbf{\Delta}\theta_e) \tag{6}$$

We now take the time derivative of both sides of (6) to go from angles to angular velocity.

$$\mathbf{\Delta}\omega_l = -\mathbf{B}_{22}^{-1}(\mathbf{B}_{21}\mathbf{\Delta}\omega_e) \tag{7}$$

Furthermore, we have

$$\mathbf{\Delta}\omega_l = \omega_l - \mathbf{1} \tag{8}$$

$$\mathbf{\Delta}\omega_e = \omega_e - \mathbf{1} \tag{9}$$

where $\mathbf{1}$ is a column vector containing only ones. Finally to arrive at the FD formula we insert (8) and (9) into (7) and rearrange.

$$\omega_l = \mathbf{1} + \mathbf{D}(\omega_e - \mathbf{1}) \tag{10}$$

where

$$\mathbf{D} = -\mathbf{B}_{22}^{-1}\mathbf{B}_{21} \tag{11}$$

The formula (10) is the same as the one presented in [1]

## III. Illustrative example

In this letter only a short example demonstrating the use of the FD formula is provided. In [1] several examples are presented comparing the FD formula to other approaches for estimation of bus frequencies, as well as examples investigating some of the assumptions made.

In the example we will use the small test system depicted in Fig. 1. The reactances, $x_1$ and $x_2$ are line reactances, and $x'_{d1}$ and $x'_{d2}$ are the transient reactances of the generators at bus 1 and bus 2 respectively. The system is tuned using the values from [2] to have a frequency response similar to the Nordic system.

The nodal susceptance matrix $\mathbf{B}$ for the system depicted in Fig. 1 using sucseptances($b = 1/x$) is.

$$\mathbf{B} = \left[\begin{array}{ccc:cc} b'_{d1} & 0 & -b'_{d1} & 0 & 0 \\ 0 & b'_{d2} & 0 & -b'_{d2} & 0 \\ \hdashline -b'_{d1} & 0 & b'_{d1}+b_1 & 0 & -b_1 \\ 0 & -b'_{d2} & 0 & b'_{d2}+b_2 & -b_2 \\ 0 & 0 & -b_1 & -b_2 & b_1+b_2 \end{array}\right] \tag{12}$$

The expression for the change in angular velocity at the bus 5 as a function of the generator speeds with $|\mathbf{B}_{22}|$ denoting the determinant of $\mathbf{B}_{22}$ is.

$$\Delta\omega_3 = \frac{(b_1b_{d2}+b_1b_2+b_2b_{d2})b_{d1}}{|\mathbf{B}_{22}|}\Delta\omega_1 + \frac{b_1b_2b_{d2}}{|\mathbf{B}_{22}|}\Delta\omega_2 \tag{13}$$

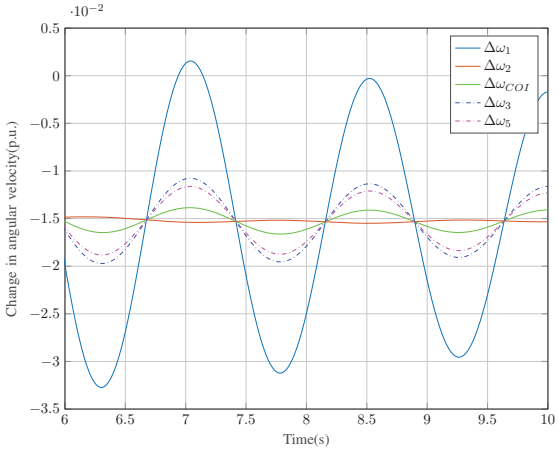


Fig. 2: Comparison of COI and FD

Similarly the expression for the angular velocity at bus 5 will be

$$\Delta\omega_5 = \frac{b_1b'_{d1}(b'_{d2}+b_2)}{|\mathbf{B}_{22}|}\Delta\omega_1 + \frac{b_2b'_{d2}(b'_{d1}+b_1)}{|\mathbf{B}_{22}|}\Delta\omega_2 \tag{14}$$

The COI speed for the system is

$$\Delta\omega_{COI} = \frac{1}{H_1+H_2}(H_1\Delta\omega_1 + H_2\Delta\omega_2) \tag{15}$$

where $H_1$ and $H_2$ are the inertia constants of the plants at bus 1 and 2 respectively.

In Fig. 2 $\Delta\omega_1$, $\Delta\omega_2$, $\Delta\omega_3$, $\Delta\omega_5$, and $\Delta\omega_{COI}$ are plotted after applying a one per unit load step. From the figure one can see how the FD formula unlike the COI formula captures the effect of bus 3 being closer to generator 1 than bus 5. Furthermore, the COI formula underestimates the amplitude of the oscillations at both buses compared to the FD formula.

## IV. Conclusions

We have shown that it is easy to derive the FD formula starting from a dc power flow assumption. This approach for deriving the FD formula should be quick and easy to grasp for both students and power system engineers.


## Acknowledgements

The work presented in this paper was carried out in the project OperaGrid funded by the Norwegian research council.


## References


[1] F. Milano and Á. Ortega, "Frequency divider," *IEEE Transactions on Power Systems*, vol. 32, no. 2, pp. 1493–1501, Mar. 2017, ISSN: 0885-8950. DOI: 10 . 1109 / TPWRS.2016.2569563.

[2] L. Saarinen, P. Norrlund, U. Lundin, E. Agneholm, and A. Westberg, "Full-scale test and modelling of the frequency control dynamics of the nordic power system," in *2016 IEEE Power and Energy Society General Meeting (PESGM)*, Jul. 2016, pp. 1–5. DOI: 10.1109/PESGM.2016.7741711.